Condensation of Refrigerants 12 and 134a in Horizontal Tubes With and Without Oil

D. K. Hinde, M. K. Dobson, J. C. Chato, M. E. Mainland, and N. Rhines

ACRC TR-26 October 1992

For additional information:

Air Conditioning and Refrigeration Center
University of Illinois
Mechanical & Industrial Engineering Dept.
1206 West Green Street
Urbana, IL 61801

(217) 333-3115

Prepared as part of ACRC Project 01
Refrigerant-Side Evaporation and Condensation Studies
J. C. Chato, Principal Investigator

The Air Conditioning and Refrigeration Center was founded in 1988 with a grant from the estate of Richard W. Kritzer, the founder of Peerless of America Inc. A State of Illinois Technology Challenge Grant helped build the laboratory facilities. The ACRC receives continuing support from the Richard W. Kritzer Endowment and the National Science Foundation. The following organizations have also become sponsors of the Center.

Acustar Division of Chrysler
Allied-Signal, Inc.
Amana Refrigeration, Inc.
Bergstrom Manufacturing Co.
Caterpillar, Inc.
E. I. du Pont de Nemours & Co.
Electric Power Research Institute
Ford Motor Company
General Electric Company
Harrison Division of GM
ICI Americas, Inc.
Johnson Controls, Inc.
Modine Manufacturing Co.
Peerless of America, Inc.
Environmental Protection Agency
U. S. Army CERL
Whirlpool Corporation

For additional information:

Air Conditioning & Refrigeration Center
Mechanical & Industrial Engineering Dept.
University of Illinois
1206 West Green Street
Urbana IL 61801

217 333 3115

CONDENSATION OF REFRIGERANTS 12 AND 134a IN HORIZONTAL TUBES WITH AND WITHOUT OILS

David Kistler Hinde, M.S.
Department of Mechanical and Industrial Engineering
University of Illinois at Urbana-Champaign, 1992
J. C. Chato, Advisor

ABSTRACT

This study investigated local condensation heat transfer and pressure drop for pure R-12, pure R-134a and R-134a/oil mixtures and examined the results based on two-phase flow patterns. Condensing conditions simulated those found in domestic refrigerator/freezers. Experiments were performed to measure internal heat transfer coefficients and pressure drops inside a 0.25 in. (6.35 mm) OD, 0.180 in. (4.57 mm) ID smooth, horizontal copper tube. Direct measurements of the temperature difference between the tube wall and the condensing fluid were made. The heat transfer coefficients and pressure drops were compared with existing prediction techniques and differences were found due primarily to differing flow patterns from those used in models and the presence of liquid entrainment in the flow. Tests with a mixture of R-134a and ester lubricant showed a slight increase in heat transfer coefficient at 1.2% concentration and a decrease at 5% concentration. Pressure drop increased with oil concentration. Heat transfer coefficients for R-134a were found to be 10% to 20% higher than for R-12 at equivalent mass flux and saturation temperature, while the difference in pressure drop was within the range of experimental error.

TABLE OF CONTENTS

NOMENCLATURE

A	area	[m^2]
C	constant in generalized Lockhart-Martinelli parameter	
C_f	skin friction coefficient	
c_p	specific heat	[kJ/kg•K]
D	diameter	[m]
f	friction factor	
F_2	constant in Traviss et. al., Eq. (2.10)	
k	thermal conductivity	[W/m•K]
G	mass flux	[kg/m^2•s]
g	acceleration due to gravity	[m/s^2]
h	heat transfer coefficient	[W/m^2•K]
h	enthalpy	[kJ/kg]
K	constant in Chisholm equation	
P	pressure	[Pa]
q	heat	[W]
T	temperature	[K]
v	specific volume	[m^3/kg]
w	mass fraction	
x	vapor quality	
y	vertical distance	[m]
y	mole fraction	
z	length	[m]

GREEK SYMBOLS

α	thermal diffusivity	[m^2/s]
χ	generalized Lockhart-Martinelli parameter as defined by Eq. (2.26)	
χ_{tt}	Lockhart-Martinelli parameter, as defined by Eq. (2.11)	
Δ	difference between liquid and vapor values	
ε_h	eddy diffusivity of heat	[m^2/s]
ε_m	eddy or momentum diffusivity	[m^2/s]
ϕ	two-phase multiplier	
μ	dynamic viscosity	[$N \cdot s/m^2$]
ν	kinematic viscosity	[m^2/s]
ρ	density	[kg/m^3]
θ	angle of inclination from horizontal in Eq. (2.1)	[degrees or radians]
τ	shear stress	[N/m^2]
ω	mass fraction	

SUBSCRIPTS

eq	equivalent value for liquid/vapor mixture
f	fluid, liquid
f	friction component
fg	change from liquid to vapor
g	gas, vapor
l	fluid, liquid
m	oil/refrigerant mixture
m	momentum component
o	oil
r	refrigerant
rd	reduced value, defined as actual value/critical value

sat	saturation value
TP	two-phase
v	gas, vapor
w	wall

SUPERSCRIPTS

m	constant in generalized Lockhart-Martinelli parameter
n	constant in generalized Lockhart-Martinelli parameter

DIMENSIONLESS GROUPS

Nu	Nusselt number	$[h \cdot D/k]$
Pr	Prandtl number	$[c_p \cdot \mu/k]$
Re	Reynolds number	$[G \cdot D/\mu]$
St_x	Stanton number	$[Nu/Re_L \cdot Pr]$

CHAPTER 1
INTRODUCTION

Recent legislation aimed at phasing out chloro-fluorocarbons (CFC's) has combined with increasingly strict energy standards for refrigeration equipment to intensify research in heat exchanger design for domestic and automotive refrigeration and air conditioning. The signing of the Montreal Protocol in 1987 mandated the eventual elimination of one of the most common refrigerants, R-12 (Dichlorodifluoromethane). Used in domestic refrigerators and air conditioners for several decades, this fluid now requires a replacement. One such replacement proposed is the hydrofluorocarbon R-134a (Tetrafluoroethane), which contains no chlorine potentially harmful to the ozone layer. R-134a has shown promise for R-12 replacement but needs further testing to fully understand its heat transfer behavior, pressure drop characteristics, and oil and material compatibilities.

Prediction of heat transfer and pressure drop behavior is essential to heat exchanger design. As materials and manufacturing methods improve the overall performance of condensing heat exchangers, it is becoming increasingly important to improve the internal condensing heat transfer coefficients. To achieve this goal, local condensation heat transfer coefficients must be predicted. These coefficients are very dependent on the two-phase flow pattern and there is a general lack of existing information and understanding of this interrelation. It is then the purpose of this project to examine local heat transfer coefficients and pressure drop characteristics of condensing flows and to correlate observations based on two-phase flow patterns.

The subject of this thesis is condensation of Refrigerant-134a in horizontal tubes and its behavior in both pure form and with the presence of oil. Oil in small amounts is necessary in domestic refrigerators for lubrication of the compressor. Local heat transfer coefficients and pressure drops are examined with emphasis on explaining results based on observed two-phase flow patterns.

Chapter 2 of this thesis is a review of the literature associated with in-tube condensation. Two-phase flow regimes for condensation are examined. The development of methods to predict condensation heat transfer is discussed and several correlations are presented. The effects of oil on refrigerant condensation is next examined. Finally, pressure drop models for two-phase flow are discussed.

Chapter 3 presents the experimental facility built for this study at the Air Conditioning and Refrigeration Center at the University of Illinois at Urbana-Champaign. The refrigerant and cooling loops are discussed placing emphasis on the test condenser and related instrumentation. Data acquisition methods for the project are also presented.

Chapter 4 summarizes typical operating conditions for domestic refrigerator condensers and outlines the experimental test designed to simulate these. Included is a discussion of operating procedures and the technique used for measurement of oil concentrations.

Chapter 5 is a detailed explanation of the procedures used in reducing and analyzing the experimental data. The first section details energy balance calculations required to establish inlet and outlet conditions of the test condenser. This is followed by a description of the methods used to determine local and average heat transfer coefficients on the tube surface.

Chapter 6 presents the data collected for this study. A comparison of measured heat transfer coefficients and pressure drops to existing prediction methods is made for both the pure refrigerant and refrigerant/oil mixtures. Special attention is given to looking at the results in terms of the observed flow regime and how this information could be used to improve prediction techniques.

Finally, Chapter 7 presents the conclusions reached in this study. Recommendations for further work are included as well as suggestions for improvements to the test facility and future test condensers.

CHAPTER 2

LITERATURE REVIEW

In past decades, much emphasis has been given to research of in-tube forced-convection and laminar-film condensation. Since Nusselt's early work with condensation on inclined flat plates to more recent studies of ozone-safe refrigerants with oils and in tubes with enhanced surfaces, forced-convection condensation has proven to be a complicated process. This literature review summarizes investigations studying condensation heat transfer coefficients, pressure drop characteristics, and flow patterns of both pure refrigerants and refrigerant-oil mixtures in smooth tubes.

2.1. Flow Mechanics of In-Tube Condensation

In condensation, heat is removed from a fluid causing vapor to change into a liquid. Fluid condensing in a tube may assume a variety of flow patterns or flow regimes as they are called. These flow patterns depend on the mass flow rate, the vapor quality, and various properties of each phase of the fluid.

Figure 2.1 shows a typical series of flow patterns for condensing fluid in a smooth, horizontal tube for the case of low velocity and high velocity flows. For the high velocity case, fluid enters the tube as a single phase vapor (quality = 1) and condenses on the tube surface where an annular film of liquid begins to form. In this high velocity *annular-flow regime*, laminar-film condensation may occur, meaning that the film is flowing in the laminar range and heat is removed from the vapor only by conduction through the liquid film. If the vapor velocity is sufficiently high, flow in the film is likely to become turbulent and liquid entrainment may occur, where small droplets of liquid are sheared from the liquid film and carried off in the vapor flow. As more vapor is condensed, the flow may enter the *slug-flow regime*, where forced-convection condensation takes over. Here, the flow is still mostly vapor and annular in nature but in some areas of the tube the film becomes thick enough to coalesce

into a slug of liquid and is carried down the tube at high velocity. With most of the vapor having been condensed, the flow enters the *plug-flow regime*, where the majority of the flow consists of all liquid but periodic plugs of vapor travel through at the liquid velocity. The *bubbly-flow regime* occurs when only a small amount of vapor is present and the liquid flow is too turbulent to allow smaller vapor bubbles to coalesce into a plug. Finally, as the last of the vapor condenses, a single-phase liquid flow (quality = 0) exits the tube.

For the lower velocity case the fluid again enters the tube as a single phase vapor and condenses on the tube surface but in contrast to the higher velocity flow, the liquid immediately begins to collect on the bottom of the tube. As the amount of liquid increases, the flow enters the *stratified-flow regime* or with slightly higher vapor velocities, the *wavy-flow regime.* Here, the majority of heat transfer takes place at the top of the tube where the liquid film is very thin. It is in these regimes where gravity effects may have a major impact on the thickness of the liquid layer. The flow then enters the *plug-flow regime* where the last of the vapor is condensed and single-phase liquid exits the tube.

Since the heat transfer coefficients and pressure drop characteristics of a two-phase flow vary with the flow geometry, it is desirable to be able to predict the flow regime given conditions such as mass flow rate, tube size, vapor quality, and liquid and vapor properties. To achieve this, it is possible to produce a *flow regime map*. Figure 2.2 shows one such map from Baker (1958) where the vapor superficial mass flux is plotted against the liquid superficial mass flux. Lines on the map mark transitions from one flow regime to another. Flow regime maps vary greatly between authors, however, since flow regime categorization is not based on measurable quantities but by subjective visual determination only. Authors widely disagree on the parameters which should be plotted on such a map. This process being somewhat blind, it would then seem more appropriate to first determine the heat transfer coefficient based on experimental data and later correlate the coefficients based on flow regime criteria.

2.2. Heat Transfer Coefficient Correlations for In-Tube Condensation

The accurate prediction of heat transfer coefficients is a main goal of most condensation research. The following sections look at the history of attempts to predict heat transfer and summarize some works which are applicable to this project for both pure refrigerants and refrigerant-oil mixtures.

2.2.1. Development of Condensation Heat Transfer Correlations

In 1916, Nusselt derived an equation for the heat transfer coefficient of a fluid film condensing on an inclined flat plate. The following assumptions were made: 1. flow of the condensate film is laminar; 2. fluid properties are constant throughout the flow; 3. subcooling of the fluid is negligible; 4. momentum changes in the film are negligible; 5. vapor is stagnant and exerts no drag on the film; 6. heat is transferred by conduction only. The equation he derived is as follows:

$$Nu(z) = \left[\frac{\rho_f (\rho_f - \rho_g)\, g \sin\theta\, h_{fg}\, z^3}{4\, \mu_f\, k_f\, (T_{sat} - T_w)} \right]^{0.25} \tag{2.1}$$

where T_w is the temperature of the plate surface and T_{sat} is the saturation temperature of the condensing fluid (Collier 1982). Subsequent studies added the effects of liquid subcooling, nonlinear temperature distribution due to convection, and more recently, the influence of drag at the liquid-vapor interface. Nusselt's extended analysis to condensation on the outside of a horizontal tube yields the following expression:

$$\bar{h} = 0.725 \left[\frac{\rho_f (\rho_f - \rho_g)\, g\, h_{fg}'\, k_f^3}{D\, \mu_f\, (T_{sat} - T_w)} \right]^{0.25} \tag{2.2}$$

where h_{fg}' is a modified latent heat of vaporization by Rohsenow (1956) and is defined as follows:

$$h_{fg}' = h_{fg} + 0.68\, c_{pf}\, (T_{sat} - T_w) \tag{2.3}$$

For sufficiently low vapor velocities such that the flow is still in the laminar region, that is, the entrance vapor Reynolds number is less than 35,000, this solution may be applied to condensation inside tubes. Chato (1962) developed a relationship for two-phase gravity-driven stratified flow in horizontal tubes and is as follows:

$$h_{TP} = 0.77\, h_{Nu} \tag{2.4}$$

where h_{Nu} is given by Eq. (2.2). Chato also showed that a slight downward slope of the tube in the flow direction can drastically reduce the depth of the bottom condensate and thereby increase the heat transfer by as much as 20%. While Eq. (2.4) has been well verified, other solutions for horizontal laminar flow attempt to correlate the two-phase heat transfer coefficient with a combination of Eq. (2.2) and the void fraction of the flow.

In forced convection condensation, where the flow is no longer in the laminar region, the effects of turbulence must be added to the equation for momentum continuity before a solution may be found. The Newtonian fluid shear stress equation is the following:

$$\tau_{yx} = \mu \frac{du}{dy} \tag{2.5}$$

For turbulent flows, the shear stress can be modeled as:

$$\tau_{yx} = \rho\, (\nu + \varepsilon_m) \frac{\partial \bar{u}}{\partial y} \tag{2.6}$$

where ε_m is the eddy diffusivity for momentum. A similar modification is made to Fourier's Law which is the following:

$$\frac{q}{A} = -k \frac{dT}{dy} \tag{2.7}$$

For turbulent flow, the equation becomes the following:

$$\frac{q}{A} = -\rho c_p (\alpha + \varepsilon_h) \frac{\partial \bar{T}}{\partial y} \tag{2.8}$$

where ε_h is the eddy diffusivity of heat. Combining Eq. (2.6) and Eq. (2.8) leads to what is termed the Reynolds-Colburn analogy for turbulent flow which is the following:

$$j = St_x \, Pr^{2/3} = \frac{C_f}{2} \tag{2.9}$$

$$St_x = \frac{Nu_x}{Re_x \, Pr} = \frac{h_x}{G \, c_p}$$

where the friction factor C_f is a function of the Reynolds number. This form of the Reynolds-Colburn analogy has been applied to several different heat transfer correlations for the Nusselt number as a function of the Prandtl and Reynolds numbers of the flow and a variety of correction factors. As will be seen in the next section, the correlations used in this study are all similar in form to the Reynolds-Colburn analogy.

2.2.2. Correlations for Pure Refrigerants

Four correlations have been chosen for this study to which experimental data will be compared. The criteria for choosing these were two-fold; the correlations were specifically tested with refrigerants, and they exhibited good agreement with previous experimental data as well as each other.

Traviss, Rohsenow, and Baron (1973) presented an equation for forced-convective, annular-flow condensation based on the solutions of the turbulent flow equations, Eq. (2.6) and Eq. (2.8), and using the von Karman universal velocity distribution. The equation is as follows:

$$Nu = F(\chi_{tt}) \frac{Pr_l \, Re_l^{0.9}}{F_2} \tag{2.10}$$

$$F(\chi tt) = 0.15 \left[\chi_{tt}^{-1} + 2.85 \, \chi_{tt}^{-0.476}\right]$$

$Re_l < 50$ $\qquad F_2 = 0.707 \, Pr_l \, Re_l^{0.5}$

$50 < Re_l < 1125$ $\qquad F_2 = 5 \, Pr_l + 5 \ln\left[1 + Pr_l \, (0.09636 Re_l^{0.585} - 1)\right]$

$Re_l > 1125$ $\qquad F_2 = 5 \, Pr_l + 5 \ln(1 + 5 \, Pr_l) + 2.5 \ln(0.00313 \, Re_l^{0.812})$

$$Re_l = \frac{GD(1-x)}{\mu_l}$$

where χ_{tt} is the Lockhart-Martinelli parameter for turbulent gas and liquid flow and is defined as follows:

$$\chi_{tt} = \left(\frac{\mu_l}{\mu_v}\right)^{0.1} \left(\frac{1-x}{x}\right)^{0.9} \left(\frac{\rho_v}{\rho_l}\right)^{0.5} \tag{2.11}$$

Experiments were performed by Traviss for condensation of R-12 and R-22 in a 3/8 in. (9.5 mm) OD, 0.315 in. (8.0 mm) ID test section. Predicted heat transfer coefficients from the above equation showed good agreement with the experimental data.

Based on the same analysis but simplified and more empirical in nature, is the correlation by Cavallini and Zecchin (1974) which is as follows:

$$Nu = 0.05\ Re_{eq}^{0.8}\ Pr^{0.33} \tag{2.12}$$

$$Re_{eq} = Re_v \left(\frac{\mu_v}{\mu_l}\right)\left(\frac{\rho_l}{\rho_v}\right)^{0.5} + Re_l$$

$$Re_l = \frac{GD(1-x)}{\mu_l}$$

$$Re_v = \frac{GDx}{\mu_v}$$

The above equation was compared with several data sets from previous authors and included the following working fluids: R-11, R-12, R-22, R-113, and R-114. In addition, the data were within the following parameters: $5000 < Re_{lo} < 500{,}000$; $0.8 < Pr < 20$. In general, Eq. (2.12) showed good agreement with the experimental data, especially those of R-22.

The third correlation looked at in this study is by Shah (1979) and is purely empirical in nature. Here, it was assumed that the two-phase heat transfer coefficient is a multiple of the liquid single-phase coefficient and that this multiplier is a function of the condensation number and the Froude number. For the liquid single-phase heat transfer coefficient, the equation by Dittus and Boelter was used and is the following:

$$h_L = 0.023\ Re_L^{0.8}\ Pr_l^{0.4}\ \frac{k_l}{D} \tag{2.13}$$

After calculating the single-phase coefficient, the experimental data were correlated with the condensation number and Froude number and the equation finally simplifies as follows:

$$h_{TP} = h_L \left[(1-x)^{0.8} + \frac{3.8\ x^{0.76}\ (1-x)^{0.04}}{P_{rd}^{0.38}} \right] \tag{2.14}$$

$$Re_L = \frac{GD}{\mu_l}$$

where P_{rd} is the reduced pressure. The data used in correlating this equation came from a variety of authors and included the following fluids: R-11, R-12, R-113, water, methanol, ethanol, and benzene. The data were within the following range of Reynolds numbers: $104 < Re_L < 69{,}000$. Although a wide range of Reynolds numbers were compared, Shah suggested that Eq. (2.14) was best applied to flows with $Re_L > 3000$.

Finally, Chen, Gerner, and Tien (1987) suggest the following correlation for annular film condensation:

$$Nu = 0.036\ A^{0.50}\ Pr_l^{0.65}\ Re_L^{0.20}\ [Re_{Lo} - Re_L]^{0.70} \tag{2.15}$$

$$A = 0.252 \left(\frac{\mu_g}{\mu_l}\right)^{0.156} \left(\frac{\rho_l}{\rho_g}\right)^{0.78}$$

$$Re_L = \frac{GD(1-x)}{\mu_l}$$

$$Re_{Lo} = \frac{GD}{\mu_l}$$

The above correlation was shown to work well for existing data obtained with R-113, R-21, and water, and for Re_{lo} from 40 to 18,000.

2.2.3. Correlations for Refrigerant-Oil Mixtures

Although there are many correlations for pure refrigerant condensation, very few exist for refrigerant-oil mixtures. Two basic approaches have been used for calculating mixture heat transfer coefficients. The first method makes use of a pure refrigerant correlation but replaces pure-refrigerant properties with properties corrected for the mixture. The second method accounts for the mixture differences by multiplying the pure-refrigerant correlation by an enhancement factor based on oil concentration or viscosity ratios (Sur and Azer 1991).

Baustian, Pate, and Bergles (1986) recommend a variety of equivalent property equations for density, specific heat, thermal conductivity, and viscosity as follows:

$$\rho_m = \frac{\rho_r}{1 - (1 - w)\left(1 - \rho_r/\rho_o\right)} \tag{2.16}$$

$$c_{pm} = c_{pr}w + c_{po}(1 - w) \tag{2.17}$$

$$k_m = k_r w + k_o (1 - w) - 0.72 (k_o - k_r)(1 - w)\, w \tag{2.18}$$

$$\mu_m = \left[y_r \mu_r^{1/3} + y_o \mu_o^{1/3}\right]^{1/3} \tag{2.19}$$

where w is the mass fraction of refrigerant, y_r is the mole fraction of refrigerant, and y_o is the mole fraction of oil. The above relations showed good agreement when compared with measured values for a mixture of R-113 and 150 SUS Naphthenic oil. Schlager, Pate, and Bergles (1990b) inserted mixture properties obtained from the above relations into the three correlations from the previous section, Eq. (2.10) to (2.14), and obtained results within 10% of experimental values for complete condensation of mixtures of R-12 and 150-SUS and 300-SUS oils.

Tichy, Macken, and Duval (1985) took the second approach to condensation of refrigerant-oil mixtures and defined an enhancement factor with which the pure refrigerant correlation could be multiplied; their equation is the following:

$$h = h_{TP}\left[0.88 + \left(\frac{Re_{lR_o}}{Re_{lR}}\right)^{1.99}\right] e^{-5.0\,\omega_o} \tag{2.20}$$

Re_{lR_o} = reference Reynolds number = 3650

$$Re_{lR} = \frac{GD}{\mu_l}$$

where h_{TP} is the pure refrigerant correlation from Shah, Eq.(2.14) and ω_o is the mass fraction of oil in the mixture. The above equation was compared with experimental data from a mixture of R-12 and 300-SUS Naphthenic oil. Agreement was found to be ±20% for 82% of the data.

Additional relationships suggested by Schlager, Pate, and Bergles (1990b) are the following:

$$h = h_{TP}\, e^{-3.2\,\omega_o} \tag{2.21}$$

$$h = h_{TP}\left[\frac{\mu_{lr}}{\mu_{lm}}\right]^{0.47} \tag{2.22}$$

where h_{TP} in Eq. (2.22) may as well be defined using the correlation by Cavallini and Zecchin, Eq. (2.12), and the liquid mixture viscosity, μ_{lm} as defined by Eq. (2.19).

2.3 Pressure Drop Correlations for In-Tube Condensation

The pressure gradient for two-phase flow in a horizontal tube may be described by the following equation:

$$\left[\frac{dP}{dz}\right] = \left[\frac{dP}{dz}\right]_f + \left[\frac{dP}{dz}\right]_m + \left[\frac{dP}{dz}\right]_g \tag{2.23}$$

where the first term is the pressure drop due to friction, the second term is the pressure drop due to momentum change as a result of condensation, and the third term is the pressure drop due to gravity, which for horizontal flow is zero (Collier 1972).

The friction component of pressure drop may be described using two-phase multipliers which are the ratios of two-phase to single-phase pressure drops. These multipliers, ϕ_l^2, ϕ_g^2, ϕ_{lo}^2, and ϕ_{go}^2 are defined as follows:

$$\left[\frac{dP}{dz}\right]_f = \phi_l^2 \left[\frac{dP}{dz}\right]_{fl} \tag{2.24a}$$

$$\left[\frac{dP}{dz}\right]_f = \phi_{lo}^2 \left[\frac{dP}{dz}\right]_{flo} \tag{2.24b}$$

$$\left[\frac{dP}{dz}\right]_f = \phi_g^2 \left[\frac{dP}{dz}\right]_{fg} \tag{2.24c}$$

$$\left[\frac{dP}{dz}\right]_f = \phi_{go}^2 \left[\frac{dP}{dz}\right]_{fgo} \tag{2.24d}$$

where the single-phase pressure drops $\left[\frac{dP}{dz}\right]_{fl}$, $\left[\frac{dP}{dz}\right]_{fg}$, $\left[\frac{dP}{dz}\right]_{fl}$, and $\left[\frac{dP}{dz}\right]_{fg}$ are described as:

$$\left[\frac{dP}{dz}\right]_{fl} = \frac{2\, f_l\, G^2\, (1-x)^2\, v_l}{D} \tag{2.25a}$$

$$\left[\frac{dP}{dz}\right]_{f_{lo}} = \frac{2\, f_{lo}\, G^2\, v_l}{D} \tag{2.25b}$$

$$\left[\frac{dP}{dz}\right]_{f_g} = \frac{2\, f_g\, G^2\, x^2\, v_g}{D} \tag{2.25c}$$

$$\left[\frac{dP}{dz}\right]_{f_{go}} = \frac{2\, f_{go}\, G^2\, v_g}{D} \tag{2.25c}$$

In the above equations, f_l, f_{lo}, f_g, and f_{go} are the liquid and vapor friction factors and can be found from either of the following equations for turbulent flow:

$$f = \frac{0.079}{Re^{0.25}} \tag{2.26a}$$

$$f = \frac{0.046}{Re^{0.2}} \tag{2.26b}$$

and for laminar flow:

$$f = \frac{64}{Re} \tag{2.26c}$$

Where the Reynolds number is dependent on the friction factor used as follows:

$$\text{For } f_l, \quad Re = \frac{GD(1-x)}{\mu_l}$$

$$\text{For } f_{lo}, \quad Re = \frac{GD}{\mu_l}$$

$$\text{For } f_g, \quad Re = \frac{GDx}{\mu_g}$$

$$\text{For } f_{go}, \quad Re = \frac{GD}{\mu_g}$$

Several correlations for determining the two-phase multiplier ϕ^2 follow and all were taken from Corradini (1991). Many of these correlations make use of the generalized Lockhart-Martinelli parameter defined as follows:

$$\chi^2 = \frac{\left[\frac{dP}{dz}\right]_{fl}}{\left[\frac{dP}{dz}\right]_{fg}} = \frac{Re_g^m}{Re_l^n} \frac{C_l}{C_g} \frac{\mu_l}{\mu_g} \frac{\rho_g}{\rho_l} \tag{2.27}$$

The constants m, n, C_l, and C_g are dependent on whether the gas and liquid flows are laminar or turbulent (Lockhart and Martinelli 1949). Typically in condensing flows, both phases will be in the turbulent regime and in this case, χ reduces to χ_{tt} as shown previously in Eq. (2.11).

The Chisholm correlation uses χ along with a flow-defined constant to determine the value of ϕ_g^2 and is the following (Chisholm 1963):

$$\phi_g^2 = \chi^2 + K\chi + 1 \tag{2.28}$$

K = 20 for turbulent liquid - turbulent gas flow
K = 12 for laminar liquid - turbulent gas flow
K = 10 for turbulent liquid - laminar gas flow
K = 5 for laminar liquid - laminar gas flow

Similarly, the Soliman correlation for the turbulent-turbulent case determines the value of ϕ_g^2 from the following (Corradini 1991):

$$\phi_g^2 = \left[1 + 2.85\ \chi^{0.523}\right]^2 \tag{2.29}$$

Three other correlations using the two-phase multiplier ϕ_{lo}^2 have shown to work well with condensing flows. First is the Homogeneous I correlation and is the following (Corradini 1991):

$$\phi_{lo}^2 = \left[1 + x \frac{\Delta \rho}{\rho_g}\right] \tag{2.30}$$

$$\mu_{TP} \equiv \mu_l$$

The Homogeneous III correlation is the following (Corradini 1991):

$$\phi_{lo}^2 = \left[1 + x \frac{\rho_f - \rho_g}{\rho_g}\right]\left[1 - x \frac{\mu_f - \mu_g}{\mu_g}\right]^{0.25} \tag{2.31}$$

$$\mu_{TP} \equiv x\,\mu_g + (1-x)\mu_l$$

Finally, the Thom correlation is the following (Thom 1964):

$$\phi_{lo}^2 = \left[\left[0.97303\,(1-x) + x \frac{\Delta \rho}{\rho_g}\right]^{0.5}\left[0.97303\,(1-x) + x\right]^{0.5} + 0.027\,(1-x)\right]^2 \tag{2.32}$$

The above correlations have all shown to predict experimental pressure drop in certain cases but tend to exhibit inconsistencies when compared for similar conditions.

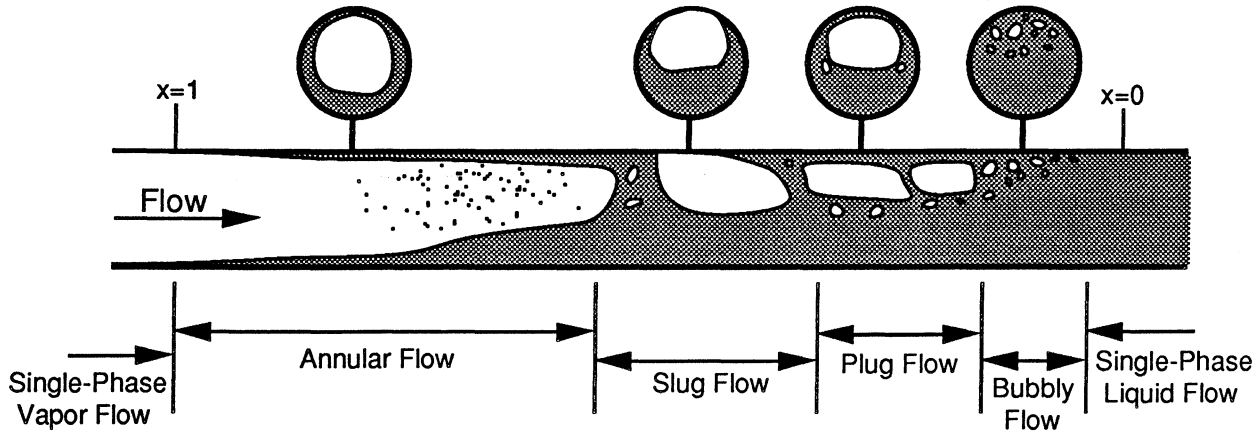

Figure 2.1a. Flow Regimes for High Velocity Flow

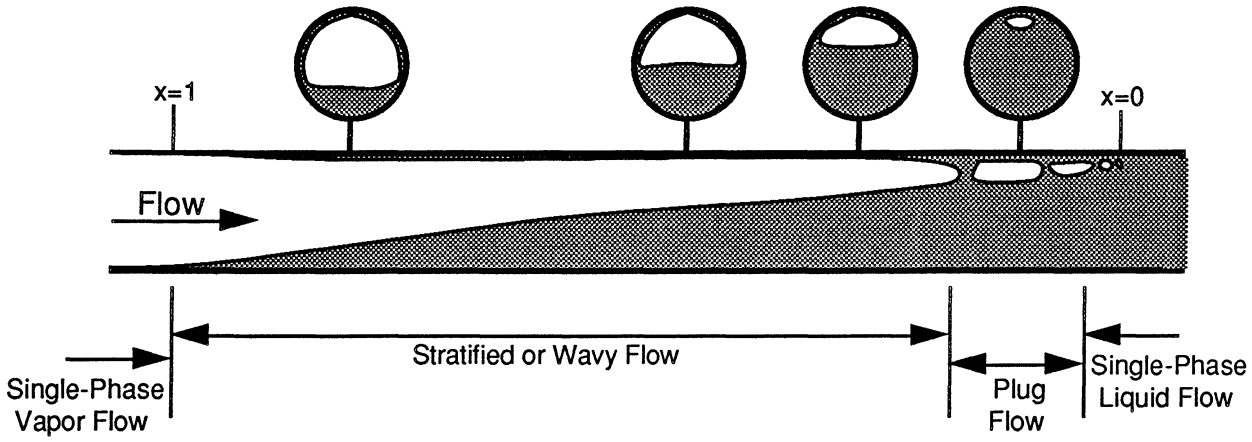

Figure 2.1b. Flow Regimes for Low Velocity Flow

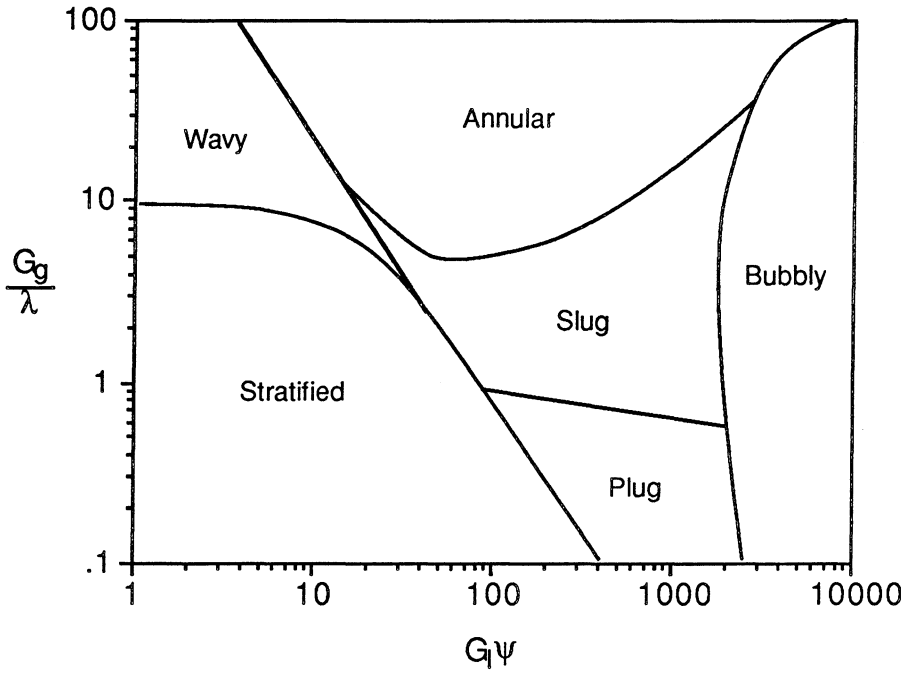

$$\lambda = \left[\left(\frac{\rho_g}{0.075}\right)\left(\frac{\rho_l}{62.3}\right)\right]^{\frac{1}{2}}$$

$$\psi = \frac{73}{\sigma}\left[\mu_l\left(\frac{62.3}{\rho_l}\right)^2\right]^{\frac{1}{3}}$$

Figure 2.2. Flow Regime Map, from Baker (1958)

CHAPTER 3

TEST FACILITY, INSTRUMENTATION, AND DATA ACQUISITION

A single tube condenser test facility was built for this project at the Air Conditioning and Refrigeration Center at the University of Illinois at Urbana-Champaign and is pictured in Figure 3.1. The components of the facility to be detailed in this chapter are the refrigerant loop, the cooling water loop, the test condenser, the instrumentation, and the data acquisition system. For a more detailed explanation of the basic design and construction of the test facility, the reader is referred to Bonhomme (1991). Modifications are described below.

3.1. Refrigerant Loop

Figure 3.2 shows a schematic of the refrigerant loop of the single tube condenser test facility. The main components of the refrigerant loop are the following: a variable speed pump, two flowmeters, a refrigerant heater, the test condenser, a void fraction measurement section, an aftercondenser, a receiver, and a bladder accumulator; a brief explanation of each of these components and their function follows. The loop itself is constructed primarily of 1/2 in. OD copper refrigeration tubing and was designed for operating pressures up to 500 psi (3450 kPa) and temperatures up to 180 °F (82 °C). The loop is completely insulated with 1 1/2 in. (3.8 cm) of Armaflex insulation.

In this facility, only the high-pressure side of a refrigeration cycle is represented, that is, there is no compressor or low-pressure side and the refrigerant is pumped through the cycle eliminating the oil contamination that a compressor would necessitate. The pump is composed of a MicroPump three-gear, variable-speed, 0.77 gpm (2.9 l/min) capacity pump head magnetically driven by a 1/3 horsepower, 3450 maximum rpm motor. The pump is digitally controlled using a Woods E-trAC AC inverter . Immediately before the pump is a refrigerant filter/dryer to remove any water vapor or particulate matter which may harm the pump and

flowmeter. Additional control of the refrigerant flow is facilitated with a bypass around the pump as well as a throttling valve farther downstream.

Following the pump, the refrigerant flows through one of two flowmeters placed in parallel. These are a Max 0-2 gpm (0-7.6 l/min) positive displacement flowmeter and a Micro Motion, 0-1 lb/min (0-0.45 kg/min) mass flowmeter. For tests reported in this thesis, the latter was used because its range was more appropriate. A bypass is included around the flowmeters as recommended by the manufacturer for situations when the refrigerant flow is not all liquid and may not provide adequate cooling to the meter's components or when the meter's capacity is greatly exceeded.

A 4 kW refrigerant heater follows the flowmeter and was designed to heat the refrigerant from a subcooled liquid to a desired two-phase or superheated outlet condition. The heater is composed of a serpentine of 3/4 in. (19 mm) OD copper tubing wrapped with resistance heater tape. Copper inserts constructed of 3/8 in. (9.5 mm) OD copper tubing wrapped with a spiral of 10 gauge solid copper wire were placed inside each row. These serve the purpose of increasing the internal heat transfer to reduce the wall temperature and minimize the possibility of heater burnout. The amount of charge required by the heater was also reduced by 50%, decreasing slightly the amount of time the refrigerant loop required to reach steady state. The heater is divided into two sections, Heater 1 and Heater 2, both with a heating capacity of 2 kW. The heater is controlled by turning on individually switched 120 W heaters and controlling the applied voltage with a 0-240 V variac. The total heat input is monitored with watt-hour transducers which are discussed in section 3.4. The tubes of the heater are individually insulated with 2 1/2 in. (63 mm) of rigid fiberglass insulation due to the possibility of temperatures developing which are higher than the 180 °F (82 °C) design limit of the Armaflex insulation.

The refrigerant next flows through the test condenser which is discussed in Section 3.3. Sight glasses are located at the entrance and exit of the test condenser. Each sight glass is composed of a 5 in. (127 mm) length of thick-walled glass tubing which has

been annealed to remove any internal stress and is rated to a pressure of 800 psi (5500 kPa). The glass has an inside diameter very close to that of the test condenser copper tube and is held in place by brass compression fittings installed with Teflon ferrules. This design allows the observation of the flow regime of the refrigerant as described in Section 2.1.

Following the test condenser is the void fraction measurement section. As it was not used for this part of the study, the reader is again referred to Bonhomme (1991) for further details.

Following the void fraction measurement section is the aftercondenser which is a 5 ton (17.6 kW) capacity, water-cooled, counterflow heat exchanger which removes heat from the refrigerant flow and returns it to the subcooled condition desired for the pump and flowmeter.

A bladder accumulator was added to the loop after initial testing had been completed and replaced the receiver used previously. The accumulator serves the purpose of absorbing the increase in refrigerant volume, when vapor is initially produced, while keeping the loop at a constant pressure. The accumulator, from Greer, has a 5 gal. (18.9 l) capacity Buna-N bladder and is pressurized with a regulated nitrogen tank. In line with the connection between the accumulator and the loop is a capillary tube which was installed to dampen any fluid movement between the two. With the installation of the bladder accumulator, the amount of time required to reach steady state was greatly reduced.

3.2. Cooling Water Loop

Figure 3.3 shows a schematic of the cooling water loop used to supply both the test condenser and the aftercondenser with water. The main components of the cooling water loop are the supply pump and tank, the water heaters, the rotameters, and the waste pump and tank. The open tank design was chosen to eliminate from the loop any fluctuations in flow rate and pressure from the water mains in the building.

Water for the test section enters the loop from the city water line and fills the supply tank, the level of which is regulated by an ordinary float valve. The water is then pumped

through a 6 kW capacity water heater and into the two halves of the test section by a 1/2 hp centrifugal supply pump and is regulated by needle valves. Water for the aftercondenser is directly supplied by the city water line. After passing through each of the three components, the water flows through either a high or low range rotameter. For all three components, the capacity of the high-range rotameters is 1-5 gpm (4-19 l/min) and the capacity of the low range rotameters is 0.1-1 gpm (0.4-3.8 l/min). The rotameters were installed only for rough measurements of the water flow rates. A graduated cylinder and a stopwatch are used to obtain accurate measurements used in data processing. The water then flows into the waste tank which is periodically emptied into the city waste line by a 1/3 hp centrifugal waste pump controlled by a float switch.

3.3. Test Condenser

The test condenser used in this study was designed to simulate a single smooth horizontal tube in a condensing heat exchanger with the purpose of measuring heat transfer coefficients and pressure drops in condensing flows. Figure 3.4 shows a schematic of the test condenser including thermocouple and pressure tap placement. The condenser is an annular counterflow heat exchanger with water flowing on the outside and the refrigerant or refrigerant/oil mixture flowing on the inside. The annulus is constructed of 3/4 in. (19 mm) ID PVC tubing and fittings. The inside tube is a 1/4 in. (6.35 mm) OD, 0.18 in. (4.57 mm) ID, hard copper tube with a cooling length of 9 ft.-8 in. (2.95 m). Two PVC mixers, spaced 1/4 in. (6.35 mm) apart are located every 12 in. (0.305 m) along the test condenser to serve the dual purpose of supporting the internal tube in the annulus and mixing the water flow. A set of U-shaped grooves in the copper tube are located after each set of mixers into which single-ended type-T (copper-constantan) thermocouples are mounted to measure the temperature of the tube wall. Dimensions of the grooves are shown in Figure 3.4. At the inlet and outlet positions of the copper tube, four thermocouples are placed, one each on the top, 60 degrees circumferentially downward, 120 degrees downward, and on the bottom. At all other

locations, the thermocouples are placed on the top and bottom only. This arrangement of thermocouples is designed to reveal any circumferential temperature differences in the tube surface which may be indicative of stratified flow.

Pressure measurement taps are located at the inlet and outlet of the test condenser for measuring the absolute pressure and the pressure drop across the test condenser. The pressure taps consist of a brass cube surrounding the copper tube with a 1/16" (1.6 mm) hole drilled through the cube and tube to keep the flow disturbance to a minimum. Specific information about the pressure measuring devices is found in the following section.

3.4. Instrumentation

Measurement devices employed in this investigation include the following: thermocouples, absolute and differential pressure transducers, watt-hour transducers, and flowmeters.

All thermocouples used in this study are type-T (copper-constantan) and were calibrated from 32-76 °F (0-80 °C) using a constant temperature bath. Thermocouples mounted in the refrigerant loop are enclosed in 1/8 in. (3.2 mm) OD stainless steel Omega protection tubes and project a minimum of 4 in. (102 mm) into the refrigerant flow. Temperature measurements in the refrigerant loop are indicated in Figure 3.2 and include the following locations: heater inlet, test section inlet, test section outlet, aftercondenser inlet, and aftercondenser outlet. Thermocouples mounted in the cooling water loop are enclosed in similar tubes of either copper or brass because of the lower pressure conditions and are directly exposed to the flow. Temperature measurements in the cooling water loop are shown in Figures 3.3 and 3.4. Single ended thermocouples are mounted at the inlet and outlet of each half of test condenser and at the inlet and outlet of the aftercondenser. Accuracy of the thermocouples is ±0.18 °F (±0.1 °C).

Absolute pressure measurements are made using 5 Setra 0-1000 psia (0-6900 kPa) pressure transducers and 1 BEC 0-300 psia (0-2070 kPa) pressure transducer. The locations of these measurements are indicated on Figure 3.2 and include the following: heater inlet,

heater outlet, test section inlet, test section outlet, aftercondenser inlet, and aftercondenser outlet. The Setra transducers were calibrated from 15-500 psia (100-3400 kPa) using a dead weight testing device and accuracy of these transducers is ±0.11% of full scale or ±1.1 psia (±7.6 kPa). Output from these transducers is a 0-5 V DC signal. The BEC transducer has an accuracy of ±0.1% of full scale or ±0.3 psia (±2.1 kPa) and an output signal of 2-10 V DC.

A differential pressure measurement is made across the test section as shown in Figure 3.2 using a Sensotec 0-15 psid (0-100 kPa) differential pressure transducer. This transducer was calibrated from 0-7 psid (0-48 kPa) using a mercury manometer and accuracy is ±0.25% of full scale or ±0.04 psid (±0.3 kPa). Output from the differential pressure transducer is a 0-20 mV DC signal.

The amount of heat input to the two refrigerant heater sections is measured using two Ohio Semitronics watt-hour transducers which measure both the voltage and current draw of the heaters and produce a pulse output for each 100 mW of energy input. Accuracy of these transducers is ±0.2% of reading.

The flow rate of refrigerant in the refrigerant loop is measured using either a Max Machinery 0-2 gpm (0-7.6 liters/min) positive displacement flowmeter or a Micro Motion 0-1 lb/min (0-0.45 kg/min) mass flowmeter. Factory calibration of the Max flowmeter was verified using a MicroMotion mass flowmeter and accuracy is ±0.31% of full scale output. Output from the Max flowmeter is a 0-10 VDC signal. The Micro Motion mass flowmeter has and accuracy of 0.1% of reading and an output signal of 2-10 VDC.

3.5. Data Acquisition

Data acquisition for this project is performed using an Apple Mac IIci computer along with data acquisition hardware from National Instruments and Campbell Scientific, and data acquisition software from National Instruments. Figure 3.5 shows a diagram of the data acquisition system. A National Instruments NB-MIO-16L multifunction I/O data acquisition board is installed in a Nubus card slot in a Macintosh IIci computer. The computer board is

connected, using shielded 50 pin cable to a National Instruments CB-50 in an isothermal enclosure to provide a total of 8 analog input channels to the computer. In addition, the serial port of the computer is connected to a Campbell Scientific 21X Datalogger which reads two 24-channel Campbell Scientific AM64 Multiplexers. Data is collected, analyzed, saved, and displayed using National Instruments' LabView 2.2 data acquisition software. This software was chosen because of its speed, flexibility, graphics capabilities, and comparatively low cost to other systems. Although LabView has strong analysis capabilities, most analysis was performed using a separate spreadsheet macro written in Excel 3.0, to be discussed further in Chapter 5.

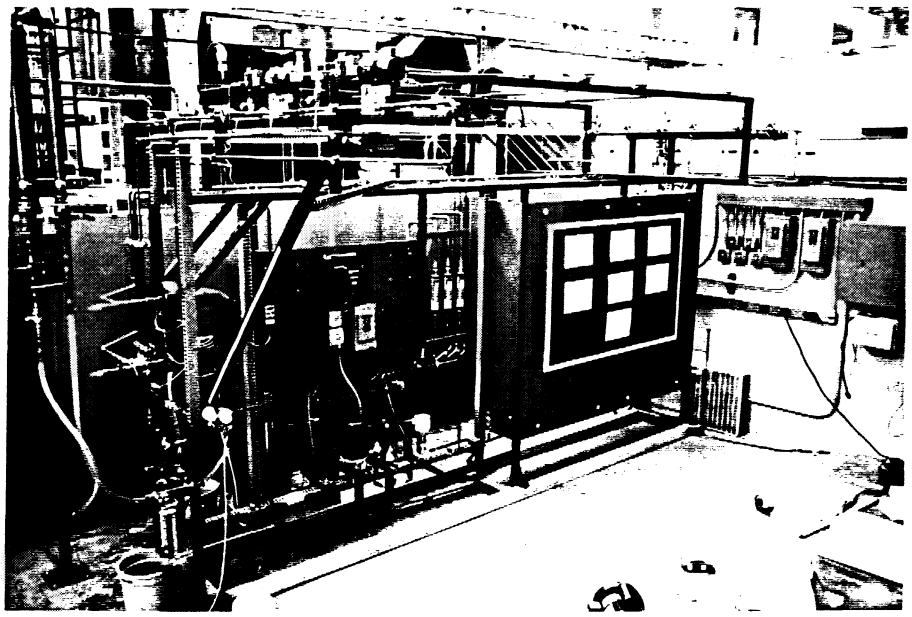

Figure 3.1. Single Tube Condenser Test Facility at the University of Illinois at Urbana-Champaign

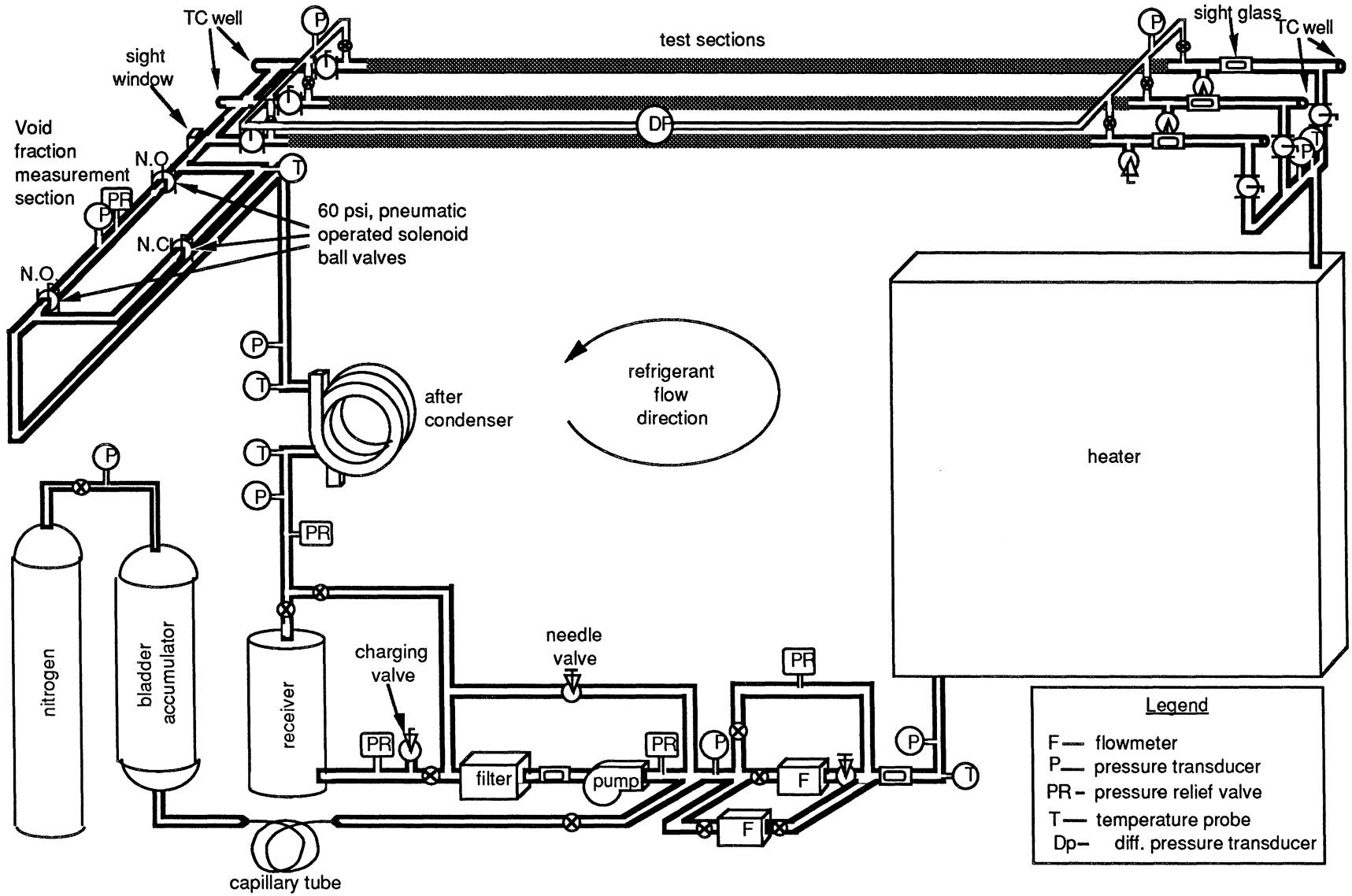

Figure 3.2. Schematic of Refrigerant Loop

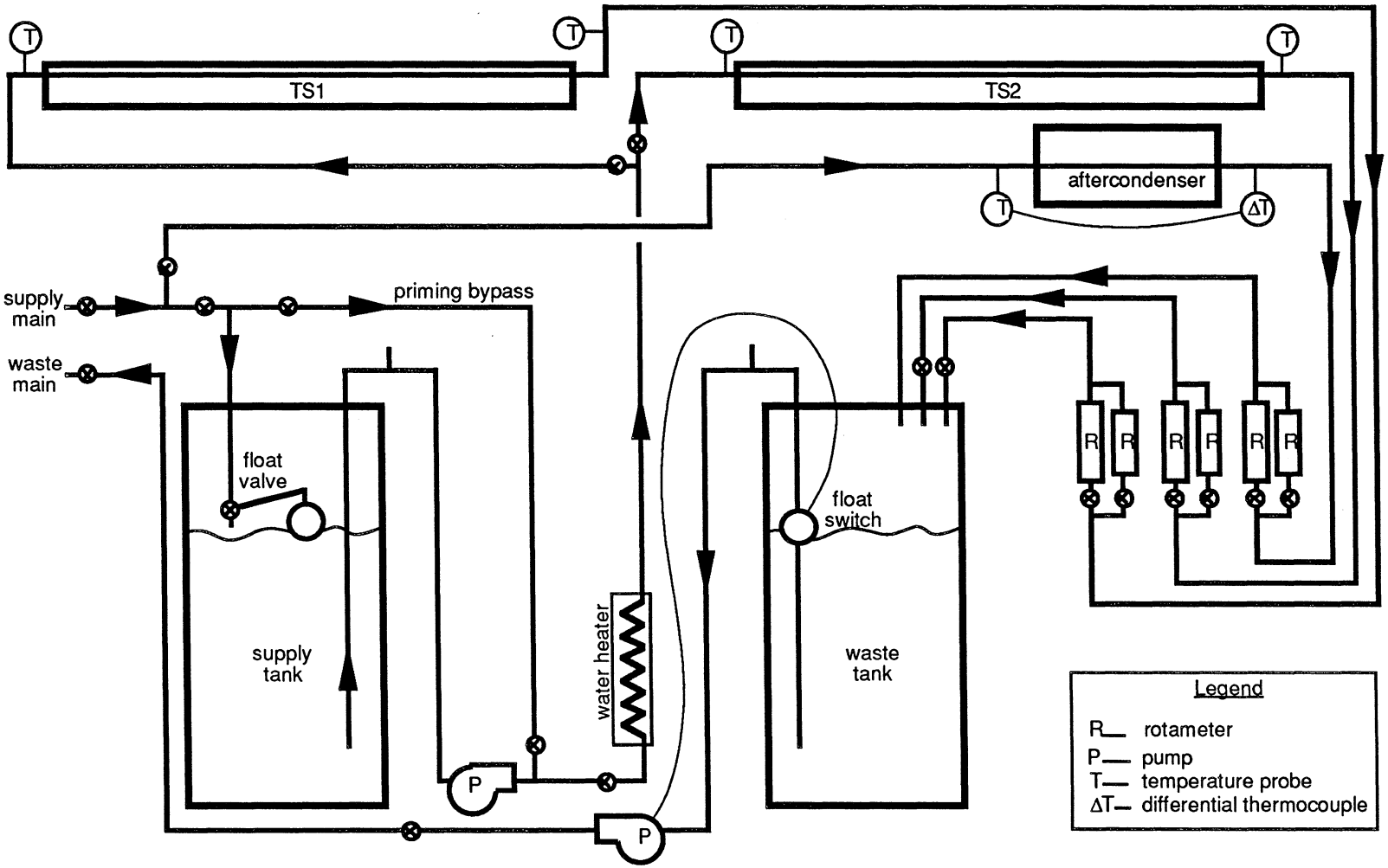

Figure 3.3. Cooling Water Loop

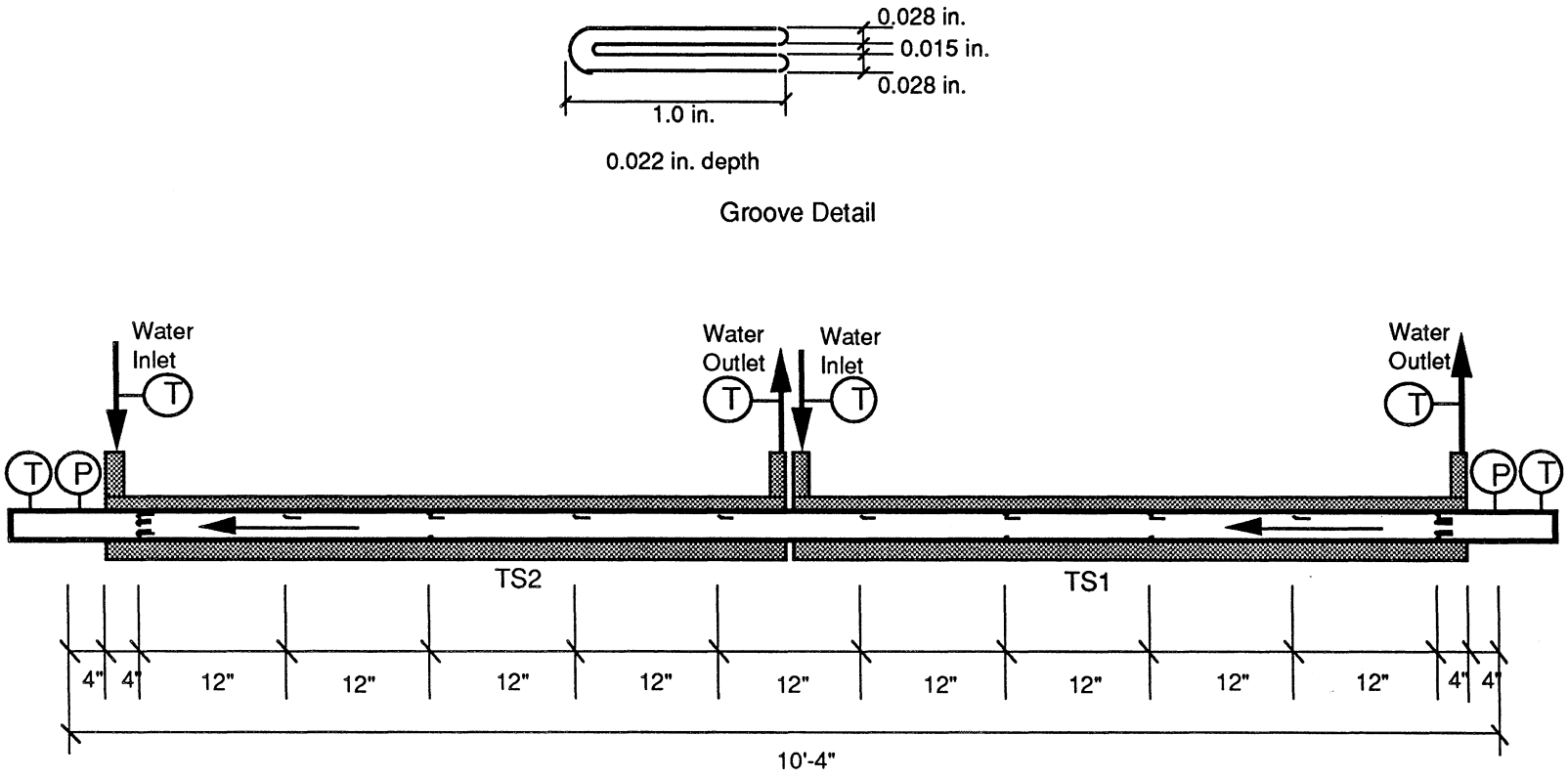

Figure 3.4. Test Condenser Design

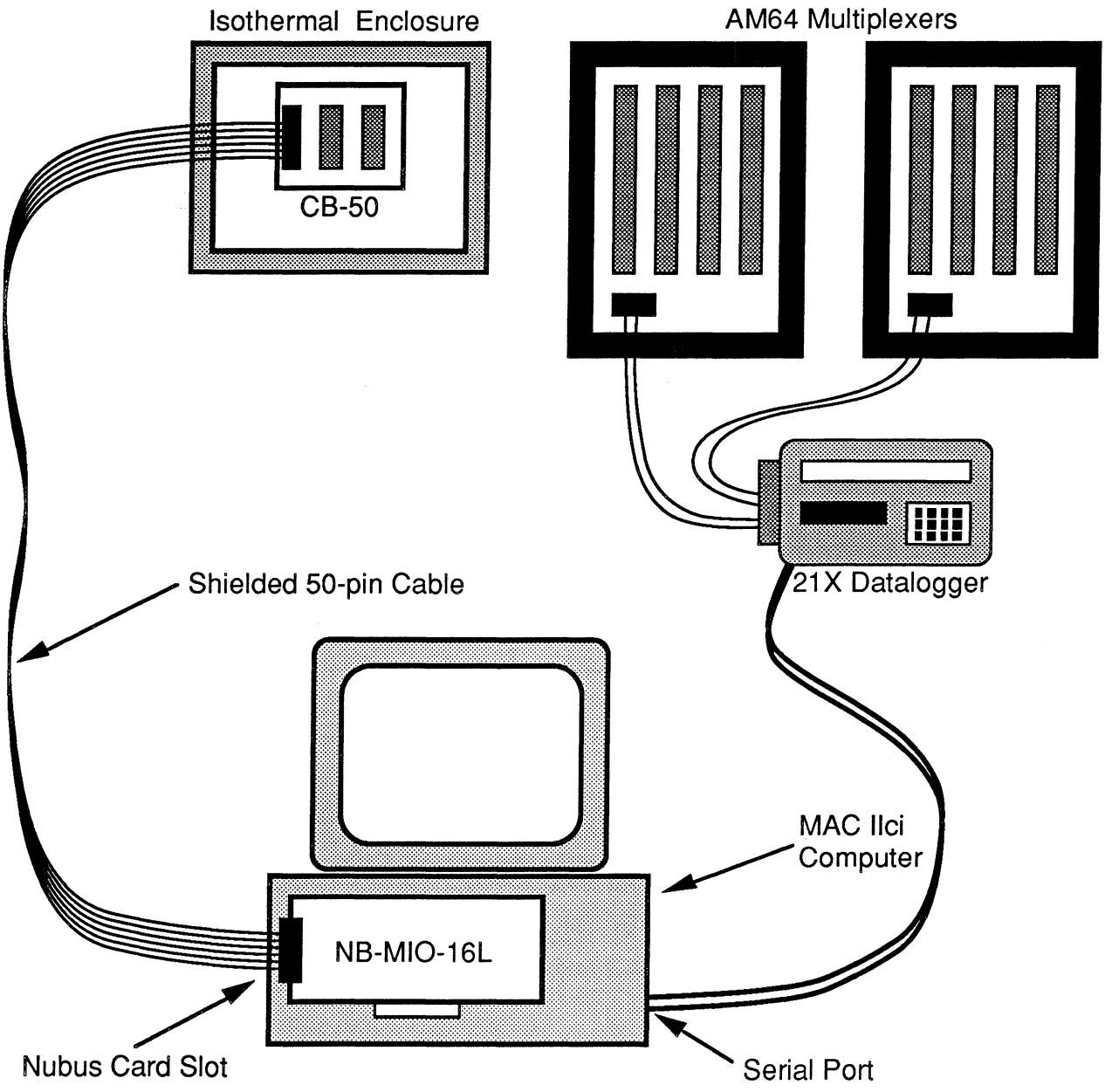

Figure 3.5. Data Acquisition System

CHAPTER 4
EXPERIMENTAL DESIGN

This chapter describes the experiments run for this study. Typical conditions are presented for simulation of domestic refrigerator/freezer simulation and are followed by a discussion of the tests performed. The procedure for measurement of oil concentration is also presented.

4.1. Condenser Conditions for Domestic Refrigerator/Freezers

The test condenser in this study was designed to simulate conditions typically found in domestic refrigerators with the ultimate purpose of prediction of heat transfer coefficients and pressure drop of two-phase, condensing flows. Parameters which may be varied to simulate these conditions are the following: mass flux, saturation temperature, vapor quality, oil type, and oil concentration. Refrigerant flow rates found in typical domestic refrigerators are from 10-40 lbm/hr (4.5-18.2 kg/hr) which corresponds to a mass flux in a 0.180 in. (4.57 mm) ID tube of 55,000-220,000 lbm/ft^{2}hr (75-300 kg/m^{2}s). Temperatures typically found in refrigerators range from 90-140 °F (32-60 °C). Oil concentration of R-12/mineral oil mixtures range from 1-5%.

4.2. Experiments

A number of two-phase experiments were run for both pure R-134a and a mixture of R-134a and oil. Table 4.1 outlines the conditions for these tests. As described in Section 3.3, the test condenser used for these experiments is a 1/4 in. (6.35 mm) OD, 0.180 in. (4.57 mm) ID smooth copper tube cooled by an annulus of water. The oil used for these experiments was obtained from Mobil Research and Development Corporation and is an ISO VG 22 version of a synthetic polyol ester-based refrigeration oil designed for use with R-134a in domestic refrigerator/freezers. Table 4.2 shows typical physical properties of this oil.

The required conditions for each experiment were achieved by adjusting controls on the test facility. These adjustments included the refrigerant flow rate, the power supplied to the refrigerant heaters, the pressure supplied to the bladder accumulator, the cooling water flow rate, and the power supplied to the cooling water heaters. A set of data was taken after the test facility had been brought to the desired conditions and steady state had been achieved. Typical inlet qualities to the test condenser ranged from 25-95% and quality changes occuring in each half of the test condenser ranged from 10% for high mass flux experiments to 35% for low mass flux experiments. Multiple samples of the measurement data on the test facility were taken and saved to a file over an approximately 5 minute time period. Analysis of the data then took place as described in Chapter 5.

Uncertainty in the calculated heat transfer coefficient proved to be a strong function of the temperature difference between the tube wall and the refrigerant. For low flow rate experiments, this temperature difference was smaller and hence, carried a higher error. Using the method of sequential pertubations (see Moffat 1988), the uncertainty for calculated heat transfer coefficients ranged from ±4% for high flow rate tests to ±19% for low flow rate tests.

4.3. Oil Concentration Measurements

Measurement of oil concentration was required for the experiments run with R-134a/oil mixtures. The technique for measuring this is based on ASHRAE Standard 41.4 with the exception that two measurements are made for each concentration, one each preceding and following the experiments run with the concentration under study. A more detailed explanation of this technique is found in Panek (1992).

The measurement procedure begins with the evacuating and weighing of a sampling cylinder which contains both liquid and vapor charging ports. A sample of liquid refrigerant/oil mixture is then let into the cylinder through the liquid charging port and the cylinder is weighed a second time. Oil samples were taken from the refrigerant loop at the entrance of the test condenser. A typical refrigerant/oil mixture sample weight was 1 lbm

(0.45 kg). The refrigerant vapor is slowly bled off through a capillary tube passing first through a filter to catch any oil which may have escaped the cylinder through the vapor port. A vacuum is pulled on the cylinder when the vapor has ceased leaving the capillary tube and is allowed to sit overnight allowing any gasses dissolved in the oil to come out of solution. A final vacuum is then pulled, the cylinder is weighed, and the oil concentration is found from the following expression:

$$\omega = \text{weight fraction} = \frac{(\text{cylinder + oil weight}) - (\text{empty cylinder weight})}{(\text{cylinder + refrigerant/oil mixture weight}) - (\text{empty cylinder weight})}$$

where ω is defined as the fraction of oil by mass in the refrigerant/oil mixture.

Table 4.1. Test Plan for 1/4 in. Test Condenser

Fluid	Temperature [F]	Mass Flux [klbm/ft^2-hr]	Quality
Pure R-134a	95	55	0.1 to 0.9
		110	0.1 to 0.9
		220	0.1 to 0.9
	140	55	0.1 to 0.9
		110	0.1 to 0.9
		220	0.1 to 0.9
R-134a/1.2% Ester Mixture	95	55	0.1 to 0.9
		110	0.1 to 0.9
		220	0.1 to 0.9
R-134a/5% Ester Mixture	95	55	0.1 to 0.9
		110	0.1 to 0.9
		220	0.1 to 0.9
Pure R-12	95	55	0.1 to 0.9
		110	0.1 to 0.9
		220	0.1 to 0.9
	140	55	0.1 to 0.9
		110	0.1 to 0.9

Table 4.2. Physical Properties of Ester Lubricant

Name	XRL 1681-1Z
ISO VG	22
Specific Gravity @ 59 °F	0.995
Flash Point	473 °F
Pour Point	--65 °F
Viscosity: @ 104 °F @ 212 °F	 23.9 cSt 4.87 cSt

CHAPTER 5

DATA REDUCTION TECHNIQUES

This chapter discusses the data reduction procedures used in determining the refrigerant-side convective heat transfer coefficients found in the test condenser. The first section details energy balance calculations required to establish inlet and outlet conditions of the test condenser. This is followed by a description of the method used to determine the local and average heat transfer coefficients on the tube surface.

5.1. Energy Balance Calculations

During operation of the test facility, heat is added to the refrigerant in the heater and removed in the test condenser and the aftercondenser. In addition, some losses to the environment may occur. Calculation of these heat quantities is necessary in determining the inlet and outlet conditions of the refrigerant in the test condenser. In this study, thermodynamic properties for R-134a have been based on curve fits obtained from data by NIST (National Institute of Standards and Technology) and by Wilson and Basu (1988) as indicated in Appendix D.

The refrigerant heater is used to heat the refrigerant from a subcooled inlet state to a desired subcooled, two-phase, or superheated outlet state. The heater inlet enthalpy is found by measuring the temperature and pressure at the heater inlet and using the following equation:

$$h_{\text{heater inlet}} = h_f + v_f\left[P_{\text{heater inlet}} - P_{\text{sat,heater inlet}}\right] \tag{5.1}$$

where h_f, v_f, and $P_{\text{sat, heater inlet}}$ are saturation values calculated at the measured heater inlet temperature. The enthalpy at the heater outlet and hence, the inlet of the first half of the test condenser, TS1, is found from the heat input to the refrigerant heater, the refrigerant flow rate, and the refrigerant temperature and pressure at the inlet and uses the following equation:

$$h_{\text{heater outlet}} = h_{\text{TS1 inlet}} = h_{\text{heater inlet}} + \frac{\dot{Q}_{\text{heater}} - \dot{Q}_{\text{loss}}}{\dot{m}_{\text{refrigerant}}} \tag{5.2}$$

where $\dot{Q}_{loss}$ is the heat loss to the environment which is estimated for typical test conditions using single-phase tests as described in Appendix B. The heat transfer from the two halves of the test condenser is found by measuring the mass flow rate and the temperature increase of the water flowing through each half. The heat balance for each half of the test condenser is described from the following equations:

$$\dot{Q}_{TS1} = \left(\dot{m} c_p \Delta T\right)_{water,TS1} \tag{5.3a}$$

$$\dot{Q}_{TS2} = \left(\dot{m} c_p \Delta T\right)_{water,TS2} \tag{5.3b}$$

where c_p is the specific heat of the water calculated at the average water temperature. The refrigerant enthalpy leaving TS1 and entering TS2 is then found from the following:

$$h_{\text{TS1 outlet}} = h_{\text{TS2 inlet}} = h_{\text{TS1 inlet}} - \frac{\dot{Q}_{TS1}}{\dot{m}_{\text{refrigerant}}} \tag{5.4}$$

Similarly, the refrigerant enthalpy leaving TS2 is found from the following:

$$h_{\text{TS2 outlet}} = h_{\text{TS2 inlet}} - \frac{\dot{Q}_{TS2}}{\dot{m}_{\text{refrigerant}}} \tag{5.5}$$

The calculation of vapor quality of the refrigerant entering and exiting the two halves of the test condenser requires knowledge of the saturation temperature at those points. Since this temperature is difficult to measure directly in two phase flow due to non-equilibrium effects,

the saturation temperature is calculated from the pressure measured at the test condenser inlet and the pressure drop measured across the test condenser. It is assumed that for small quality changes, the pressure drop in the test condenser changes linearly. In this manner then, the saturation temperatures at the inlet and outlet of TS1 and TS2 are the following:

$$T_{sat,\,TS1\ inlet} = T_{sat}(P_{TS\ inlet}) \tag{5.6a}$$

$$T_{sat,\,TS1\ outlet} = T_{sat,\,TS2\ inlet} = T_{sat}\left(P_{TS\ inlet} - \frac{\Delta P_{TS}}{2}\right) \tag{5.6b}$$

$$T_{sat,\,TS2\ outlet} = T_{sat}\left(P_{TS\ inlet} - \Delta P_{TS}\right) \tag{5.6c}$$

Average saturation temperatures are then found for each half of the test condenser and are the following:

$$\overline{T}_{sat,TS1} = \frac{T_{sat,\,TS1\ inlet} + T_{sat,\,TS1\ outlet}}{2} \tag{5.7a}$$

$$\overline{T}_{sat,TS2} = \frac{T_{sat,\,TS2\ inlet} + T_{sat,\,TS2\ outlet}}{2} \tag{5.7b}$$

The equations above are true for both single-phase and two-phase experiments, however, subsequent calculations differ for the two cases. In the case of two-phase flow an average quality is calculated for the refrigerant in the test condenser, while for single-phase flow an average temperature is calculated. The sections below describe these calculations.

5.1.1. Two-Phase Experiments

For two-phase experiments, the vapor qualities are calculated at the inlet and outlet of each half of the test condenser from the following:

$$x_{TS1\ inlet} = \frac{h_{TS1\ inlet} - h_f(T_{sat,\ TS1\ inlet})}{h_{fg}(T_{sat,\ TS1\ inlet})} \tag{5.8a}$$

$$x_{TS1\ outlet} = x_{TS2\ inlet} = \frac{h_{TS1\ outlet} - h_f(T_{sat,\ TS1\ outlet})}{h_{fg}(T_{sat,\ TS1\ outlet})} \tag{5.8b}$$

$$x_{TS2\ outlet} = \frac{h_{TS2\ outlet} - h_f(T_{sat,\ TS2\ outlet})}{h_{fg}(T_{sat,\ TS2\ outlet})} \tag{5.8c}$$

where h_f is the saturated liquid enthalpy and h_{fg} is the enthalpy of vaporization at the appropriate saturation temperature. Average vapor qualities are also calculated for each half of the test condenser and are the following:

$$\bar{x}_{TS1} = \frac{x_{TS1\ inlet} + x_{TS1\ outlet}}{2} \tag{5.9a}$$

$$\bar{x}_{TS2} = \frac{x_{TS2\ inlet} + x_{TS2\ outlet}}{2} \tag{5.9b}$$

The average refrigerant temperatures and average vapor qualities thus found, combined with wall temperatures, allow the convective heat transfer coefficient to be calculated.

5.1.2. Single-Phase Experiments

In this study, single-phase experiments served the dual purpose of verifying single-phase correlations and providing a check on energy balances applied to the refrigerant heater and the test condenser. The latter purpose allows the calculation of heat losses to the environment, which are difficult to calculate analytically. Single-phase temperature measurements, in general, are not greatly affected by non-equilibrium situations. We may then

measure the refrigerant temperatures at the inlet and outlet of the test condenser directly. The enthalpy at the heater outlet is calculated for single-phase liquid tests using:

$$h_{heater,inlet} = h_f(T_{heater,inlet}) + v_f\left[P_{heater,inlet} - P_{sat,heater,inlet}\right] \tag{5.10a}$$

where h_f, v_f, and P_{sat} are evaluated at the heater outlet temperature. The enthalpy at the same location is calculated for single-phase vapor tests using:

$$h_{TS1\ inlet} = h_g + c_{p,\,vap}\left[T_{TS1\ inlet} - T_{sat,\,TS1\ inlet}\right] \tag{5.10b}$$

where h_g and $c_{p,\,vap}$ are evaluated at $T_{sat,\,TS1\ inlet}$,. For heat loss calculations, this enthalpy can be compared to that predicted by Eq. (5.2) with $\dot{Q}_{loss}$=0 such that the loss to the environment in the refrigerant heater is given by:

$$\dot{Q}_{loss,\,heater} = \dot{m}_{refrigerant}\left[h_{Eq.\ (5.2)} - h_{Eq.\ (5.10a,b)}\right] \tag{5.11}$$

Similarly, the refrigerant enthalpy may be calculated for the outlet of the test condenser for subcooled liquid using Eq. (5.10a) and evaluating h_f, v_f, and P_{sat} at the test condenser outlet temperature, or for superheated vapor using Eq. (5.10b) and evaluating h_g and $c_{p,\,vap}$ at the saturation temperature at the test condenser outlet.

Heat transfer coefficient calculations require the average refrigerant temperature for each half of the test condenser and assuming a linear temperature drop through the test condenser, these may be found from the following:

$$\overline{T}_{TS1} = T_{TS1\ inlet} - \frac{1}{4}\left(T_{TS1\ inlet} - T_{TS2\ outlet}\right) \tag{5.12a}$$

$$\overline{T}_{TS2} = T_{TS1\ inlet} - \frac{3}{4}\left(T_{TS1\ inlet} - T_{TS2\ outlet}\right) \tag{5.12b}$$

where $T_{TS1\ inlet}$ and $T_{TS2\ outlet}$ are the measured temperatures at the inlet and outlet of the test condenser.

5.2. Convective Heat Transfer Coefficient Calculations

The refrigerant-side convective heat transfer coefficient is calculated for all tests using the law of cooling which is generally attributed to Newton as follows:

$$q" = h(T_s - T_\infty) \tag{5.13}$$

where q" is the convective heat flux from the surface, h is the convective heat transfer coefficient, and T_s and T_∞ are the surface and fluid temperatures, respectively (e.g. Incropera and DeWitt, 1981). For this investigation, we used the following form:

$$\dot{Q} = hA(\overline{T}_{sat,\ refrigerant} - \overline{T}_{wall}) \tag{5.14}$$

where $\dot{Q}$ is the heat transfer out of the test condenser, A is the inside surface area of the cooling length of the test condenser, $\overline{T}_{sat,\ refrigerant}$ is the average refrigerant saturation temperature as calculated in the previous section, and $\overline{T}_{wall}$ is the average measured wall temperature of the test condenser as defined below.

The calculation of an average wall temperature requires a close look at the geometry of the test condenser. Figure 5.1 shows a dimensioned schematic of the test condenser with an alphabetic designation for each significant axial location. Pressure taps for the absolute and differential pressure transducers are located at points A and P. The cooling length, defined as the portion of the copper test section exposed to cooling water, runs from points B to H in TS1 and points I to O in TS2, 58 in.(1.473 m) for both halves. Temperature measurements of the tube wall and the water annulus in contact with it are located at points C through G for TS1 and

points J through N for TS2. Additional water temperature measurements are located at points B, H, I, and O.

The assumption is made that a given wall temperature measurement accurately reflects the wall temperature for the area surrounding it. We may then say that the temperature measurement at point C reflects the wall temperature for the 10 in. (254 mm) from point B to halfway between points C and D, the temperature measurement at point D represents the wall temperature the 12 in. (305 mm) from halfway between points C and D to halfway between points D and E, and so on. In this manner then, the average wall temperatures for the two halves of the test condenser are described with the following:

$$\overline{T}_{wall,TS1} = \frac{10 \cdot T_{wall,C} + 12 \cdot T_{wall,D} + 12 \cdot T_{wall,E} + 12 \cdot T_{wall,F} + 12 \cdot T_{wall,G}}{58} \tag{5.15a}$$

$$\overline{T}_{wall,TS2} = \frac{12 \cdot T_{wall,J} + 12 \cdot T_{wall,K} + 12 \cdot T_{wall,L} + 12 \cdot T_{wall,M} + 10 \cdot T_{wall,N}}{58} \tag{5.15b}$$

Applying Newton's law of cooling, Eq. (5.11), to both halves of the test condenser, we may calculate the convective heat transfer coefficients with the following:

$$h_{TS1} = \frac{\dot{Q}_{TS1}}{A_{TS1}\left(\overline{T}_{sat,TS1} - \overline{T}_{wall,TS1}\right)} \tag{5.16a}$$

$$h_{TS2} = \frac{\dot{Q}_{TS2}}{A_{TS2}\left(\overline{T}_{sat,TS2} - \overline{T}_{wall,TS2}\right)} \tag{5.16b}$$

where the inside surface area of the cooling lengths of TS1 and TS2 is defined as $A_{inside} = \pi D_{inside} L_{cooling}$. The actual value is 32.80 in^2 (0.02116 m^2) for each half.

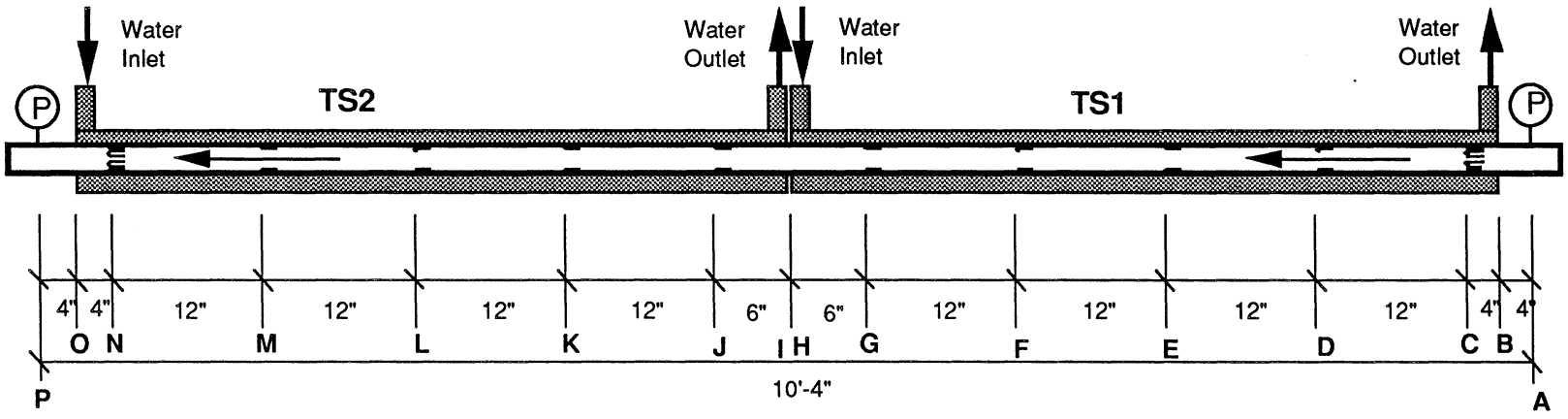

Figure 5.1. Dimensioned Schematic of Test Condenser

CHAPTER 6

EXPERIMENTAL RESULTS

Experimental tests were performed using pure R-134a, pure R-12, and R-134a/oil mixtures as outlined in Table 4.1 and subsequently analyzed as described in Chapter 5. This chapter presents the results of those experiments, compares the results with existing prediction techniques, and discusses how the results may be used to improve prediction techniques. Tabulated data for all two-phase tests are located in Appendix C.

6.1. Results for Pure Refrigerant

Tests using pure R-134a were performed for three mass fluxes and two temperatures giving a total of 65 data points. Figure 6.1 is a graph of heat transfer coefficient versus average quality for those tests. As shown, heat transfer tends to increase with increasing quality.

For these tests, the flow pattern of the refrigerant was observed to have a large effect on the measured heat transfer coefficients. Tests run at a mass flux of 220 klbm/ft^{2}hr were observed to be in an annular flow pattern. Tests at 110 klbm/ft^{2}hr were in a wavy flow pattern at the lowest qualities ($x<0.35$), a wavy-annular flow pattern at intermediate qualities ($0.35<x<0.8$), and an annular flow pattern at the highest qualities ($x>0.8$) for the 95 °F conditions. For the same mass flux at a saturation temperature of 140 °F, the flow regime was wavy below qualities of around 70% and wavy-annular for higher qualities. Finally, tests run at 55 klbm/ft^{2}hr were in a wavy or wavy-stratified flow pattern across the range of quality.

Figure 6.2 shows a graph of heat transfer coefficient versus average vapor quality for all test performed at T_{sat} = 95 °F. The highest coefficients were obtained at a mass flux of 220 klbm/ft^{2}hr and the lowest were obtained at 110 klbm/ft^{2}hr. Figure 6.3 shows a similar graph for T_{sat} = 140 °F. At higher qualities, the trend is identical to the 95 °F graph but at lower qualities, heat transfer coefficients are almost identical for the different mass fluxes.

Figure 6.4 shows a graph of heat transfer coefficient versus average quality for tests run at a mass flux of 220 klbm/ft^{2}hr. Below vapor qualities of 0.6, the coefficients at 95 °F are slightly higher than those at 140 °F. For the annular flow pattern, heat must conduct through the liquid annulus and at 140 °F, the liquid conductivity is 12% lower than the value at 95 °F. The higher vapor shear which occurs at lower temperatures also augments the heat transfer for annular flow conditions. Figures 6.5 and 6.6 show similar graphs for mass fluxes of 110 klbm/ft^{2}hr and 55 klbm/ft^{2}hr, respectively. For these two graphs, coefficients were slightly higher for the 140 °F tests. This is not explainable based upon property values, since stratified flow correlations such as those of Chato (1962) predict higher heat transfer coefficients at 95 °F than at 140 °F. The proposed reason for this phenomenon is that at lower temperatures, the increase in vapor shear resulted in the flow pattern being more wavy-annular than wavy at the same conditions. This would tend to thicken the liquid film on the upper part of the tube and thereby reduce the heat transfer. This tendency was probably offset somewhat by more favorable property values at the lower temperature, resulting in a slight increase in heat transfer coefficient with increasing temperature.

Figure 6.7 shows a graph of heat transfer coefficient versus mass flux for a saturation temperature of 95 °F. The three curves represent data with average qualities of 0.28, 0.49, and 0.70, respectively. This presentation of the data clearly illustrates that at low mass fluxes the heat transfer coefficient is independent of mass flux while it does depend on quality. At higher mass fluxes, the heat transfer coefficient shows the usual dependence on mass flux as predicted by most correlations. The region where heat transfer is independent of mass flux includes the wavy-flow regime and part of the transition from wavy to wavy-annular flow. This is an interesting phenomenon in that the flow-regime must progress well into the wavy-annular region before any positive impact from increasing the mass flux is noticed. This illustrates the positive effects of stratification due to gravity on condensation, since stratified or wavy flows tend to have a much thinner film on the upper part of the tube than annular flows. Superimposed on Figure 6.7 are predictions of the Chen correlation, which was developed for

annular flow conditions. It is seen to predict the heat transfer coefficients reasonably well in the lower mass flux range of the annular region, although it tends to overestimate the effect of mass flux. It should be noted that the some of the data included on Figure 6.7 were run at unusually high mass fluxes to test the limits of annular flow correlations. Up to the highest typical mass flux that we ran, 220 klb_m/ft^2-hr, the Chen correlation predicts heat transfer coefficients well.

. Figures 6.8 and 6.9 show graphs of experimental and predicted heat transfer coefficients versus average vapor quality at a mass flux of 220 $klbm/ft^2hr$ and saturation temperatures of 95 °F and 140 °F, respectively. For both cases, the Chen correlation predicts the coefficients well at lower qualities but deviates from the experimental values at higher qualities. At qualities around 0.7 and 0.6 for the 95 °F and 140 °F tests, respectively, an increase in slope is noticed. This is possibly caused by liquid entrainment in the flow which would have the effect of thinning the liquid annulus and hence, increasing the heat transfer. Since the models do not address the possibility of entrainment occuring, deviation from experimental values is expected. Also, the high quality experiments tend to have lower temperature differences and higher uncertainties so trends from them should be viewed with caution.

Figures 6.10 and 6.11 show graphs of experimental and predicted heat transfer coefficients versus average vapor quality at a mass flux of 110 $klbm/ft^2hr$ and saturation temperatures of 95 °F and 140 °F, respectively. For the 95 °F tests, experimental values are higher than those predicted by the Chen correlation but are closer to the Cavallini, Traviss, and Shah correlations. At this condition, wavy-annular flow was observed except at qualities above 0.85, where annular flow was seen. For the 140 °F tests, experimental values are consistently higher than predicted. At this condition, wavy flow was observed up to qualities of 0.55, above which wavy-annular flow was seen. Since most of the correlations were developed using an annular flow pattern, the deviation is again expected.

Figures 6.12 and 6.13 show graphs of experimental and predicted heat transfer coefficients versus average vapor quality at a mass flux of 55 klbm/ft^{2}hr and saturation temperatures of 95 °F and 140 °F, respectively. The experimental values are substantially higher than predicted, indicating inapplicability of the correlations to the observed wavy or wavy-stratified flow patterns.

Figures 6.14 and 6.15 show experimental heat transfer coefficients plotted against predicted heat transfer coefficients for a mass flux of 220 klbm/ft^{2}hr and saturation temperatures of 95 °F and 140 °F, respectively. Plots of this nature give an indication of which prediction techniques show better agreement with the experiments. For both temperatures, the Chen correlation predicts this annular data better at the lower qualites, however, large deviations occur at higher qualities when entrainment possibly occurs. Overall, the Shah and Traviss correlations do an acceptable job but, as before, show the wrong trends at higher qualities.

Figure 6.16 shows a graph of frictional pressure drop versus average vapor quality for saturation temperatures of 95 °F and 140 °F at a mass flux of 220 klbm/ft^{2}hr. As expected, the lower temperature tests exhibited a significantly higher pressure drop due mainly to higher liquid viscosity combined with increased density ratio and hence, higher vapor velocities. Figure 6.17 shows a similar graph but at a mass flux of 110 klbm/ft^{2}hr. Since pressure drop is a strong function of fluid velocity, the magnitude of these values are considerably lower than those for the higher mass flux test. The same trend with respect to temperature is also observed, though more scatter in the data is present. This is due mainly to the uncertainty of the differential pressure measurements. At lower mass fluxes, the uncertainty begins to approach the same order of magnitude as the values being measured. For this reason, pressure drop measurements for a mass flux of 55 klbm/ft^{2}hr are not reported.

Figures 6.18 and 6.19 show experimental and predicted frictional pressure drop versus average vapor quality for a mass flux of 220 klbm/ft^{2}hr and saturation temperatures of 95 °F and 140 °F, respectively. The predicted values were obtained by the Chisholm correlation and

the Soliman correlation using the two-phase multiplier ϕ_g^2, as described in Section 2.3. For the 95 °F graph, the correlations overpredict the experimental values by 15-25% at lower qualities. However, the Chisholm correlation predicts the experimental values within 10% at qualities greater than 70%. For the 140 °F graph, the correlations overpredict the experimental values by 50-100% but again, the error lessens at the highest qualities.

6.2. Results for Refrigerant/Oil Mixtures

Tests using a mixture of R-134a and Ester lubricant were performed at oil concentrations of 0%, 1.2%, and 5% by weight. Experiments with oil were performed at three mass fluxes, all at a saturation temperature of 95 °F. This gave a total of 27 data points at 1.2% oil concentration and 21 points at 5% oil concentration.

The addition of oil to the pure refrigerant caused an increase in the saturation temperature often known as boiling point elevation or apparent superheat. Both an experimental method and an analytical method were developed to quantify this phenomenon. The details of these methods are provided in Appendix E. While the analytical and experimental methods predicted apparent superheat within 0.18 °F of one another, the experimental method was used to correct the data presented herein. Future test-sections will utilize refrigerant thermocouples which are located directly at the inlet and outlet of each test-section so that such corrections are unnecessary.

Figure 6.20 shows heat transfer coefficient versus average vapor quality for all tests with R-134a and 1.2% Ester at T_{sat}=95 °F. The heat transfer coefficients were essentially equal for mass fluxes of 55 and 110 klbm/ft^{2}hr, while they increased as the mass flux was raised to 220 klbm/ft^{2}hr. Figure 6.21 shows heat transfer coefficient versus average vapor quality for all tests with R-134a and 5% Ester at T_{sat}=95 °F. Again, the heat transfer coefficients were unaffected by the increase in mass flux from 55 to 110 klbm/ft^{2}hr, while they did increase as the mass flux was increased to 110 klbm/ft^{2}hr. For both oil concentrations, the

flow regime was predominantly wavy at 55 and 110 klbm/ft^{2}hr, while at 220 klbm/ft^{2}hr the flow regime was wavy below qualities of around 15% and wavy-annular or annular at higher qualities. The fact that the heat transfer coefficient is independent of mass flux in the wavy-flow or stratified-flow regimes is predicted by correlations such as those of Chato (1962).

Figures 6.22 shows heat transfer coefficent versus average vapor quality for pure and refrigerant/oil mixture tests at T_{sat}=95 °F and a mass flux of 220 klbm/ft^{2}hr. The flow-regime was predominantly annular at this mass flux. An increase in heat transfer was observed across the range of quality with the addition of 1.2% Ester oil, with the magnitude being about 15% at 50% quality. At 5% oil concentration at the same mass flux, the heat transfer coefficients were unaffected at low qualities and degraded at higher qualities. The degradation was approximately 20% at 70% quality, although an average across the quality range would be significantly less than this.

Figure 6.23 and Figure 6.23a show heat transfer coefficient and heat transfer coefficient times wall to refrigerant temperature difference raised to the 0.25 power, respectively, versus vapor quality for refrigerant/oil mixtures at T_{sat}=95 °F and a mass flux of 110 klbm/ft^{2}hr. At this mass flux, the flow-regime was wavy at qualities below approximately 60%, and wavy-annular or purely annular at higher qualities. For the wavy-flow regime, the heat-transfer coefficient is proportional to $1/\Delta T^{0.25}$, so Figure 6.22a presents the heat transfer coefficient multiplied by $\Delta T^{0.25}$ to account for varying temperature differences between tests. This presentation reduces the scatter of the data in the stratified and wavy-stratified regimes. In the wavy-annular regime, the importance of the temperature difference is not clear, while it is presumed to be unimportant for purely annular flow. For this reason, Figure 6.23 does not account for varying temperature differences and should be used for comparing tests at high qualities. With these complexities in mind, the two figures show that the heat transfer coefficient at this mass flux was relatively insensitive to the oil concentration. At very low qualities, it appeared that the heat transfer coefficient increased slightly with oil concentration based on Figure 6.23a. At the highest qualities, seen in Figure 6.23, the addition

of 1.2% oil increased the heat transfer coefficient slightly over pure refrigerant, while the addition of 5% oil degraded the heat transfer coefficient. At qualities around 50%, the heat transfer coefficients were approximately equal for all concentrations.

Figure 6.24 presents heat transfer coefficient times $\Delta T^{0.25}$ for refrigerant/oil mixtures at T_{sat}=95 °F and a mass flux of 55 klbm/ft^{2}hr. The flow-regime for these tests was wavy across the range of quality, so the quarter power correction should be applicable for all the tests. At qualities less than 30%, the heat transfer coefficients seemed to be insensitive to oil concentration. Past this point, the heat transfer coefficients decreased with increasing quality and increasing oil concentration.

While the trends regarding the effect of oil on heat transfer seem difficult to discern, several general statements can be drawn. First, the effect of oil on the heat transfer coefficient at concentrations of 5% or less seem to be rather small. Second, the addition of larger amounts of oil seems to make the variation of heat transfer coefficient with quality less pronounced. Third, in the annular flow regime the addition of 1.2% oil seemed to increase the heat transfer coefficient while the addition of 5% oil decreased the heat transfer coefficient. This is consistent with findings regarding the effect of oil on purely convective evaporation, where heat transfer is initially improved by the addition of oil then decreased at higher concentrations [Chato (1992)]. The physical reasoning behind this phenomenon is that lubricants typically have higher conductivities than liquid refrigerant by 46 to 100%, and higher viscosities than liquid refrigerant by around two orders of magnitude [Baustian et al. (1986)]. The higher conductivity is helpful, while the higher viscosity degrades the heat transfer by thickening the film . These properties could also explain a modest increase in heat transfer with the addition of oil in the wavy-flow or stratified-flow regimes. Here, the heat transfer coefficient is proportional to $k_l^{0.75}/\mu_l^{0.25}$ so that the increase in conductivity might overcome the increase in viscosity. Clearly, the results might depend significantly on the oil properties, which we were unable to obtain. This might explain discrepancies between different researchers.

Figure 6.25 shows a graph of pressure drop versus average vapor quality for both pure R-134a and R-134a/Ester mixtures for a mass flux of 220 klbm/ft^{2}hr. As shown, the addition of oil increased the pressure drop significantly at higher qualities, with a small effect at low qualities. This is reasonable since the oil concentration in the liquid phase becomes higher as quality increases. The 1.2% oil mixture increased the pressure drop up to 20% over the pure refrigerant, with an average increase over the quality range of approximately 10%. The 5% oil mixture increased the pressure drop up to 33% over the pure refrigerant in the quality range we tested. If one extrapolates the curves over the full quality range, the average increase for the 5% oil mixture appears to be around 25%. These findings are consistent with other results from the literature. Figure 6.26 shows a similar graph for a mass flux of 110 klbm/ft^{2}s. Here, however, pressure drop for the 1.2% oil experiments appears to be consistently lower than that of the pure tests. The 5% oil experiments had higher pressure drops than those from the pure tests. The discrepancy in the 1.2% oil experiments is likely due to experimental error as described above.

6.3 Comparisons with Data for R-12

A reduced matrix consisting of only pure refrigerant tests was run with R-12 to allow comparisons between R-134a and its replacement fluid. At a saturation temperature of 95 ^{o}F, testing was performed at mass fluxes of 55, 110, and 220 klbm/ft^{2}hr. At a saturation temperature of 140 ^{o}F, tests were run at mass fluxes of 55 and 110 klbm/ft^{2}hr.

Figure 6.27 compares the heat transfer coefficients of R-12 and R-134a at a mass flux of 220 klbm/ft^{2}hr and a saturation temperature of 95 ^{o}F. The heat transfer coefficients for the R-134a experiments were 14% to 20% higher than those of the R-12 experiments across the range of quality. This is consistent or slightly lower than the findings of other researchers who report 20 to 30% increases in condensation heat transfer coefficients for R-134a. These data were primarily in the annular flow regime for both refrigerants.

Figures 6.28 and 6.29 show heat transfer coefficient times $\Delta T^{0.25}$ versus average vapor quality for R-12 and R-134a at a saturation temperature of 95 °F and mass fluxes of 110 and 55 klbm/ft^{2}hr, respectively. The data were primarily in the wavy-flow regime, so the quarter power dependence was used to correct for variations in temperature difference between the experiments. The heat transfer coefficients for the R-134a experiments were 10 to 15% higher than those of R-12 for both mass fluxes. The Chato (1962) correlation, which is applicable for stratified flows, predicts around a 10% increase in heat transfer coefficient for R-134a, due primarily to higher heat of vaporization and higher liquid conductivity.

Figure 6.30 presents heat transfer coefficient times $\Delta T^{0.25}$ versus average vapor quality for R-12 and R-134a at a saturation temperature of 140 °F and a mass flux of 110 klbm/ft^{2}hr. Again, the heat transfer coefficients for R-134a were approximately 10% higher than those of R-12. The data were primarily concentrated in the wavy-flow regime for both fluids at this mass flux and temperature.

Figure 6.31, 6.32, and 6.33 compare the pressure drop for R-12 and R-134a. Figures 6.31 and 6.32 are both for a saturation temperature of 95 °F and mass fluxes of 220 and 110 klbm/ft^{2}hr, respectively. Figure 6.33 is for a mass flux of 110 klbm/ft^{2}hr and a saturation temperature of 140 °F. The data presented in Figure 6.31 had the highest pressure drops and hence the lowest percentage uncertainties, and showed that the pressure drop for R-12 and R-134a was essentially identical. Figures 6.32 and 6.33 were both for a lower mass flux, and thus had lower pressure drops and higher percentage uncertainties. The results of these two sets of data are contradictory, with R-12 having the higher pressure drop at low temperature and R-134a having the higher pressure drop at the higher temperature. Pressure drop correlations predict little difference between the two refrigerants at these temperatures, which seems to be consistent with our data when the uncertainties are considered.

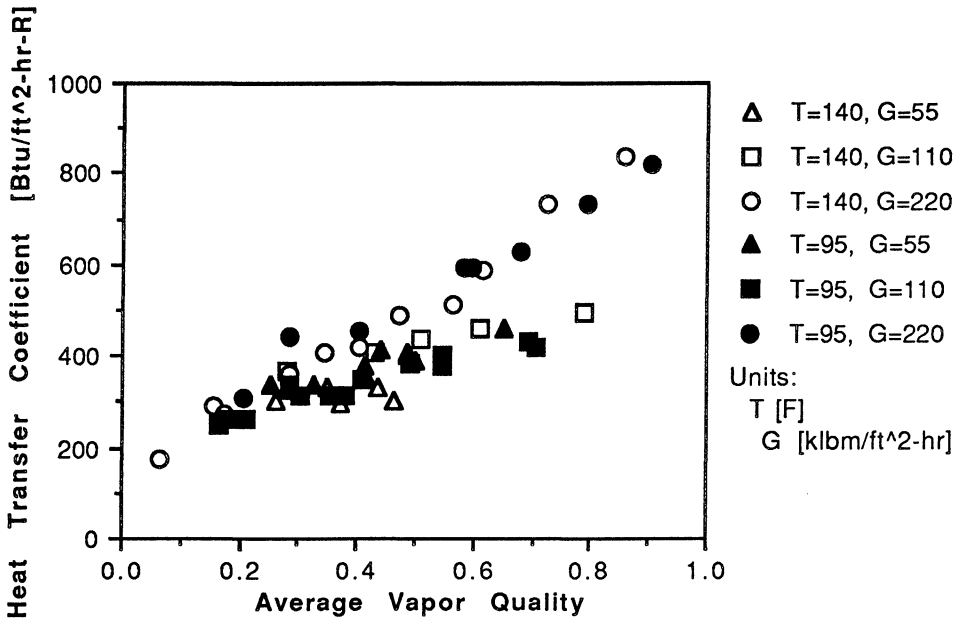

Figure 6.1. Heat Transfer Coefficient versus Average Vapor Quality for Pure R-134a

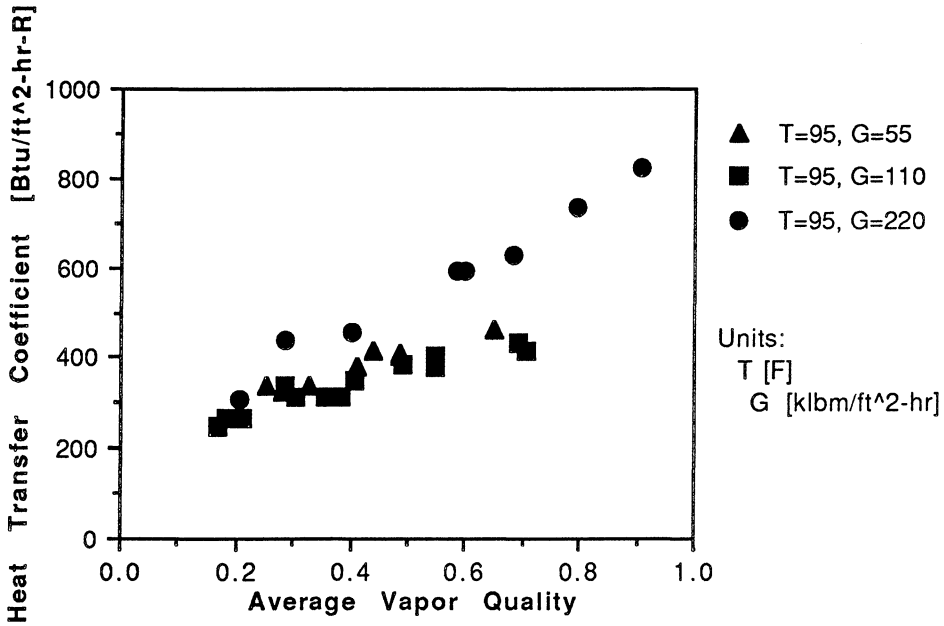

Figure 6.2. Heat Transfer Coefficient versus Average Vapor Quality for T_{sat}=95 °F

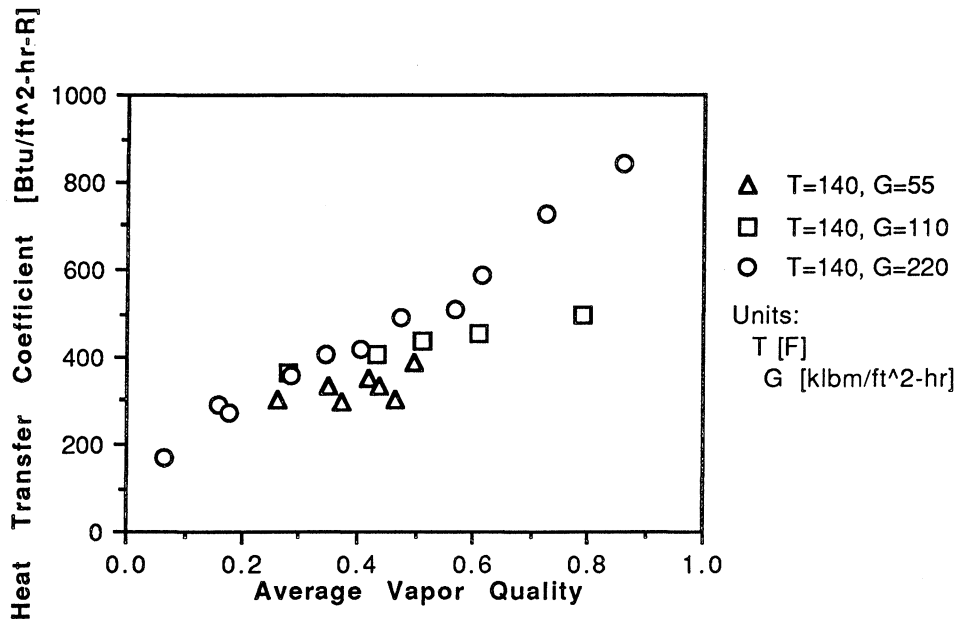

Figure 6.3. Heat Transfer Coefficient versus Average Vapor Quality for T_{sat}=140 °F

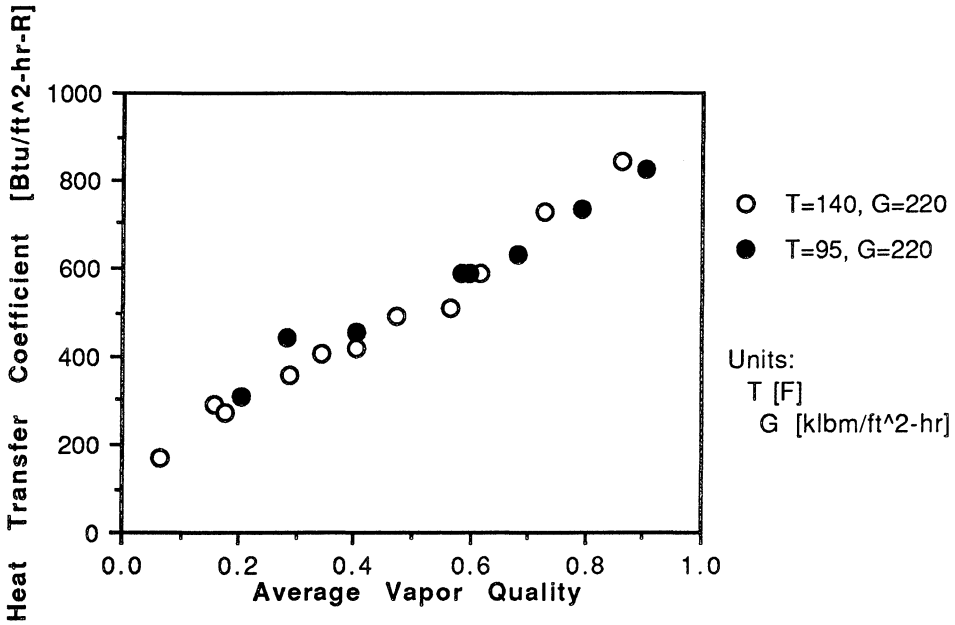

Figure 6.4. Heat Transfer Coefficient versus Average Vapor Quality for G=220 klbm/ft^{2}hr

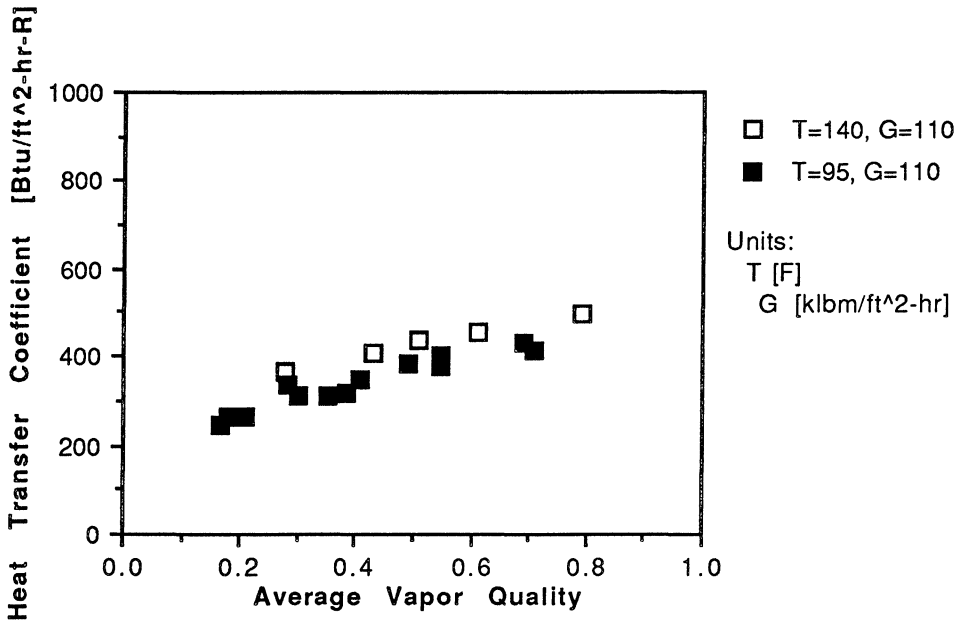

Figure 6.5. Heat Transfer Coefficient versus Average Vapor Quality for G=110 klbm/ft^{2}hr

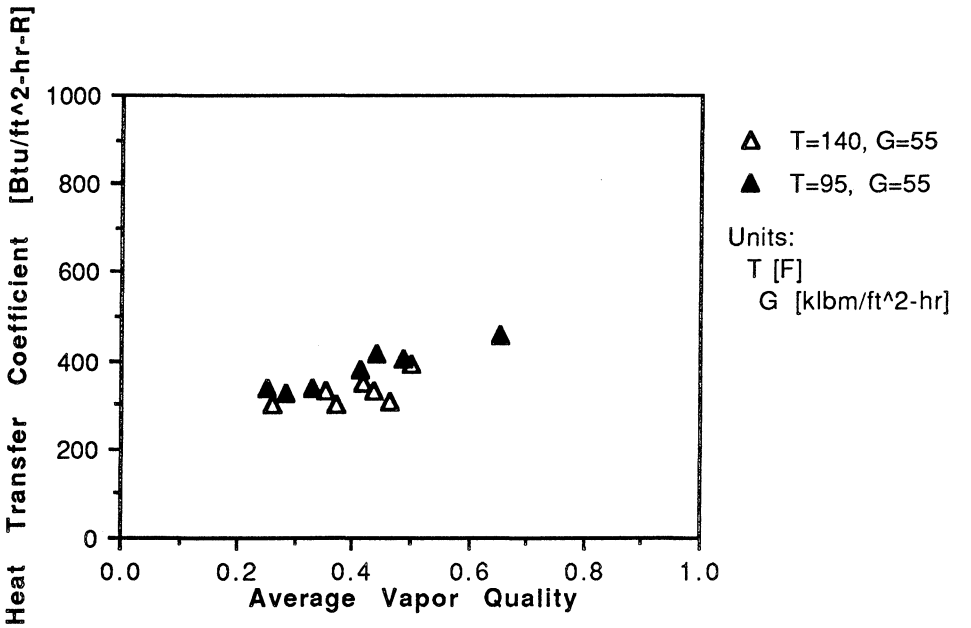

Figure 6.6. Heat Transfer Coefficient versus Average Vapor Quality for G=55 klbm/ft^{2}hr

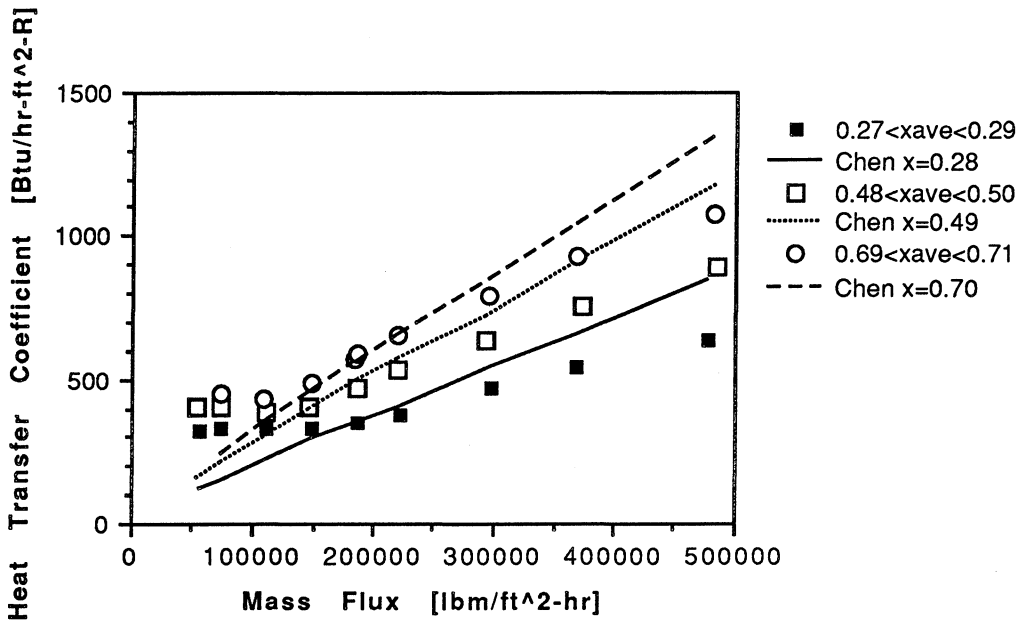

Figure 6.7 - Heat Transfer Coefficient versus Mass Flux at T_{sat}=95 °F

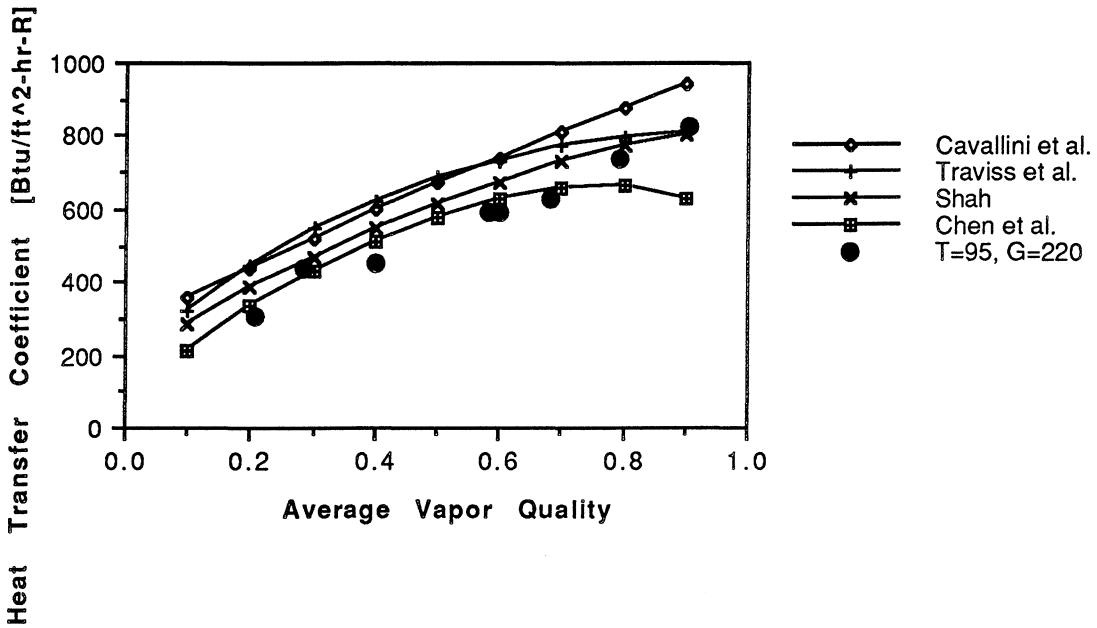

Figure 6.8. Experimental and Predicted Heat Transfer Coefficients versus Quality for G=220 klbm/ft^{2}hr, Tsat=95 °F

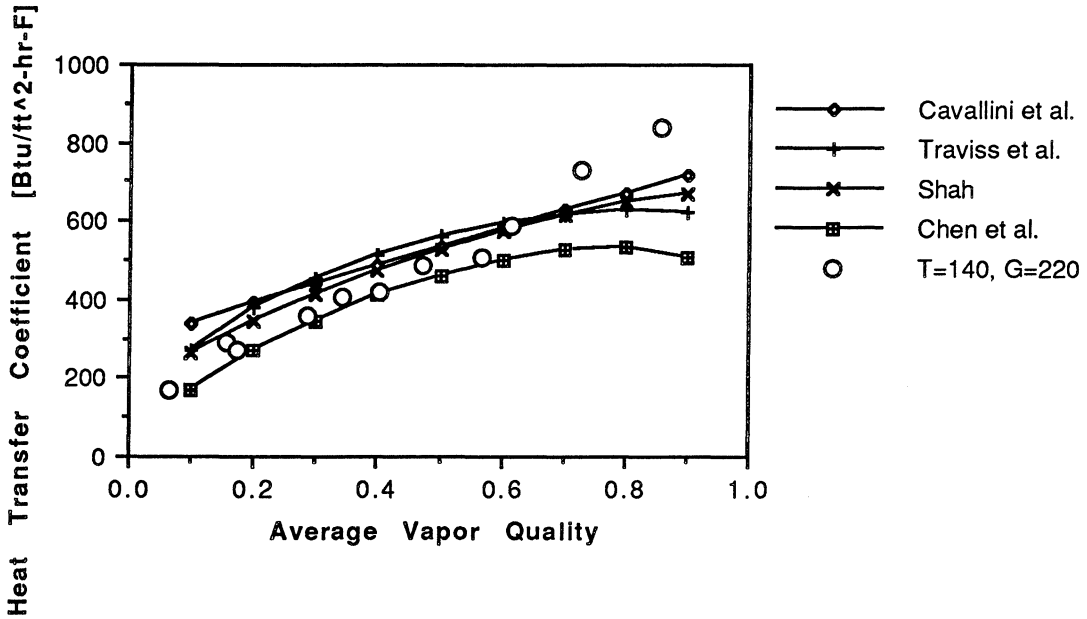

Figure 6.9. Experimental and Predicted Heat Transfer Coefficients versus Quality for G=220 klbm/ft^{2}hr, Tsat=140 °F

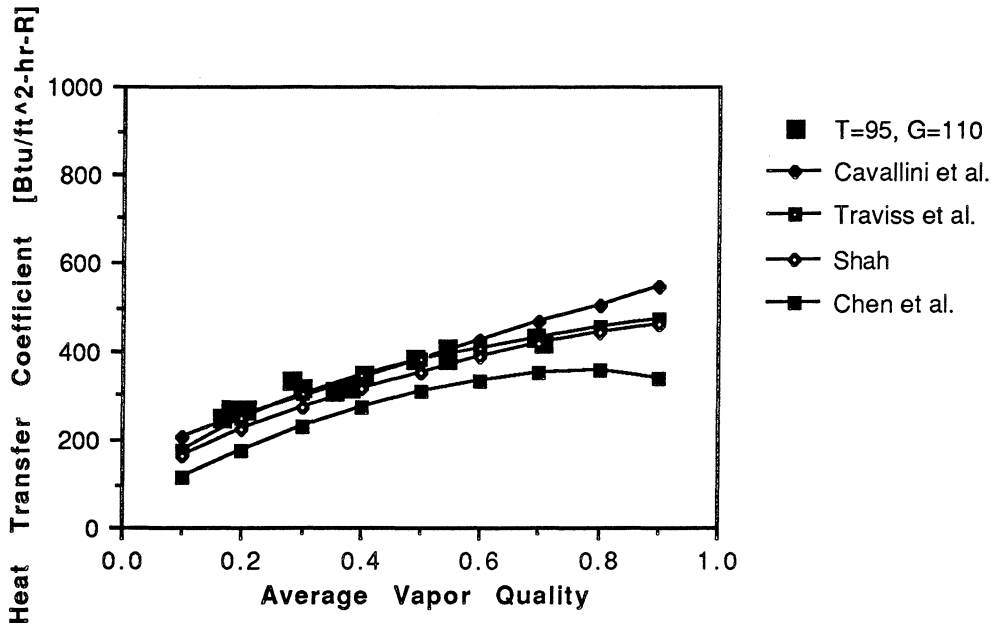

Figure 6.10. Experimental and Predicted Heat Transfer Coefficients versus Quality for G=110 klbm/ft^{2}hr, Tsat=95 °F

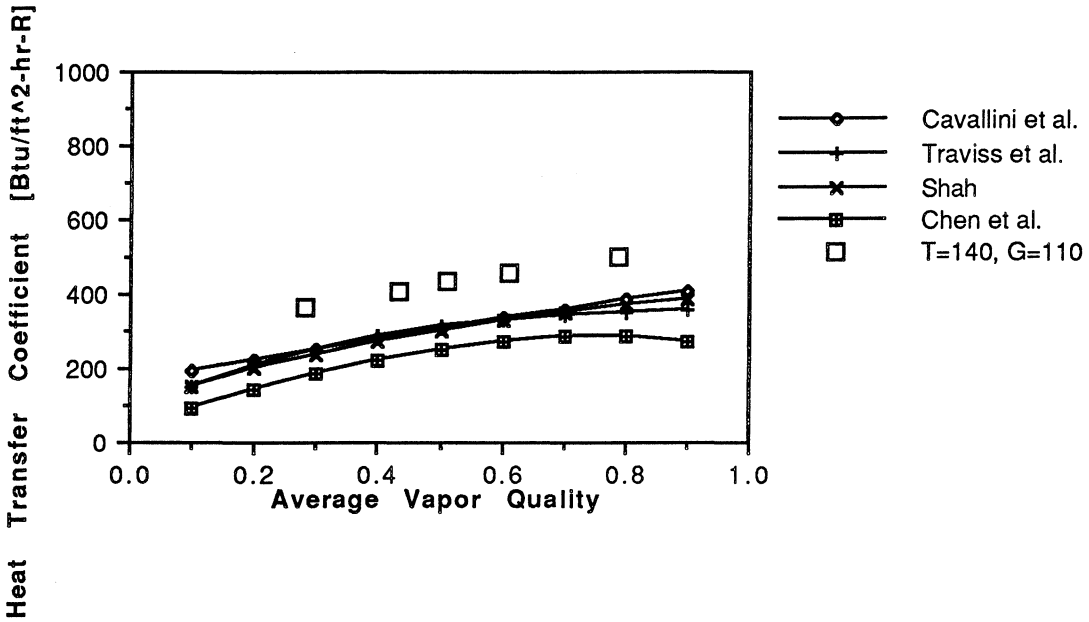

Figure 6.11. Experimental and Predicted Heat Transfer Coefficients versus Quality for G=110 klbm/ft^{2}hr, Tsat=140 °F

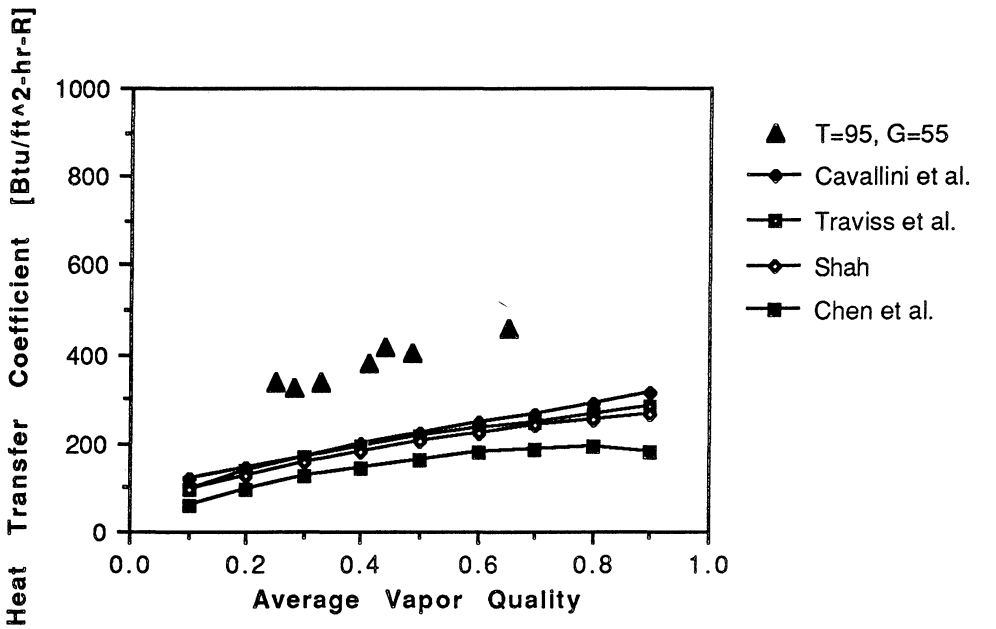

Figure 6.12. Experimental and Predicted Heat Transfer Coefficients versus Quality for G=55 klbm/ft^{2}hr, Tsat=95 °F

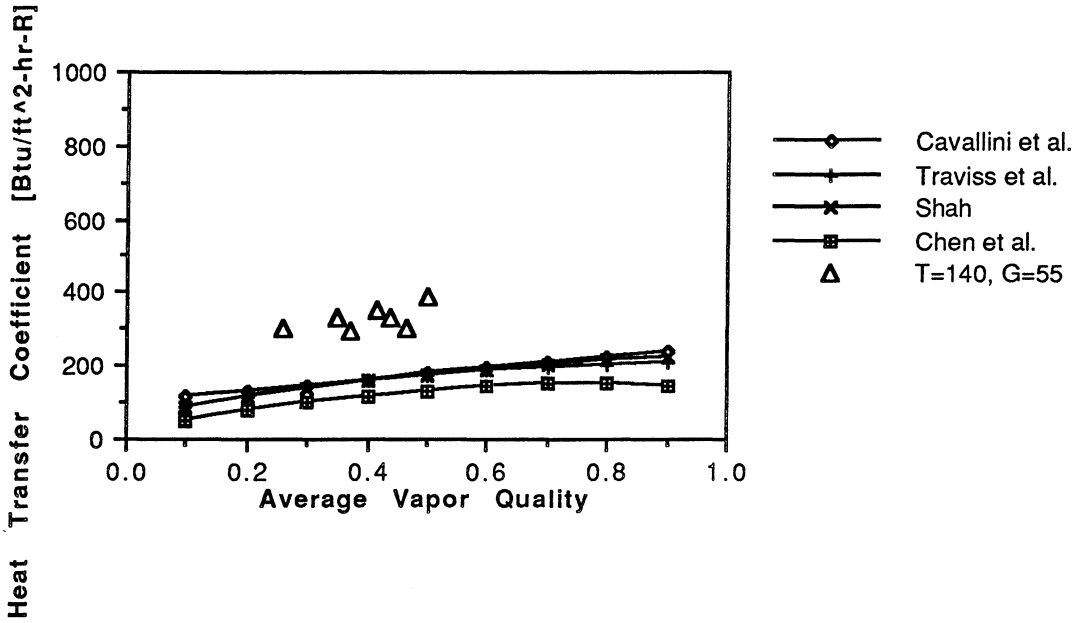

Figure 6.13. Experimental and Predicted Heat Transfer Coefficients versus Quality for G=55 klbm/ft^{2}hr, Tsat=140 °F

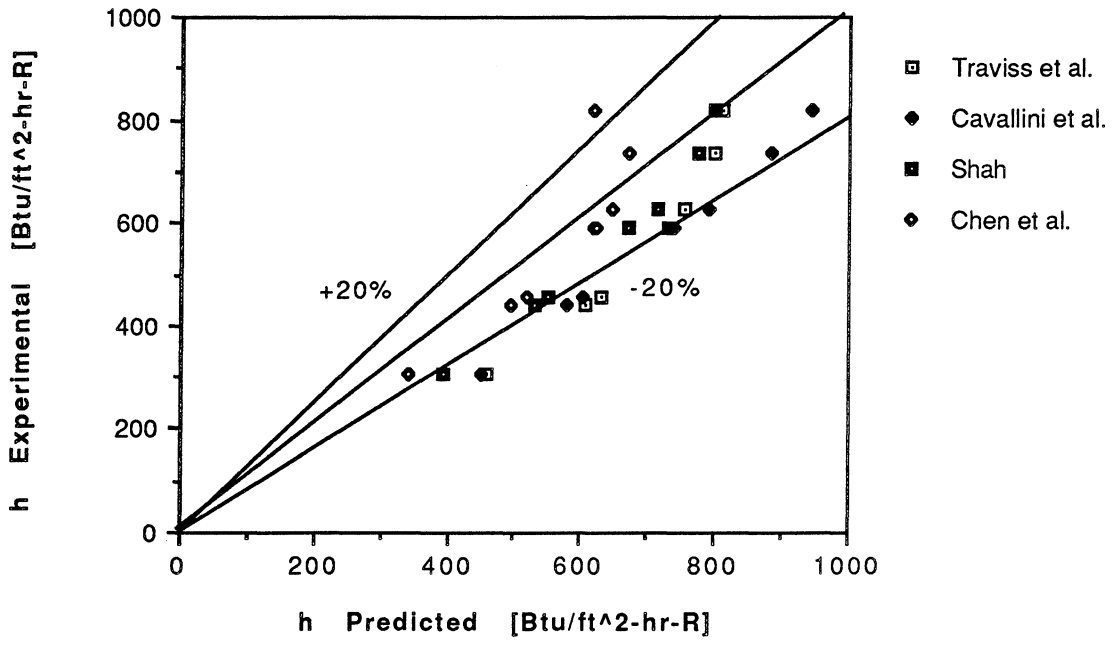

Figure 6.14. Experimental versus Predicted Heat Transfer Coefficient for G=220 klbm/ft^{2}hr, Tsat=95 °F

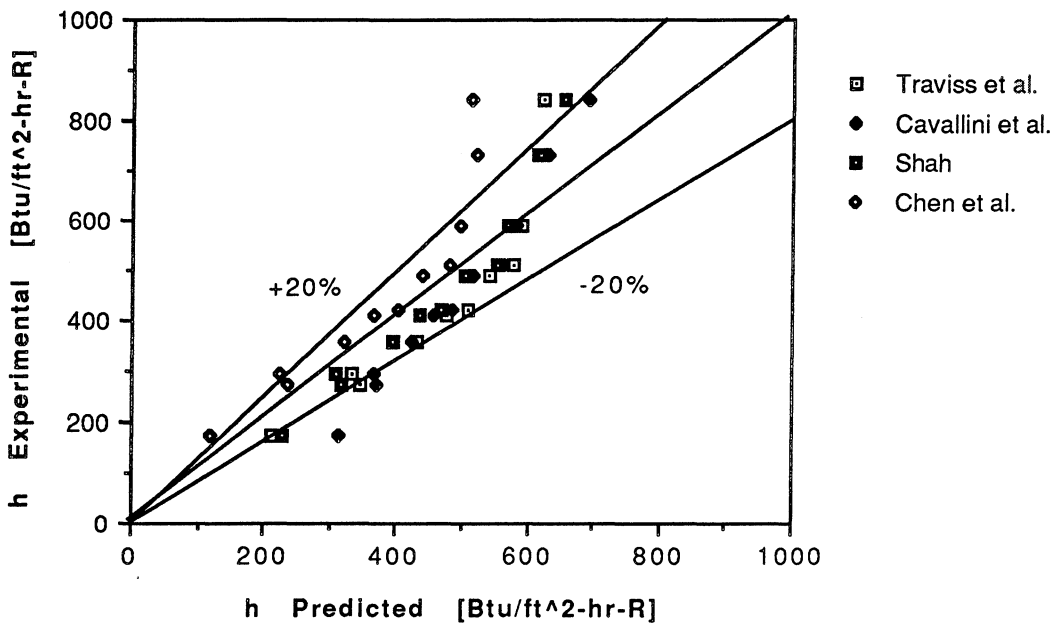

Figure 6.15. Experimental versus Predicted Heat Transfer Coefficient for G=220 klbm/ft^{2}hr, Tsat=140 °F

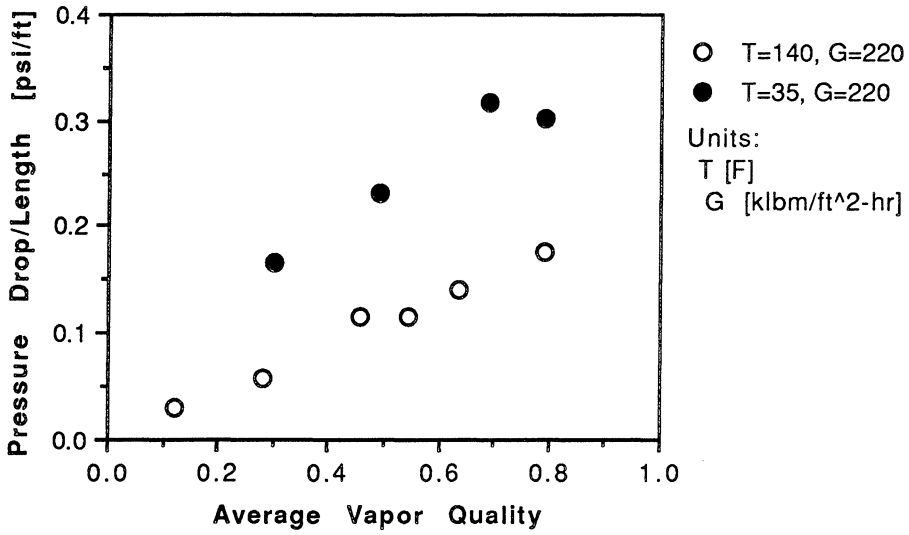

Figure 6.16. Pressure Drop versus Average Vapor Quality for G=220 klbm/ft^{2}hr

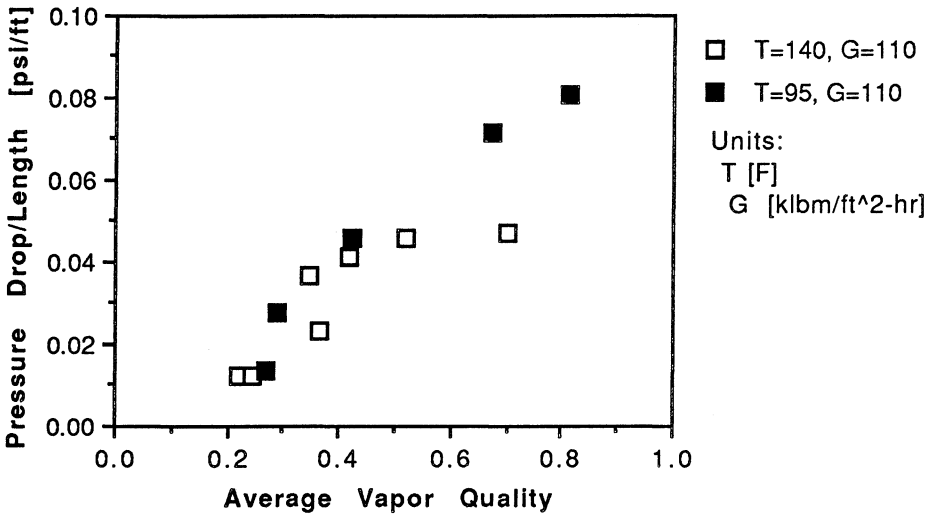

Figure 6.17. Pressure Drop versus Average Vapor Quality for G=110 klbm/ft^{2}hr

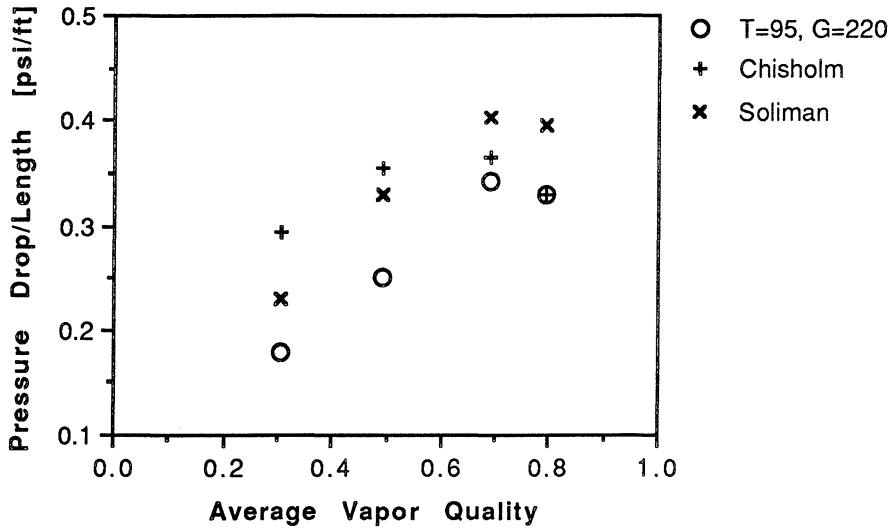

Figure 6.18. Experimental and Predicted Frictional Pressure Drops versus Average Vapor Quality for T_{sat}=95 °F, G=220 klbm/ft^{2}hr

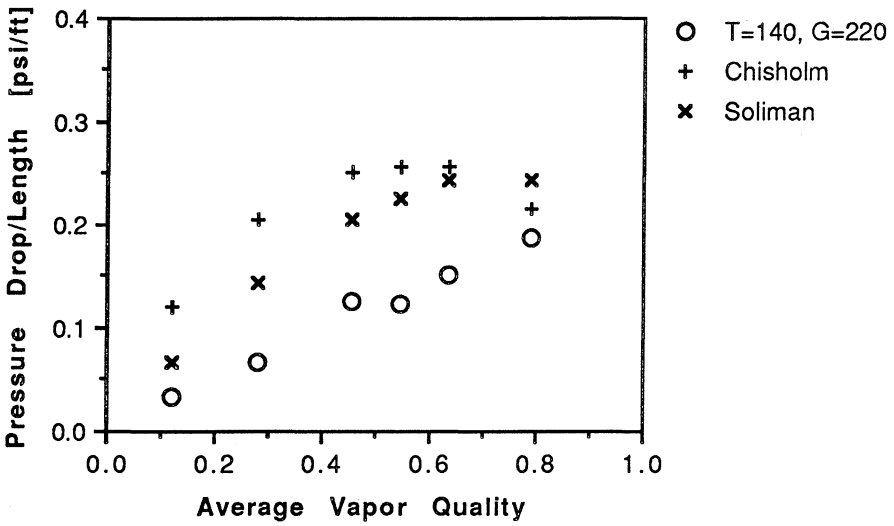

Figure 6.19. Experimental and Predicted Frictional Pressure Drops versus Average Vapor Quality for T_{sat}=140 °F, G=220 klbm/ft^{2}hr

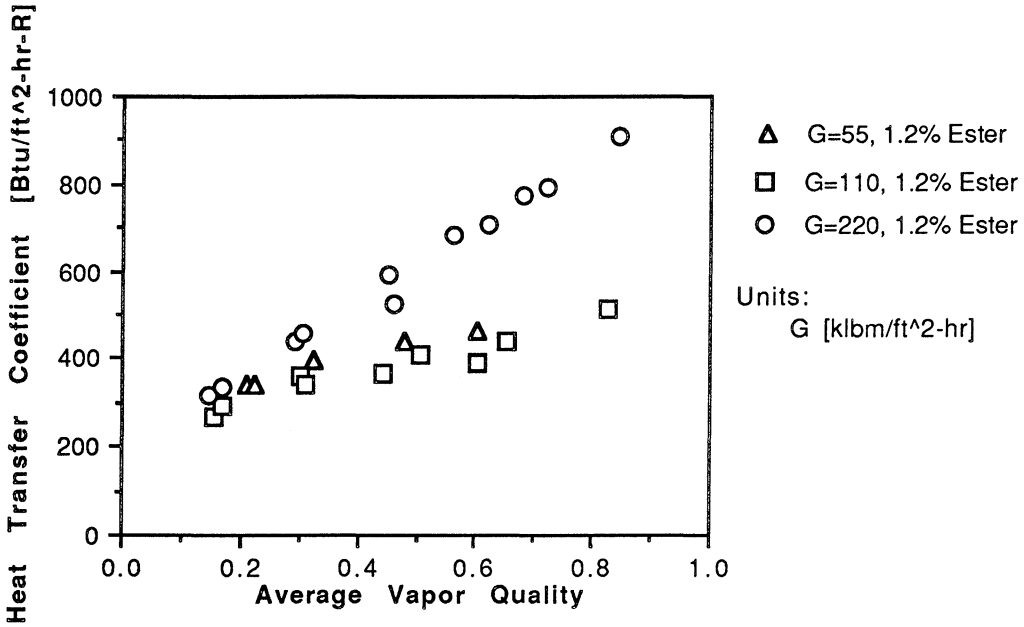

Figure 6.20. Heat Transfer Coefficient versus Average Vapor Quality for All R-134a/1.2% Ester Mixture Tests at T_{sat}=95 °F

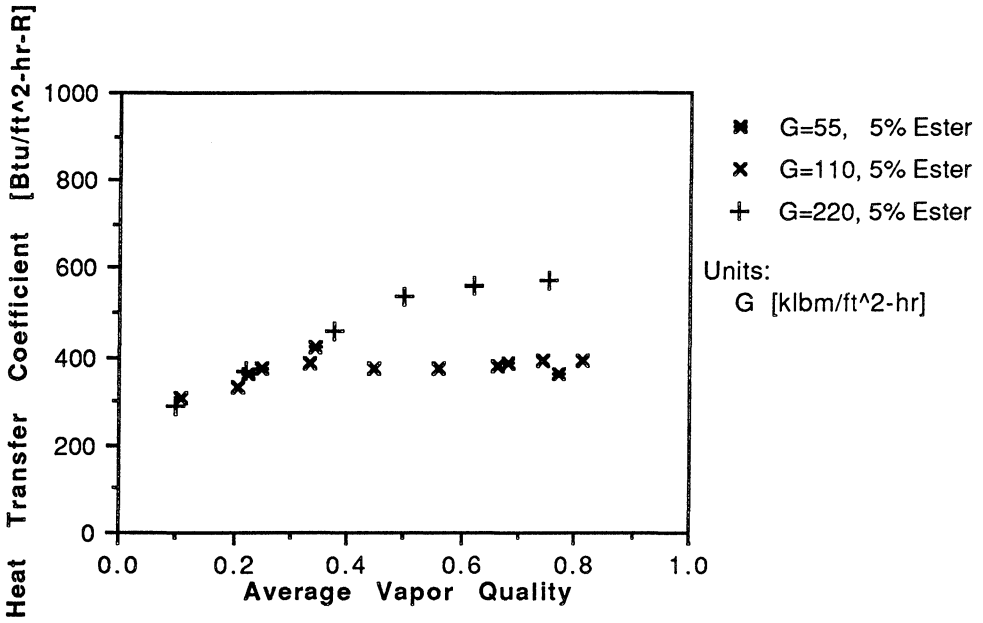

Figure 6.21. Heat Transfer Coefficient versus Average Vapor Quality for All R-134a/5% Ester Mixture Tests at T_{sat}=95 °F

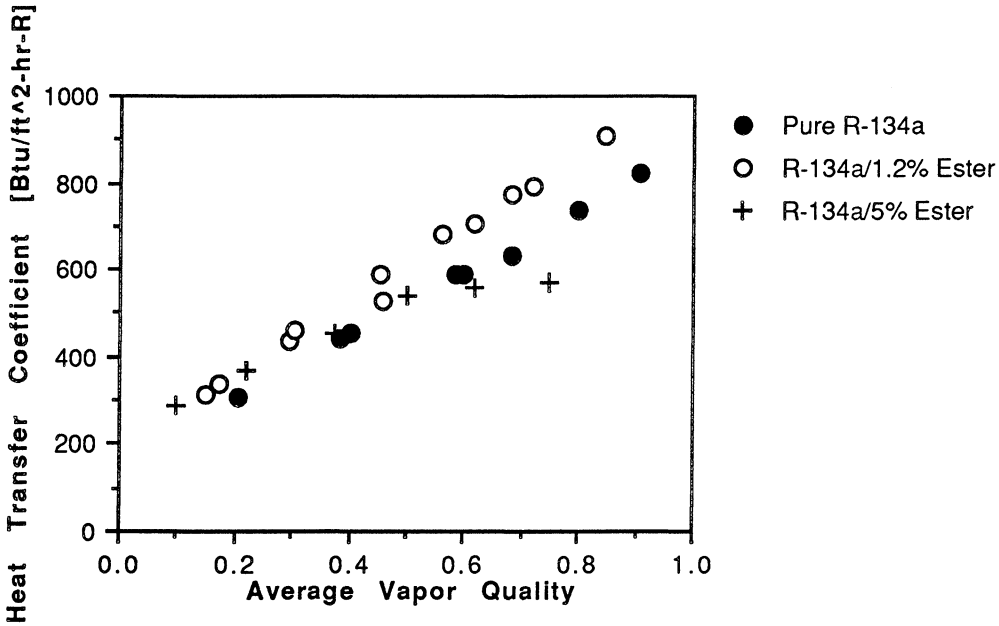

Figure 6.22. Heat Transfer Coefficient versus Average Vapor Quality for Pure and Oil Mixture Tests for G=220 klbm/ft^{2}hr, T_{sat}=95 °F

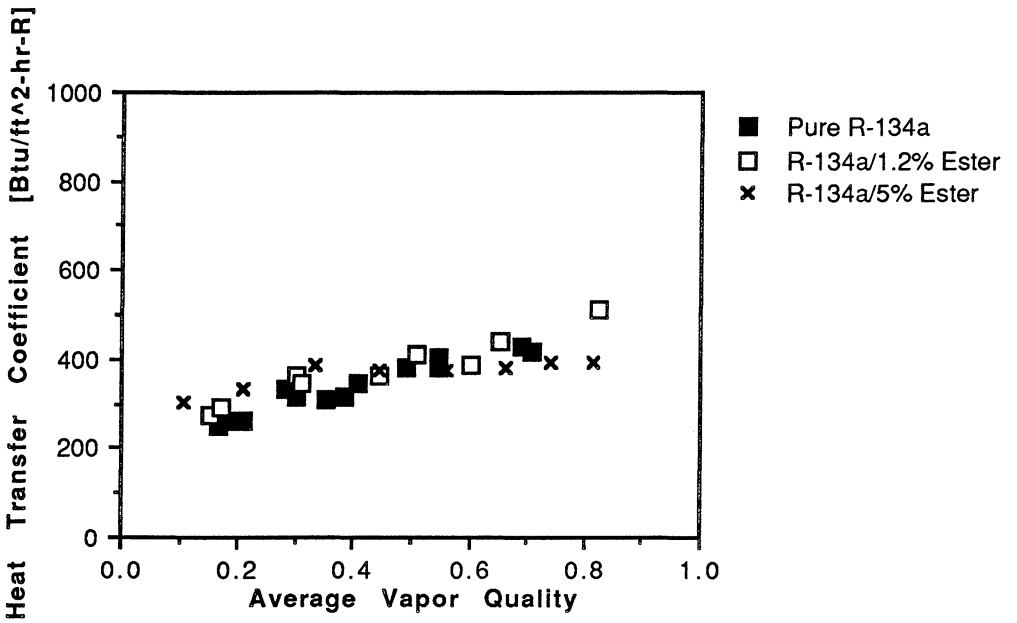

Figure 6.23. Heat Transfer Coefficient versus Average Vapor Quality for Pure and Oil Mixture Tests for G=110 klbm/ft^{2}hr, T_{sat}=95 °F

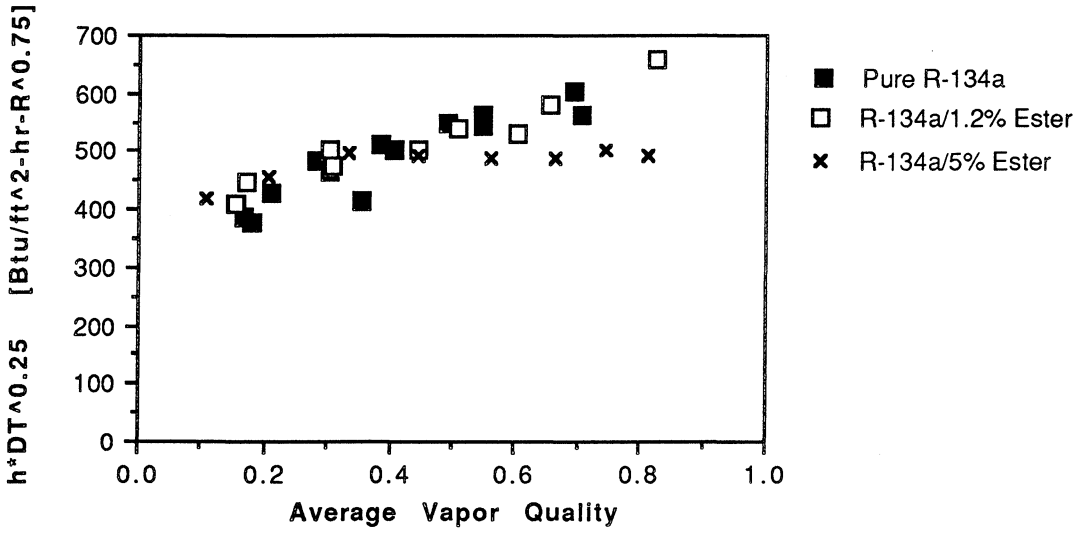

Figure 6.23a. Heat Transfer Coefficient times $\Delta T^{0.25}$ versus Average Vapor Quality for Pure and Oil Mixture Tests for G=110 klbm/ft^{2}hr, T_{sat}=95 °F

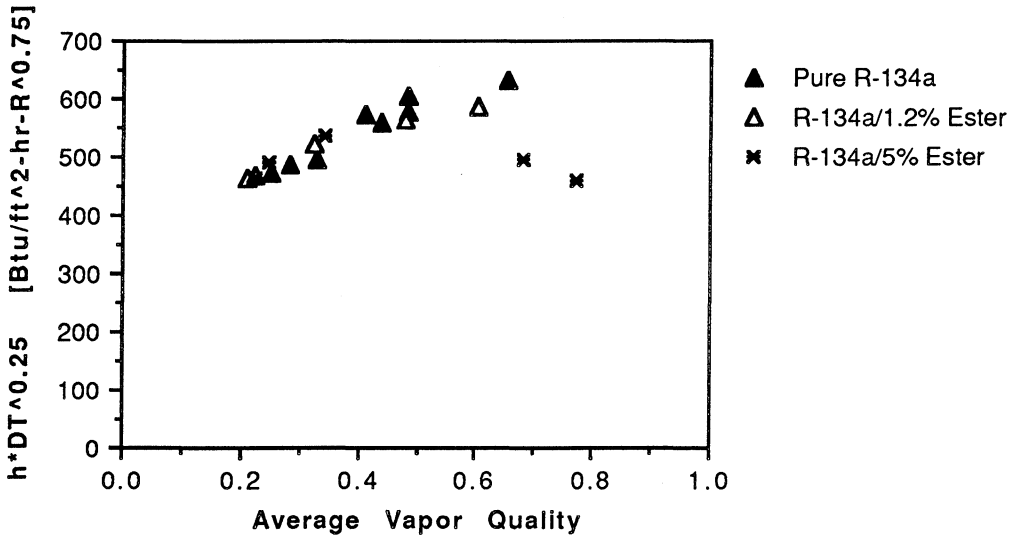

Figure 6.24. Heat Transfer Coefficient times $\Delta T^{0.25}$ versus Average Vapor Quality for Pure and Oil Mixture Tests for G=55 klbm/ft^{2}hr, T_{sat}=95 °F

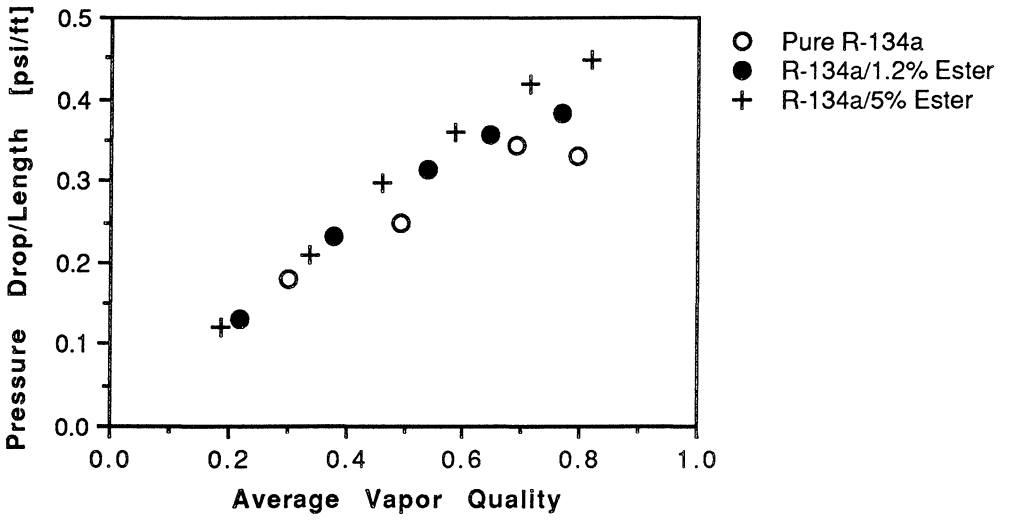

Figure 6.25. Pressure Drop versus Average Vapor Quality for Pure R-134a and R-134a/Ester Mixture Tests for G=220 klbm/ft^{2}hr, T_{sat}=95 °F

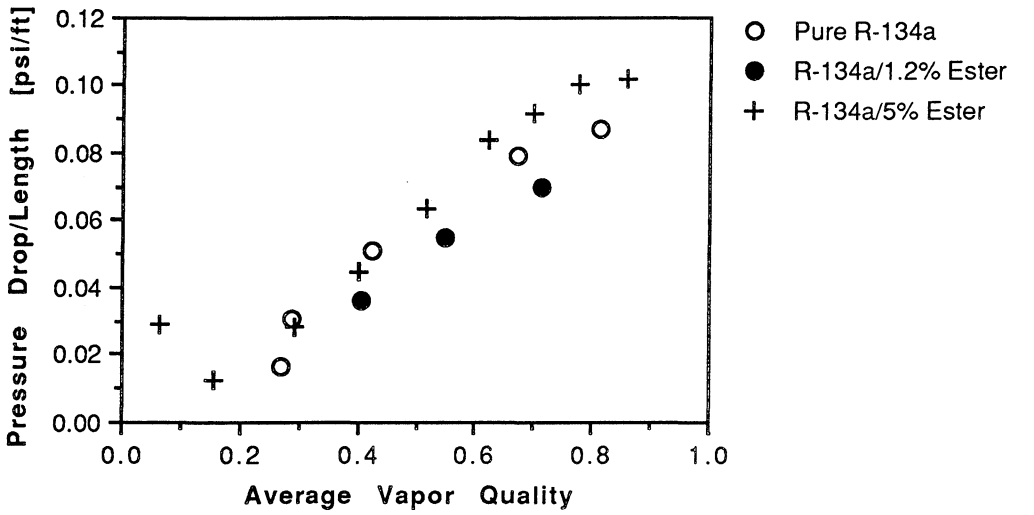

Figure 6.26. Pressure Drop versus Average Vapor Quality for Pure R-134a and R-134a/ Ester Mixture Tests for G=110 klbm/ft^{2}hr, T_{sat}=95 °F

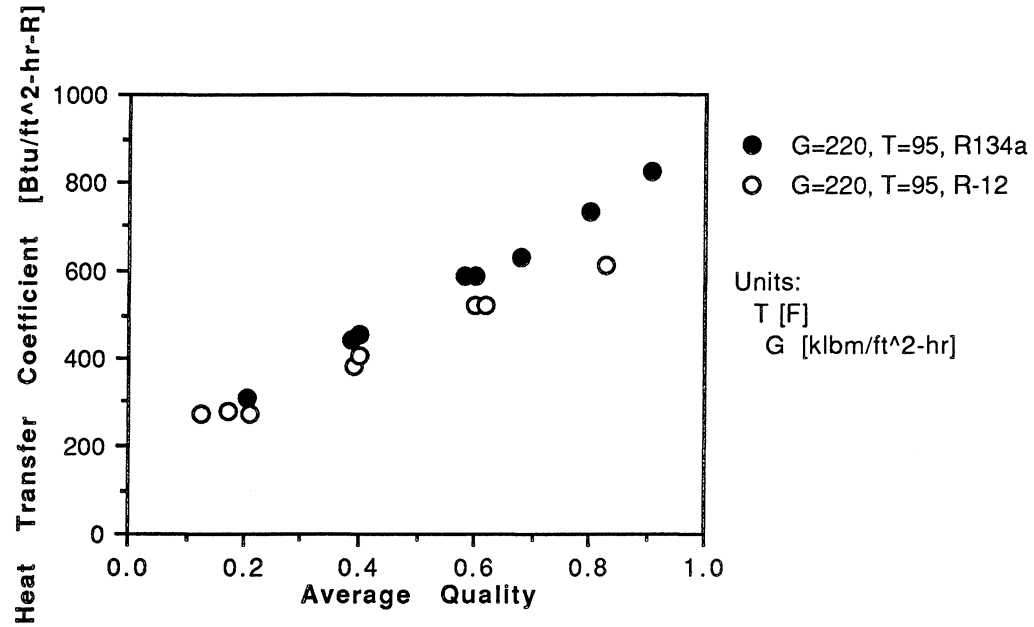

Figure 6.27. Heat Transfer Coefficient versus Average Vapor Quality for Pure R-134a and R-12 for G=220 klbm/ft^{2}hr, T_{sat}=95 °F

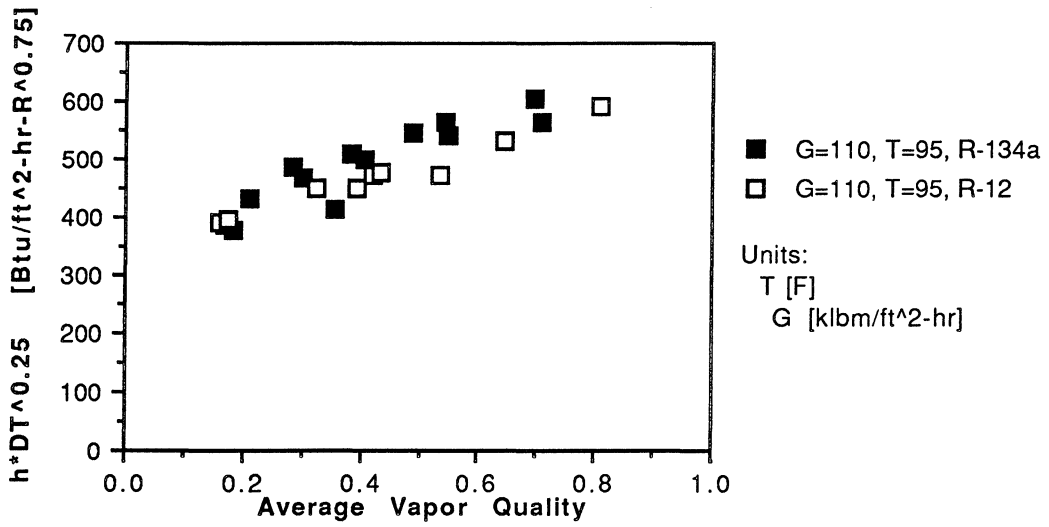

Figure 6.28. Heat Transfer Coefficient times $\Delta T^{0.25}$ versus Average Vapor Quality for Pure R-134a and R-12 for G=110 klbm/ft^{2}hr, T_{sat}=95 ^oF

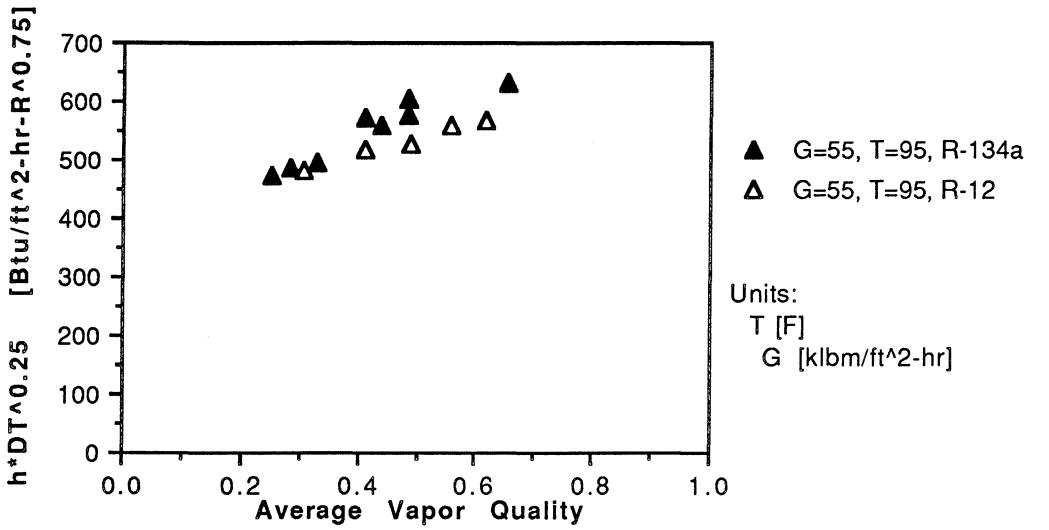

Figure 6.29. Heat Transfer Coefficient times $\Delta T^{0.25}$ versus Average Vapor Quality for Pure R-134a and R-12 for G=55 klbm/ft^{2}hr, T_{sat}=95 ^oF

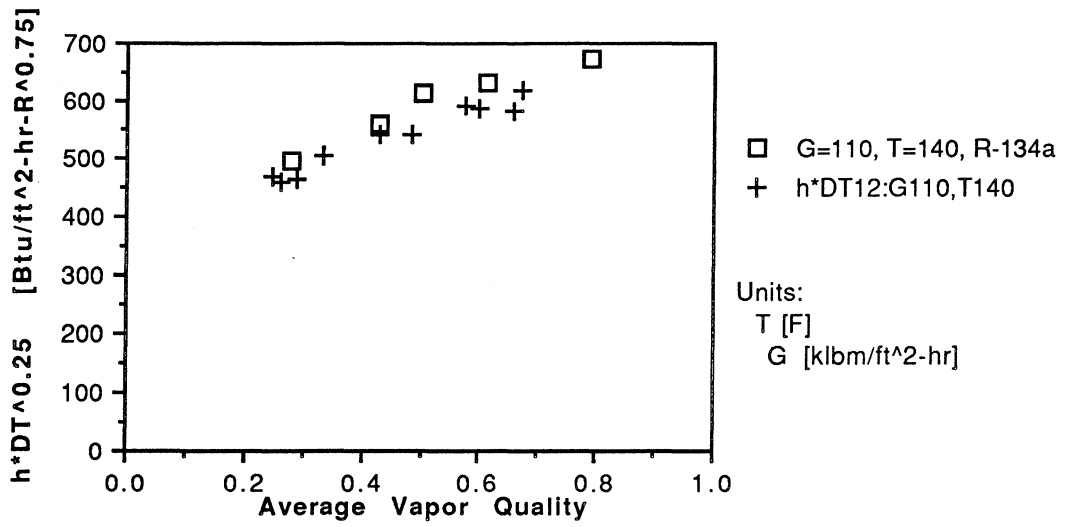

Figure 6.30. Heat Transfer Coefficient times $\Delta T^{0.25}$ versus Average Vapor Quality for Pure R-134a and R-12 for G=110 klbm/ft^{2}hr, T_{sat}=140 ^oF

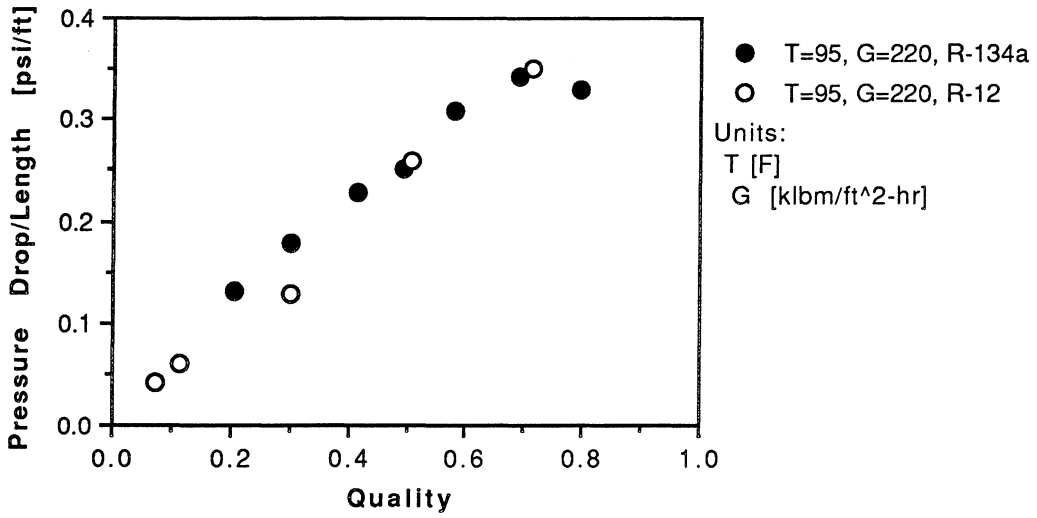

Figure 6.31. Frictional Pressure Drop Comparison for Pure R-134a and R-12 for G=220 klbm/ft^{2}hr, T_{sat}=95 ^oF

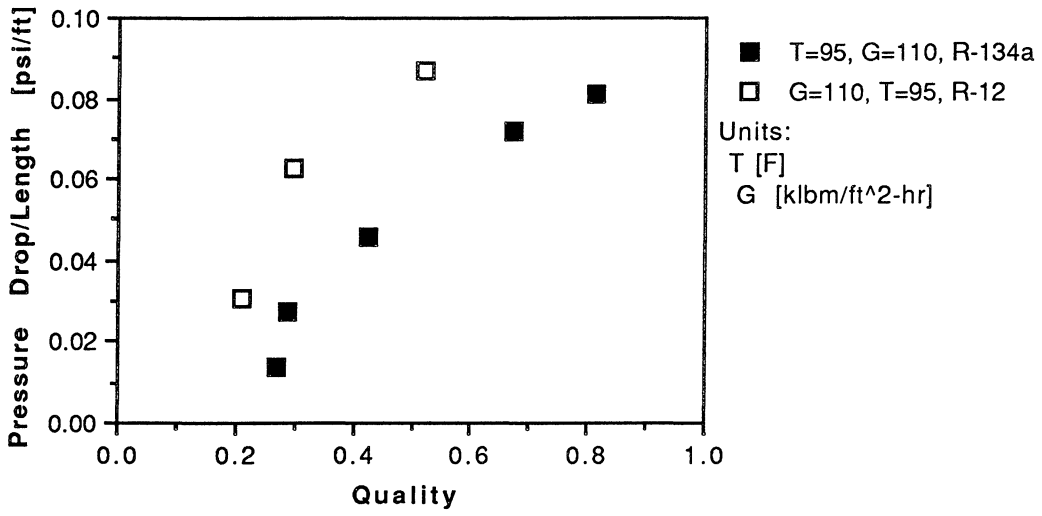

Figure 6.32. Frictional Pressure Drop Comparison for Pure R-134a and R-12 for G=110 klbm/ft^{2}hr, T_{sat}=95 ^oF

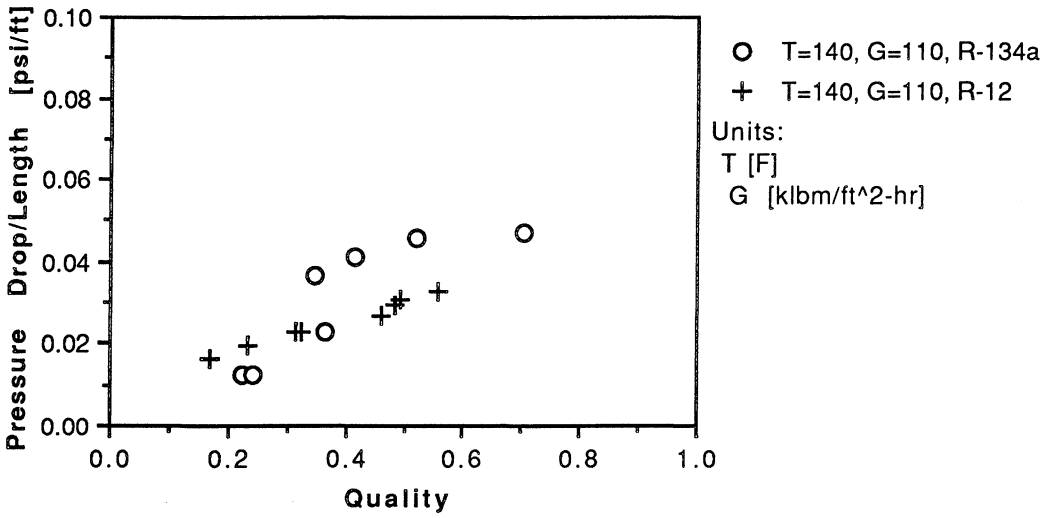

Figure 6.33. Frictional Pressure Drop Comparison for Pure R-134a and R-12 for G=110 klbm/ft^{2}hr, T_{sat}=140 ^oF

CHAPTER 7

CONCLUSIONS AND RECOMMENDATIONS

The purpose of this work was to obtain experimental data for condensing flows under conditions expected in domestic refrigerator/freezers. Tests were performed using pure R-134a, pure R-12, and mixtures of R-134a with 1.2% and 5% Ester lubricant. Special emphasis was placed on explaining the results of the experiments in terms of the two-phase flow pattern of the refrigerant flow.

7.1. Conclusions

The results of the pure R-134a two-phase experiments showed that the prediction methods used from the literature were consistent with experimental data only in those tests for which an annular two-phase flow pattern was observed, and then only when the possibility of liquid entrainment was not present. The correlations drastically underpredicted the experimental values for situations where a wavy or wavy-stratified flow pattern was observed. Clearly, a better method of predicting these coefficients based on flow regime is needed.

The addition of 1.2% Ester oil to the R-134a slightly increased the heat transfer coefficients measured in the test facility for the high mass flux. At the lower mass flux, however, the increase was almost negligible. At the 5% concentration the oil slightly increased the heat transfer coefficients only at low vapor qualities and decreased it at the high vapor qualities. The pressure drop increased with oil concentration, with the most significant increases occurring at high qualities.

Comparisons between pure R-12 and R-134a showed that R-134a had 10% to 15% higher heat transfer coefficients than R-12 across the range of flow regimes, based on an equivalent mass flux. For the wavy flow regime, the heat transfer coefficient is independent of mass flux so comparisons based on an equivalent cooling capacity should yield the same results. No measurable change in pressure drop was observed between R-12 and R-134a.

7.2. Recommendations for Future Work

Experimental results for this study have shown that the test facility is capable of accurately measuring local heat transfer coefficients of condensing refrigerant flows. Although several tests were performed with pure R-134a and R-134a/Ester oil mixtures, many additional tests are required to establish a comprehensive database for this study. Additional tests recommended for the facility include the following:

1. Tests with other R-12 replacements including DuPont's MP-39, a near azeotropic blend of R-22, R-152a, and R-124.
2. Tests with R-22 and R-32/R-125 azeotrope.
3. Tests with a smaller tube diameter to explore the possible limits of the correlations developed for "large" tubes.

Suggested improvements to the test condenser and related equipment could also be made and include the following:

1. Use a smaller annulus to promote higher water-side heat transfer coefficients, which will tend to lower the experimental uncertainty.
3. Measure refrigerant temperatures directly at the inlet and outlet of the test-sections.
3. Measure refrigerant temperature and pressure between the two test-sections.
4. Utilize a shorter test condenser to facilitate smaller quality changes.
5. Change to a more sensitive/lower-range differential pressure transducers to accommodate test conditions at low flow rates.

REFERENCES

Baker, O., 1954, "Simultaneous Flow of Oil and Gas," *The Oil and Gas Journal*, July 26, pp. 185-195.

Baustian, J.J., M.B. Pate, and A.E. Bergles, 1986, "Properties of Oil-Refrigerant Liquid Mixtures with Applications to Oil Concentration Measurement: Part 1 - Thermophysical and Transport Properties," *ASHRAE Transactions*, Vol. 92, Part 1, pp. 55-73.

Bonhomme, D., 1991, "Condensation of Ozone-Safe Refrigerants in Horizontal Tubes: Experimental Test Facility and Preliminary Results," M.S. Thesis, University of Illinois at Urbana-Champaign.

Cavallini, A., and R. Zecchin, 1974, "A Dimensionless Correlation for Heat Transfer in Forced Convection Condensation," *Proceedings of the Fifth International Heat Transfer Conference*, Tokyo, Sept. 3-7, Japan Society of Mechanical Engineers, Vol. 3, pp. 309-313.

Chato, J.C., 1962, "Laminar Condensation Inside Horizontal and Inclined Tubes," *ASHRAE Journal*, No. 4, pp. 52-60.

Chato, J.C., Jabardo, J.M.S., Christofferson, B., de Souza, Adriano, Dobson, Monte, Gaibel, Joshua, Hinde, D., Mainland, M., Panek, J., Wattelet, J., 1992, "Refrigerant-Side Evaporation and Condensation Studies", FY 92 Annual Report, Air Conditioning and Refrigeration Center, Department of Mechanical and Industrial Engineering, University of Illinois at Urbana-Champaign.

Chen, S.L., F.M. Gerner, and C.L. Tien, 1987, "General Film Condensation Correlations," *Experimental Heat Transfer*, Vol. 1, pp. 93-107.

Chisholm, D., 1963, "The Pressure Gradient Due to Friction During the Flow of Boiling Water," *Engng. and Boiler House Rev.*, Vol. 78, No. 9, pp. 287-289.

Collier, J., 1972, *Convective Boiling and Condensation.*, McGraw-Hill, London.

Corradini, M.L., J. Delhaye, M. Ishii, and G. Kocamustafaogullari, 1991, *Multiphase Flow and Heat Transfer for Industrial Applications*, Department of Engineering Professional Development, College of Engineering, University of Wisconsin-Madison.

Incropera, F., and D. DeWitt, 1981, *Fundamentals of Heat and Mass Transfer, 2nd ed.*, John Wiley and Sons, New York.

Lockhart, R.W., and R.C. Martinelli, 1949, "Proposed Correlation of Data for Isothermal Two-Phase Two-Component Flow in Pipes," *Chemical Engineering Progress*, Vol. 45, No. 1, pp. 39-48

Moffat, J.M., 1988, "Describing the Uncertainties in Experimental Results," *Experimental Thermal and Fluid Science*, Vol. 1, pp. 3-17

Panek, J., 1992, "Evaporation Heat Transfer and Pressure Drop in Ozone-Safe Refrigerants and Refrigerant-Oil Mixtures," M.S. Thesis, University of Illinois at Urbana-Champaign.

Rosenow, W.M., 1956, "Heat Transfer and Temperature Distribution in Laminar Film Condensation," *Transaction of ASME*, Vol. 78, pp. 1645-1648

Schlager, L.M., M.B. Pate, and A.E. Bergles, 1990a, "Performance Predictions of Refrigerant-Oil Mixtures in Smooth and Internally Finned Tubes - Part 1: Literature Review," *ASHRAE Transactions*, Vol. 96, Part 1, pp. 161-169.

Schlager, L.M., M.B. Pate, and A.E. Bergles, 1990b, "Performance Predictions of Refrigerant-Oil Mixtures in Smooth and Internally Finned Tubes - Part 2: Design Equations," *ASHRAE Transactions*, Vol. 96, Part 1, pp. 170-182.

Shah, M.M., 1979, "A General Correlation for Heat Transfer During Film Condensation inside Pipes," *International Journal of Heat and Mass Transfer*, Vol. 22, pp. 547-556.

Sur, B., and N.Z. Azer, 1991, "Effect of Oil on Heat Transfer and Pressure Drop during Condensation of Refrigerant-113 inside Smooth and Internally Finned Tubes," *ASHRAE Transactions*, Vol. 93, Part 1, pp. 393-416.

Thom, J.R.S., 1964, "Prediction of Pressure Drop During Forced Circulation Boiling Water," *International Journal of Heat and Mass Transfer*, Vol. 7, pp. 709-724.

Tichy, J.A., J. Duque-Rivera, N.A. Macken, and W.M.B. Duval, 1986, "An Experimental Investigation of Pressure Drop in Forced-Convection Condensation and Evaporation of Oil Refrigerant Mixtures," *ASHRAE Transactions*, Vol. 92 Part 2, pp. 461-472.

Tichy, J.A., N.A. Macken, and W.M.B. Duval, 1985, "An Experimental Investigation of Heat Transfer in Forced Convection Condensation of Oil-Refrigerant Mixtures," *ASHRAE Transactions*, Vol. 91, Part 1a, pp. 297-308.

Traviss, D.P., W.M. Rohsenow, and A.B. Baron, 1973, "Forced-Convection Condensation inside Tubes: A Heat Transfer Equation For Condenser Design," *ASHRAE Transactions*, Vol. 79, Part 1, pp. 157-165.

Wilson, D., and R. Basu, 1988, "Thermodynamic Properties of a New Stratospherically Safe Working Fluid -- Refrigerant 134a," *ASHRAE Transactions*, Vol. 94, Part 2, pp. 2095-2118.

APPENDIX A

STARTUP AND SHUTDOWN PROCEDURES

Startup Procedure:

1. Turn computer on, open Larry (data acquisition program), and start program.
2. Check for pressurization of refrigerant, i.e. $P > P_{sat}$ ($T_{ambient}$).
3. Make ice baths in dewars and install thermocouples.
4. Check that all water heater switches are OFF and 120 V heaters are plugged into quad outlets behind apparatus. Make sure red and green plugs are in separate quad outlet or current overload may occur.
5. Set nitrogen pressure in bladder accumulator at approximately the desired value corresponding to the required saturation temperature.
6. Open main valves for water: supply slightly open, waste fully open.
7. Turn waste pump switch ON (switch located on wall).
8. Open water supply valve to aftercondenser and set to 1.5 gpm.
9. Let the water in the aftercondenser run for a moment then test priming of the waste pump by lifting up float switch and observing water level in waste tank.
10. If water level in waste tank does not lower, turn waste pump switch OFF, close water supply valve to aftercondenser, prime waste pump, and test again.
11. Open test section water supply valves (needle valves near aftercondenser), test section control valves (needle valves below low-range rotameters), and water backpressure valves (blue gate valves above rotameters).
12. Turn supply pump switch ON (switch located on wall).
13. Check for priming of supply pump by observing rotameters for test sections.
14. If water is not flowing through test section rotameters, turn supply pump switch OFF, prime supply pump, and test again.
15. Check for leaks in test sections.
16. Partially open supply tank supply valve (located before supply tank float valve) to balance water level in tank.

17. Slowly close water backpressure valves until low-range rotameter read between 0.8 and 0.9 gpm or until bubbles in flow do not appear.

18. Slowly close test section control valves until desired water flowrate is reached.

19. Check that valves throughout refrigerant loop are open so as to create a complete circuit and that flow goes through the flowmeter bypass.

20. Turn ON inverter and refrigerant pump and set to desired flowrate.

21. Turn ON water heaters to obtain desired water temperature.

22. Turn OFF all refrigerant heater switches and set variac to zero.

23. Turn ON 240 V refrigerant heater disconnect switch (located on wall).

24. Turn ON refrigerant heaters and slowly bring system to desired conditions.

25. Open valves surrounding flowmeter corresponding to desired flow rate and close flowmeter bypass valves.

Shutdown Procedure:

1. Turn OFF all refrigerant heaters, set variac to zero, and turn off refrigerant heater disconnect switch (located on wall).

2. Turn OFF all water heater switches, unplug 120 V heaters from quad outlets (located behind refrigerant heater), and turn OFF 240 V water heater disconnect if used (located on wall).

3. Allow system to cool to below 30 °C

4. Turn OFF supply pump switch.

5. Close test section water supply valves, supply tank supply valve, aftercondenser supply valve, and main supply valve.

6. Empty waste tank by lifting up float switch to engage waste pump.

7. Turn OFF waste pump switch.

8. Close main waste valve.

9. Turn OFF refrigerant pump and inverter.

10. Lower pressure in bladder accumulator until two-phase condition is observed in sight glasses at inlet and outlet of test section, then close ball valves at inlet and outlet to isolate test section. (Note: This step is optional to reduce risk of sight glass leakage)

11. Stop Larry (data acquisition program) and quit LabView.

APPENDIX B

HEAT LOSS CALCULATIONS

To calculate the enthalpy of the refrigerant leaving the refrigerant heater during a typical two-phase test, it is necessary to be able to predict the amount of heat which is lost to the environment. This prediction is used in Eq. (5.2) and is based on experimental data obtained from single-phase tests as described in section 5.1.2..

Two single-phase tests were performed for each combination of mass flux and saturation temperature tested. The first was a single-phase liquid test run with a heater outlet temperature which was no more than 1.8° F (1 °C) subcooled below the saturation temperature. The heat loss for this test was calculated from Eq. (5.11) which becomes the following:

$$\dot{Q}_{loss,\,x=0} = \dot{m}_{refrigerant}\left[h_{Eq.\,(5.2)} - h_{Eq.\,(5.10a)}\right]$$

where in Eq. (5.2), $\dot{Q}_{loss}$=0. The second test was a single-phase vapor test run at no more than 1.8° F (1 °C) superheat above the saturation temperature. The heat loss for this test was also calculated from Eq. (5.11) which becomes the following:

$$\dot{Q}_{loss,\,x=1} = \dot{m}_{refrigerant}\left[h_{Eq.\,(5.2)} - h_{Eq.\,(5.10b)}\right]$$

For subsequent two-phase tests run at the same mass flux and saturation temperature combination, the heat loss from the refrigerant heater to the environment is assumed to increase linearly with quality and is given by:

$$\dot{Q}_{loss,\,heater} = \dot{Q}_{loss,\,x=0} + x_{estimated}\left[\dot{Q}_{loss,\,x=1} - \dot{Q}_{loss,\,x=0}\right]$$

where $x_{estimated}$ is the heater outlet vapor quality predicted with a 5% loss to the environment. Values for $\dot{Q}_{loss,\,x=0}$ and $\dot{Q}_{loss,\,x=1}$ for each of the mass flux and saturation temperature combinations are shown in the table below.

Heat Loss Predictions from Single-Phase Tests for R-134a

Mass Flux [klb$_m$/ft^{2}hr]	Saturation Temp. [°F]	$Q_{loss,\,x=0}$ [W]	$Q_{loss,\,x=1}$ [W]
220	35	4	17
220	60	32	38
110	35	3	17
110	60	20	38
55	35	4	15
55	60	25	38

Heat Loss Predictions from Single-Phase Tests for R-12

Mass Flux [klb$_m$/ft^{2}hr]	Saturation Temp. [°F]	$Q_{loss,\,x=0}$ [W]	$Q_{loss,\,x=1}$ [W]
220	95	3	26
110	95	4	21
110	140	29	51
55	95	6	29
55	140	31	48

APPENDIX C

EXPERIMENTAL DATA

Table C.1. Data for Pure R-134a at T=95 °F, G=220 klb_m/ft^2hr

ΔT [F] (C)	x [%]	Δx [%]	h [Btu/ft^2-hr-R] (W/m^2-K)	Filename
7.76 (4.31)	20.5	18.8	307 (1742)	19920610-1212
5.90 (3.28)	28.4	20.8	440 (2498)	19920610-1245
5.74 (3.19)	40.2	20.6	454 (2579)	19920610-1212
4.41 (2.45)	58.3	20.6	591 (3356)	19920610-1335
4.64 (2.58)	59.8	22.0	590 (3355)	19920610-1245
4.34 (2.41)	68.1	22.0	629 (3576)	19920610-1404
3.71 (2.06)	79.3	21.5	734 (4172)	19920610-1335
3.44 (1.94)	90.5	22.8	821 (4666)	19920610-1404

Table C.2. Data for Pure R-134a at T=95 °F, G=110 klb_m/ft^2hr

ΔT [F] (C)	x [%]	Δx [%]	h [Btu/ft^2-hr-R] (W/m^2-K)	Filename
5.87 (3.26)	16.7	23.5	247 (1404)	19920611-1116
4.23 (2.35)	18.1	18.3	264 (1500)	19920610-1644
6.97 (3.87)	20.9	30.1	264 (1502)	19920806-1105
4.39 (2.44)	28.3	24.2	335 (1903)	19920804-1244
4.86 (2.70)	30.3	24.2	314 (1784)	19920611-1148
3.17 (1.76)	35.4	16.4	312 (1770)	19920610-1644
6.71 (3.73)	38.3	34.7	316 (1796)	19920812-1134
4.30 (2.39)	40.7	24.4	348 (1975)	19920611-1116
4.16 (2.31)	49.0	26.0	382 (2171)	19920806-1105
3.78 (2.10)	54.5	24.2	403 (2292)	19920611-1148
4.14 (2.30)	54.6	25.2	380 (2159)	19920611-1233
3.83 (2.13)	69.2	27.0	431 (2448)	19920812-1134
3.31 (1.84)	70.7	21.7	416 (2364)	19920611-1310

Table C.3. Data for Pure R-134a at T=95 °F, G=55 klb_m /ft^2hr

ΔT [F] (C)	x [%]	Δx [%]	h [Btu/ft^2-hr-R] (W/m^2-K)	Filename
3.78 (2.10)	25.2	18.8	307 (1742)	19920610-1212
4.84 (2.69)	28.1	20.8	440 (2498)	19920610-1245
4.70 (2.61)	32.7	20.6	454 (2579)	19920610-1212
5.20 (2.89)	41.2	20.6	591 (3356)	19920610-1335
3.31 (1.84)	44.0	22.0	590 (3355)	19920610-1245
4.95 (2.75)	48.4	22.0	629 (3576)	19920610-1404
4.25 (2.36)	48.4	21.5	734 (4172)	19920610-1335
3.58 (1.99)	65.1	22.8	821 (4666)	19920610-1404

Table C.4. Data for Pure R-134a at T=140 °F, G=220 klb_m/ft^2hr

ΔT [F] (C)	x [%]	Δx [%]	h [Btu/ft^2-hr-R] (W/m^2-K)	Filename
7.99 (4.44)	15.7	23.4	293 (1662)	19920622-1828
4.43 (2.46)	17.5	12.5	273 (1549)	19920622-1644
7.63 (4.24)	26.3	24.7	332 (1887)	19920911-1222
6.95 (3.86)	27.2	23.3	335 (1901)	19920911-1340
7.07 (3.93)	28.6	25.7	360 (2043)	19920622-1747
5.31 (2.95)	34.3	21.5	409 (2321)	19920622-1913
6.21 (3.45)	40.3	25.9	420 (2384)	19920622-1828
5.90 (3.28)	52.3	27.0	458 (2604)	19920911-1340
5.31 (2.95)	55.9	24.2	452 (2567)	19920911-1520
4.61 (2.56)	56.6	23.1	510 (2895)	19920622-1913
4.59 (2.55)	81.7	27.5	595 (3381)	19920911-1520

Table C.5. Data for Pure R-134a at T=140 °F, G=110 klb_m/ft^2hr

ΔT [F] (C)	x [%]	Δx [%]	h [Btu/ft^2-hr-R] (W/m^2-K)	Filename
3.31 (1.84)	28.6	24.7	365 (2076)	19920706-1503
4.14 (2.30)	42.9	32.6	391 (2219)	19920706-1754
4.03 (2.24)	50.0	35.5	433 (2462)	19920706-1808
3.71 (2.06)	61.0	34.2	457 (2594)	19920706-1828
3.37 (1.87)	79.0	33.5	497 (2822)	19920706-1849

Table C.6. Data for Pure R-134a at T=140 °F, G=55 klb_m/ft^2hr

ΔT [F] (C)	x [%]	Δx [%]	h [Btu/ft^2-hr-R] (W/m^2-K)	Filename
4.03 (2.24)	26.0	49.4	301 (1709)	19920824-1705
4.21 (2.34)	39.9	58.1	334 (1896)	19920825-1142
3.65 (2.03)	37.0	47.4	299 (1696)	19920819-1153
4.34 (2.41)	41.7	62.2	351 (1995)	19920825-1220
3.55 (1.97)	43.0	50.3	333 (1892)	19920819-1313
4.25 (2.36)	46.3	52.0	305 (1733)	19920824-1811
3.92 (2.18)	54.8	62.1	389 (2211)	19920825-1303

Table C.7. Data for R-134a/1.2% Ester Mixture at T=95 °F, G=220 klb_m/ft^2hr

ΔT [F] (C)	x [%]	Δx [%]	h [Btu/ft^2-hr-R] (W/m^2-K)	Filename
5.49 (3.05)	14.8	14.0	315 (1788)	19920716-1207
5.60 (3.11)	17.1	15.1	336 (1907)	19920716-1126
4.30 (2.39)	29.4	15.5	437 (2482)	19920716-1207
4.03 (2.24)	30.4	14.5	458 (2601)	19920716-1228
3.29 (1.83)	45.2	45.3	591 (3358)	19920716-1228
3.64 (2.02)	46.0	15.4	527 (2995)	19920716-1248
3.51 (1.95)	56.1	15.3	553 (3140)	19920716-1310
2.84 (1.58)	61.9	16.4	708 (4025)	19920716-1248
2.61 (1.45)	68.2	16.1	774 (4400)	19920716-1336
3.40 (1.89)	71.9	16.3	601 (3412)	19920716-1310
2.34 (1.30)	84.7	17.1	906 (5146)	19920716-1336

Table C.8. Data for R-134a/1.2% Ester Mixture at T=95 °F, G=110 klb_m/ft^2hr

ΔT [F] (C)	x [%]	Δx [%]	h [Btu/ft^2-hr-R] (W/m^2-K)	Filename
5.29 (2.94)	15.5	23.8	271 (1540)	19920717-1207
4.54 (2.52)	16.9	20.6	277 (1574)	19920716-1513
3.78 (2.10)	30.3	23.0	361 (2052)	19920717-1231
3.62 (2.01)	30.9	20.1	344 (1957)	19920717-1309
3.58 (1.99)	44.5	21.0	363 (2063)	19920717-1332
3.02 (1.68)	50.8	20.1	410 (2329)	19920717-1309
3.47 (1.93)	60.4	22.0	389 (2210)	19920717-1355
2.93 (1.63)	65.4	21.1	442 (2510)	19920717-1332
2.68 (1.49)	82.5	22.7	514 (2923)	19920717-1355

Table C.9. Data for R-134a/1.2% Ester Mixture at T=95 °F, G=55 klb_m/ft^2hr

ΔT [F] (C)	x [%]	Δx [%]	h [Btu/ft^2-hr-R] (W/m^2-K)	Filename
3.42 (1.90)	21.0	38.2	341 (1938)	19920717-1546
3.47 (1.93)	22.3	38.9	344 (1955)	19920717-1700
3.08 (1.71)	32.2	39.7	395 (2242)	19920717-1601
2.75 (1.53)	48.1	39.1	437 (2481)	19920717-1620
3.26 (1.81)	60.3	37.8	354 (2010)	19920717-1700

Table C.10. Data for R-134a/5% Ester Mixture at T=95 °F, G=220 klb_m/ft^2hr

ΔT [F] (C)	x [%]	Δx [%]	h [Btu/ft^2-hr-R] (W/m^2-K)	Filename
5.02 (2.79)	9.8	11.5	290 (1648)	19920721-1225
4.72 (2.62)	21.9	13.4	367 (2083)	19920721-1311
4.12 (2.29)	37.5	14.8	455 (2588)	19920721-1354
3.60 (2.00)	49.8	15.0	539 (3062)	19920721-1412
3.22 (1.79)	61.8	13.9	559 (3176)	19920721-1434
4.28 (2.38)	74.9	13.9	571 (3243)	19920721-1448

Table C.11. Data for R-134a/5% Ester Mixture at T=95 °F, G=110 klb_m/ft^2hr

ΔT [F] (C)	x [%]	Δx [%]	h [Btu/ft^2-hr-R] (W/m^2-K)	Filename
3.51 (1.95)	10.6	17.3	305 (1734)	19920723-1431
3.40 (1.89)	20.7	18.7	334 (1899)	19920723-1450
2.79 (1.55)	33.5	17.3	384 (2184)	19920723-1506
2.95 (1.64)	44.6	17.5	376 (2138)	19920723-1526
2.88 (1.60)	55.9	17.3	374 (2127)	19920723-1549
2.74 (1.52)	66.2	16.7	381 (2163)	19920723-1601
2.72 (1.51)	74.2	16.8	391 (2221)	19920723-1622
2.48 (1.38)	81.4	15.8	392 (2230)	19920723-1645

Table C.12. Data for R-134a/5% Ester Mixture at T=95 °F, G=55 klb_m/ft^2hr

ΔT [F] (C)	x [%]	Δx [%]	h [Btu/ft^2-hr-R] (W/m^2-K)	Filename
2.81 (1.56)	22.4	33.0	359 (2041)	19920724-1309
2.86 (1.59)	24.7	34.7	376 (2135)	19920724-1323
2.57 (1.43)	34.3	36.1	425 (2412)	19920724-1358
2.66 (1.48)	68.0	33.2	386 (2193)	19920724-1445
2.65 (1.47)	77.1	32.2	360 (2045)	19920724-1500

Table C.13. Data for R-12 at T=95 °F, G=220 klb_m/ft^2hr

ΔT [F] (C)	x [%]	Δx [%]	h [Btu/ft^2-hr-R] (W/m^2-K)	Filename
4.48 (2.49)	12.7	12.4	272 (1544)	19920918-1041
4.73 (2.63)	17.4	13.6	282 (1600)	19920918-1128
5.63 (3.13)	20.9	15.6	272 (1546)	19920918-1206
5.36 (2.98)	39.1	20.7	381 (2166)	19920918-1206
4.61 (2.56)	40.1	18.8	405 (2301)	19920918-1250
3.74 (2.08)	59.9	19.8	520 (2957)	19920918-1319
4.70 (2.61)	61.7	24.6	522 (2968)	19920918-1250
4.14 (2.30)	82.8	25.9	615 (3493)	19920918-1319

Table C.14. Data for R-12 at T=95 °F, G=110 klb_m/ft^2hr

ΔT [F] (C)	x [%]	Δx [%]	h [Btu/ft^2-hr-R] (W/m^2-K)	Filename
4.14 (2.30)	10.0	20.7	247 (1403)	19920921-1154
4.37 (2.43)	16.1	25.4	270 (1533)	19920921-1230
4.01 (2.23)	17.4	22.7	279 (1587)	19920921-1327
3.71 (2.06)	32.4	24.1	323 (1837)	19920921-1154
3.40 (1.89)	39.4	23.1	334 (1897)	19920921-1348
3.94 (2.19)	42.0	26.5	334 (1896)	19920921-1327
4.14 (2.30)	43.6	29.5	333 (1892)	19920921-1230
3.47 (1.93)	53.6	24.4	346 (1965)	19920921-1408
3.42 (1.90)	64.5	27.1	389 (2211)	19920921-1348
3.35 (1.86)	80.6	29.7	438 (2489)	19920921-1408

Table C.15. Data for R-12 at T=95 °F, G=55 klb_m/ft^2hr

ΔT [F] (C)	x [%]	Δx [%]	h [Btu/ft^2-hr-R]	Filename
4.05 (2.25)	30.4	51.1	339 (1927)	19920921-1559
3.69 (2.05)	41.1	54.7	373 (2121)	19920921-1615
4.16 (2.31)	48.9	58.4	369 (2098)	19920921-1643
3.67 (2.04)	55.5	63.3	405 (2298)	19920921-1702
3.56 (1.98)	61.6	60.2	413 (2348)	19920921-1714

Table C.16. Data for R-12 at T=140 °F, G=110 klb_m/ft^2hr

ΔT [F] (C)	x [%]	Δx [%]	h [Btu/ft^2-hr-R]	Filename
3.92 (2.18)	24.5	31.3	575 (3268)	19920923-1245
3.89 (2.16)	25.9	31.1	585 (3325)	19920923-1309
9.14 (5.08)	28.9	58.7	538 (3055)	19920923-1639
3.65 (2.03)	33.4	33.2	523 (2971)	19920923-1354
3.53 (1.96)	42.7	34.6	456 (2592)	19920923-1447
7.79 (4.33)	48.3	61.5	392 (2227)	19920923-1652
3.51 (1.95)	57.4	37.5	351 (1992)	19920923-1521
3.49 (1.94)	59.8	36.4	213 (1210)	19920923-1608
7.02 (3.90)	65.8	62.4	266 (1509)	19920923-1706
3.56 (1.98)	67.2	39.2	279 (1587)	19920923-1546

Table C.17. Data for R-12 at T=140 °F, G=73 klb_m/ft^2hr

ΔT [F] (C)	x [%]	Δx [%]	h [Btu/ft^2-hr-R]	Filename
3.20 (1.78)	29.2	43.3	371 (2106)	19920924-1431
3.91 (2.17)	62.7	55.0	383 (2174)	19920924-1525
3.31 (1.84)	63.0	49.8	409 (2324)	19920924-1453
3.85 (2.14)	77.4	59.8	427 (2428)	19920924-1513

APPENDIX D

THERMODYNAMIC AND TRANSPORT PROPERTIES OF R-134a

Properties of the fluid R-134a were obtained from three different sources. Thermodynamic properties were taken from curve fits from data by Wilson & Basu (1988). Conductivity and dynamic viscosity data were obtained from personal communications with General Electric Appliances. Liquid specific heat data was taken from EES (Engineering Equation Solver, from F-Chart Software). The table below shows the property curves used in this study.

Table D.1. Thermodynamic and Transport Properties of R-134a

Property Correlation	Units	Source
$h_f = 49.469 + 1.3245\ T + 2.5867E\text{-}3\ T^2$	[kJ/kg]	W & B
$h_g = 247.13 + 0.57456\ T - 6.5564E\text{-}4\ T^2 - 3.2831E\text{-}6\ T^3 - 1.9976E\text{-}7\ T^4$	[kJ/kg]	W & B
$\rho_f = 1294.8 - 3.1664\ T - 6.7362E\text{-}3\ T^2 - 1.346E\text{-}4\ T^3$	[kg/m^3]	W & B
$\rho_g = 4.842 + 1.4697T - 2.1958E\text{-}2\ T^2 + 3.3934E\text{-}4\ T^3$	[kg/m^3]	W & B
$c_{pf} = 1.3135 + 3.9928E\text{-}3\ T + 1.7497E\text{-}6\ T^2 + 4.4304E\text{-}7\ T^3 - 1.6215E\text{-}8\ T^4 + 2.0192E\text{-}10\ T^5$	[kJ/kg-K]	EES
$\mu_f = -0.00244+3.322E\text{-}6\ (T+273.15) + 0.4944/\ (T+273.15)$	[Pa-s]	GE
$\mu_g = 1.53E\text{-}6 + 4.252E\text{-}8\ (T+273.15)$	[Pa-s]	GE
$k_f = 0.1798 - 3.481E\text{-}4\ (T+273.15)$	[W/m-K]	GE
$k_g = (12.47\text{-}0.09965\ (T+273.15) + 3.989E\text{-}4\ (T+273.15)^2)/1000$	[W/m-K]	GE
$P_{sat} = 4{,}555{,}063.92 \exp\ (-2633.437/\ (T_{sat}+273.15))$	[kPa]	W & B
$Tsat = 2633.437/\ (15.3317\text{-}\ln\ (P_{sat})) - 273.15$	[C]	W & B
$\sigma = 0.05537\ (1-\ (T+273.15)/374.3)^{1.208}$	[N/m]	GE

APPENDIX E

SATURATION TEMPERATURE CORRECTION FOR OIL EXPERIMENTS

The addition of oil to pure refrigerant results in an increase in the saturation temperature referred to as apparent superheat. This means that if the saturation temperature was initially computed based on the measured pressure, as was the case for this study, some correction must be made to the computed saturation temperature to account for the presence of oil. Before explaining the correction methods, it should be noted that this would not be necessary if reliable measurements of the refrigerant temperature were available at the inlet and outlet of each test-section. This was not the case for the present test-section, however, since the refrigerant temperature was measured approximately 2 feet before the inlet of the test-section. In this 2 foot length of tube, there was a change in diameter and connections at the inlet and outlet of the sight-glass. These transitions resulted in a drop in pressure, and therefore in saturation temperature, such that the measured temperature was higher than the temperature entering the test-section. The thermocouple at the exit of the test-section was similarly located. For the pure refrigerant experiments, this phenomenon was unimportant since the saturation temperature was computed based on the pressure which was measured only 2 inches from the inlet to the test-section. Also, the magnitude of this drop in saturation temperature was small, less than 0.4 ^{o}F in most cases. Since the temperature differences were generally around 4 ^{o}F, though, it was important to correct for this effect. This problem will be corrected in subsequent test-sections so that both temperature and pressure will be measured at the inlet and outlet of each test-section.

Presented herein will be both a theoretical method and an experimental method for correcting for apparent superheat. Comparisons between predictions of the theoretical and experimental method will also be presented. The experimental method of correcting for the apparent superheat relied on plotting the saturation temperature for a pure refriegerant based on pressure, T_{sat} (P), minus the measured temperature near the test-section inlet, T_{meas}, as a

function of quality. Separate curves were plotted for tests with pure refrigerant, 1.2% Ester oil, and 5% Ester oil in Figure E.1. The curve for the pure data accounts for the pressure drop and deviations between theoretical and experimental behavior of the saturation temperature-pressure relationship. The three curves were for a constant mass flux of 55 klb_m/ft^2-hr, and hence nearly constant pressure drop. Assuming this to be true, the difference between the pure curve and the curves with oil represents the apparent superheat caused by the oil. Curves were fit to each set of data and utilized to compute the mixture saturation temperature according to the formula:

$$T_{sat,mix}\ (P,x) = T_{sat,pure}\ (P) + \text{Apparent Superheat}\ \ (x) \qquad \text{(E.1)}$$

A theoretical attempt to predict the apparent superheat was made using Raoult's law. For equilibrium to exist between the vapor and liquid phases of component A, the fugacities of the two phases must be equal:

$$f_A^V = f_A^L \qquad \text{(E.2)}$$

Assuming that the vapor behaves as an ideal gas, its fugacity is given by:

$$f_A^V = \bar{y}_A P \qquad \text{(E.3)}$$

where: $\bar{y}_A$ = moles of component A in vapor/moles of vapor

The fugacity of the liquid phase of component A is given by:

$$f_A^L = \bar{x}_A P_A^{SAT} \qquad \text{(E.4)}$$

where: $\bar{x}_A$ = moles of component A in liquid/moles of liquid

For a binary mixture, equations (E.2) through (E.4) hold for each phase, so the complete set of equations governing the phase-equilbrium is:

$$\bar{x}_A P_A^{SAT} = \bar{y}_A P \qquad \text{(E.5)}$$

$$\bar{x}_B P_B^{SAT} = \bar{y}_B P \qquad \text{(E.6)}$$

$$\bar{x}_A + \bar{x}_B = 1 \qquad \text{(E.7)}$$

$$\bar{y}_A + \bar{y}_B = 1 \qquad \text{(E.8)}$$

Assuming component A to be the refrigerant and component B to be the oil, equations (E.5) and (E.6) can be added, then combined with (E.7) to yield:

$$P = \bar{x}_A P_A^{SAT} + \bar{x}_B P_B^{SAT} \tag{E.9}$$

Since the saturation pressure of the oil is several orders of magnitude lower than that of the refrigerant, except for cases where $\bar{x}_B$ is nearly equal to 1, equation (E.9) can be approximated as:

$$P \cong \bar{x}_A P_A^{SAT} \tag{E.10}$$

Comparing (E.10) with (E.5), we conclude that $\bar{y}_A = 1$ and $\bar{y}_B = 0$, that is all the oil remains in the liquid phase. Since $\bar{x}_A$ will be less than 1, equation (E.10) requires that P_A^{SAT} be greater than the total pressure, P, so that the saturation temperature is increased. To allow (E.10) to be used, though, the mole fraction of component A in the liquid phase must be known. The quantity which is measured is ω_A, the overall mass fraction of refrigerant. This is not equal to the liquid mass fraction at any point, so additional manipulations and assumptions are required to obtain $\bar{x}_A$ from ω_A.

If one analyzes an infinitesimal length, dz, of a tube with two-phase flow, the mass of the liquid in this volume is:

$$m_L = \rho_L A_L dz = \rho_L A(1-\alpha)dz \tag{E.11}$$

The mass of vapor in the same volume is given by:

$$m_V = \rho_V A_V dz = \rho_V A\alpha dz \tag{E.12}$$

If we denote q as the ratio of the vapor mass in the element to the total mass in the element, equations (E.11) and (E.12) can be used to show that:

$$q = \frac{\rho_V \alpha}{\rho_V \alpha + \rho_L (1-\alpha)} \tag{E.13}$$

Conservation of species A in the cross-section dictates that:

$$m_A = m[(1-q)x_A + qy_A] \tag{E.14}$$

We have already discerned that $y_A = 1$ since no oil vaporizes. Dividing (E.14) by m and realizing that m_A / m is equal to ω_A, which is known, equation (E.14) can be rearranged to solve for x_A:

$$x_A = \frac{\omega_A - q}{1-q} \tag{E.15}$$

The selection of a void-fraction model allows q to be computed based on the local quality, so that all quantities on the right hand side of (E.15) are known. The void-fraction model we utilized was that of Lockhart-Martinelli [Carey, 1991]:

$$\alpha = \frac{1}{1+\chi_{TT}^{0.791}} \tag{E.16}$$

In this correlation, it was assumed that the liquid density was that of pure refrigerant at the same pressure, a reasonable approximation for low oil-concentrations. Finally, we must relate the mass fraction given by (E.15) to the mole fraction needed in (E.10), as:

$$\bar{x}_A = \frac{x_A}{x_A(1-\frac{M_A}{M_B})+1} \tag{E.17}$$

where: M_A = molecular weight of R-134a = 102

M_B = molecular weight of the oil = 430

These equations were used to solve for the apparent superheat at a pressure corresponding to the saturation pressure of pure R-134a at 95 F in the following method:

1. The quantity q was computed by equation E.13 given the quality.
2. q and ω_A were used to compute x_A by equation (E.15).
3. x_A was used to compute $\bar{x}_A$ by equation (E.17).
4. P_{SAT} was computed from E.10.
5. $T_{SAT,mix}$ was computed from the pure refrigerant tables.
6. The apparent superheat was as $T_{SAT,MIX} - T_{SAT,PURE}$

Figure E.2 presents the predictions of apparent superheat computed from Raoult's law with those estimated by the experimental method of equation E.1 for both concentrations of 1.2% and 5%. The agreement is generally within 0.15 F, which is quite satisfactory considering the number of assumptions used. The most serious question probably concerns the applicability of Raoult's law, which is developed in non-flow, equilibrium situations, to a system with the two-phases flowing at different velocities. Our derivation assumed that the

proper mole fraction was that which would exist if the flow were stopped and a sample trapped, i.e. it was based on the mass of the phases which was in the cross-section at a particular time and not on the mass flow through that same cross-section. These two quantities are different because the liquid and vapor phases move with different velocities. The only other similar model we found in the literature [Sur and Azer, 1991] was based on the mass flow rate, which implicitly assumes a slip-ratio of one.

ADDITIONAL REFERENCES

Carey, Van P., *Vapor-Liquid Phase-Change Phenomena- An Introduction to the Thermodynamics and Thermophysics of Phase-Change Processes*, Pergamon Press, 1991.

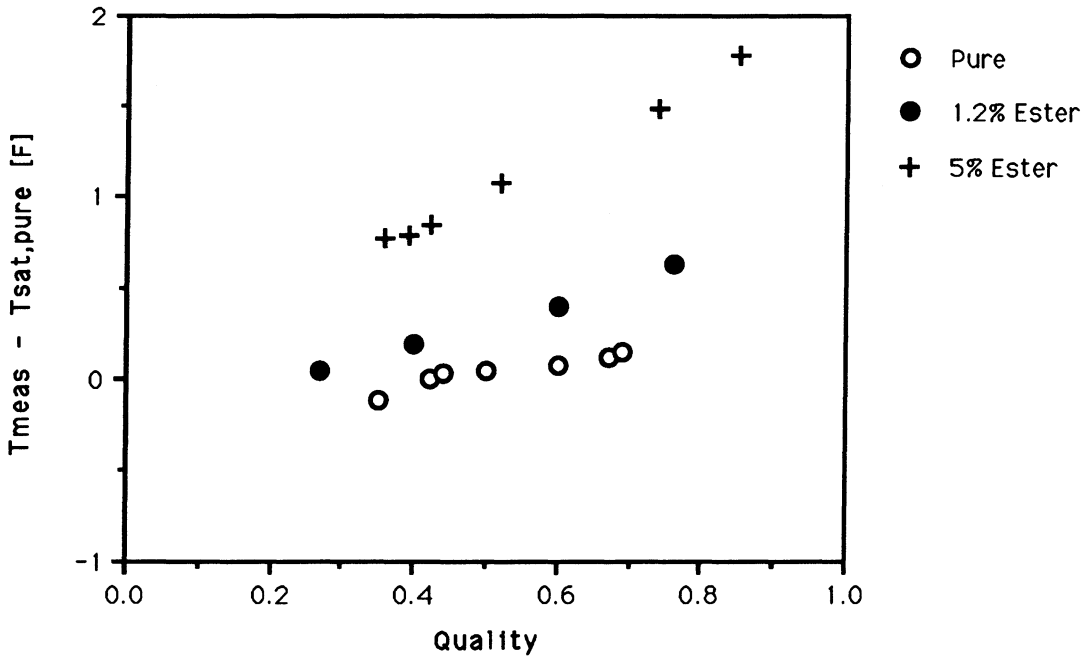

Figure E.1 - Effect of Oil Concentration and Quality on the Difference Between Measured and Saturation Temperature

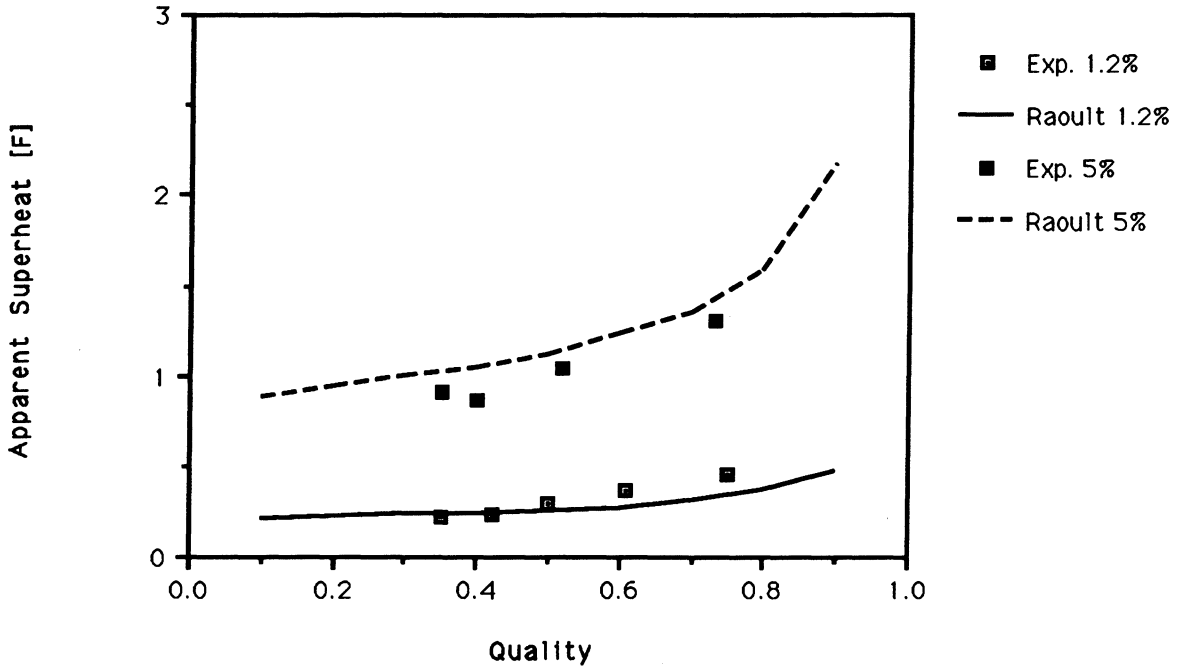

Figure E.2 - Comparison of Raoult's Law Predictions and Experimentally Measured Values of Apparent Superheat at 1.2% and 5% Oil Concentrations